Correlation Functions of Heavy Operators in AdS/CFT

by

Jacob Abajian

A thesis
presented to the University of Waterloo
in fulfillment of the
thesis requirement for the degree of
Doctor of Philosophy
in
Physics

Waterloo, Ontario, Canada, 2024

© Jacob Abajian 2024

Examining Committee Membership

The following served on the Examining Committee for this thesis. The decision of the Examining Committee is by majority vote.

External Examiner:	Thomas Hartman Department of Physics Cornell University
Supervisor:	Pedro Vieira Perimeter Institute for Theoretical Physics
Co-supervisor:	Davide Gaiotto Perimeter Institute for Theoretical Physics
Co-supervisor:	Jaume Gomis Perimeter Institute for Theoretical Physics
Committee Member:	Niayesh Afshordi Department of Physics and Astronomy University of Waterloo
Committee Member:	Luis Lehner Department of Physics and Astronomy University of Waterloo
Internal/External Examiner:	Eduardo Martin-Martinez Department of Applied Mathematics University of Waterloo

Author's Declaration

This thesis consists of material all of which I authored or co-authored: see Statement of Contributions included in the thesis. This is a true copy of the thesis, including any required final revisions, as accepted by my examiners.

I understand that my thesis may be made electronically available to the public.

Statement of Contributions

Chapter 2 consists of material from the published paper [1], co-authored with Francesco Aprile, Robert C. Myers, and Pedro Vieira.

Chapter 3 consists of material from the published paper [2], co-authored with Francesco Aprile, Robert C. Myers, and Pedro Vieira.

Substantial portions of the writing, editing, and figure-making were contributed by the author of the present thesis, who also contributed meaningfully to the research that led to the results explained therein.

Abstract

In this thesis we investigate the holographic dual description of correlation functions of heavy operators in conformal field theory. These heavy operators have scaling dimension that scales with the CFT central charge in the large central charge limit, and they are dual to objects propagating through the bulk whose gravitational backreaction cannot be neglected. We reproduce the expected CFT correlation functions through a gravitational path integral calculation–one that requires the introduction of special terms associated to the horizons of black holes appearing in the gravitational configurations. The results for two point functions apply in arbitrary dimensions. We also discuss heavy-heavy-light-light correlation functions in various dimensions. We find results for the three point functions in two-dimensional CFT that are consistent with the expected universal behavior of heavy operator structure constants. This is consistent with the interpretation of three-dimensional Einstein gravity as the holographic dual to an ensemble of CFT_2's.

Acknowledgments

During the course of my doctoral studies, I have become indebted to a great number of people. It is a privilege to have an opportunity now to thank some of them. First, I'd like to thank my supervisors Davide Gaiotto, Jaume Gomis, and especially Pedro Vieira. Their guidance has led me to grow as a scientist and as a person more than I would have thought possible. The many adventures of my time as a graduate student have been a gift that I will never forget.

I'd like to thank my collaborators Francesco Aprile and Rob Myers, without whom this thesis wouldn't exist.

I'd like to thank Jeevan Chandra, Gabriele Di Ubaldo, Yikun Jiang, Beatrix Mühlmann, and Joshua Sandor for enjoyable and helpful conversations.

I'd also like to thank my peers at Perimeter Institute for making my time here so special. In particular, I'd like to acknowledge the stimulating, enlightening, and entertaining conversations I've had with Jacob Barnett, Dawit Belayneh, Carlos Bercini, Kasia Budzik, Juan Cayuso, Ramiro Cayuso, Nicolas Cresto, Guillaume Dideron, Batia Friedman-Shaw, Nikita Grygoryev, Alexendre Homrich, Eivind Jorstad, Ji Hoon Lee, Amalia Madden, Harish Murali, Ali SaraerToosi, Mykola Semenyakin, and Vasudev Shyam.

Most of all, I'd like to thank Justin Kulp and Adrián Lopez Raven for making my time at Perimeter much more enjoyable.

I'd like to thank my brother Matthew, my parents, and my grandparents for encouraging me to pursue my academic ambitions, but especially for reminding me to put my well-being first.

Above all, I owe any success I have reached to Cassandra Alvarado. Without her love and support, I wouldn't be the person I am today.

Table of Contents

List of Figures

Chapter 1

Introduction

1.1 The AdS/CFT Correspondence

Perhaps the largest gap in our understanding of fundamental physics pertains to the reconciliation of quantum mechanics with the gravitational dynamics of general relativity. Attempting to treat gravity as just another quantum field theory may seem natural. However, due to the non-renormalizability of the observed gravitational interactions, this most straightforward approach to quantizing gravity fails beyond the low-energy regime. Many proposals have been made for how this problem might be resolved. The most promising candidate at the moment was discovered through careful study of the dynamics of relativistic strings.

Once quantized, the spectrum of relativistic strings was universally found to contain massless spin-2 particles. The behavior of these particles is guaranteed on general grounds to match that of a graviton. Beyond this, the consistency conditions for the propagation of quantum strings were found to imply that the spacetime on which they propagate satisfy the equations of motion of general relativity (or extensions thereof). Crucially, the behavior of quantum strings at high energy is much better than that of particles. It is believed that string theory is well-defined in the UV. Thus, it was found that string theory was really a theory of quantum gravity.

With these insights in hand, the non-perturbative aspects of string theory became a subject of great interest. Many interesting discoveries were made, including the existence of branes and the conjectured unification of all known consistent theories of strings. For the purposes of this thesis, the most important discovery was that of the AdS/CFT correspondence. The correspondence is a conjectured equivalence between the physics of quantum gravity in Anti-de Sitter (AdS) space with that of a conformal field theory (CFT) defined on the conformal boundary of AdS. The correspondence was originally discovered through explicit constructions in string theory [3]. It has since grown into a general proposal based on fundamental principles of gravity in AdS.

The AdS/CFT correspondence offers a window into both quantum gravity *and* the dynamics of strongly coupled conformal field theory. This is because it is a "weak/strong" duality. The weakly coupled regime of gravity in AdS is equivalent to the strongly coupled

regime of conformal field theory, and vice versa. So, when one theory is intractable due to it being strongly coupled, it is nevertheless possible to make statements about its behavior by leveraging the dual, weakly-coupled description. Thus, a better understanding of AdS/CFT promises to reveal insights into the structure of both strongly-coupled quantum field theory and quantum gravity.

1.1.1 CFT Correlation Functions and Holography

The basic observables in any quantum field theory are the correlation functions. By definition, every quantum field theory contains an algebra of local observables, and the correlation functions capture the expectation value of elements of this algebra in the vacuum state. These correlation functions can be packaged into generating function, the partition function with sources.

The AdS/CFT correspondence implies a large dictionary of equivalences between gravitational and conformal field theoretic observables. One family of such equivalences is the relationship between conformal field theory correlation functions and quantum gravitational scattering amplitudes in AdS. This relationship can be summarized as

$$\mathcal{Z}_{\text{AdS}}(\mathcal{J}) = \mathcal{Z}_{\text{CFT}}(J) \tag{1.1.0}$$

where $\mathcal{Z}_{\text{AdS}}$ is the partition function of quantum gravity on AdS, with boundary conditions specified as $\mathcal{J}$, and $\mathcal{Z}_{\text{CFT}}$ is the partition function of the dual conformal field theory in the presence of sources J. These act as generating functions for AdS scattering amplitudes and CFT correlation functions respectively. The exact relationship between the boundary conditions, $\mathcal{J}$, of the quantum gravitational theory and the sources, J, of the conformal field theory is not known in general. In fact, the left hand side of equation (1.1.1) isn't even defined in general. However, it is understood for some special cases. For example, the large central charge limit of the CFT corresponds to the semiclassical regime of the gravitational theory. In this regime, each field in the bulk effective field theory should correspond to an operator in the boundary CFT, see *e.g.* [4].

In this thesis, we will be concerned with a version of equation (1.1.1) that is less well understood. Namely, when the CFT operators involved have very large scaling dimension. These are what we call "heavy" operators, and by "very large" scaling dimension, we mean dimensions that scale with the central charge of the theory, in the large central charge limit. In this limit, heavy operator insertions correspond to heavy objects propagating through the bulk. Depending on how heavy the operators are, they could correspond to different types of objects. They could be heavy particles, strings, branes, or even black holes. The key results of this thesis will be how to properly treat the gravitational path integral involving such objects in order to reproduce the corresponding CFT correlation functions.

1.2 Wormholes and Ensemble Averages in Holography

The role of wormholes in the gravitational path integral has long been a topic of interest. In the 1980's it was understood by that the inclusion of small wormholes had the effect of introducing random couplings to the low energy effective field theory. It was difficult to make any assertions about whether such wormholes should be included, since a guiding principle for quantum gravity wasn't known which could resolve this question. The question was significantly sharpened once AdS/CFT came onto the scene. With the duality in hand, we can make non-perturbative predictions about how quantum gravity should behave in AdS, and compare this with predictions with and without wormholes.

1.2.1 Wormholes and Factorization

The inclusion of wormholes in the gravitational path integral seems to conflict with the basic structure of holography. To see this, consider the effect of including a wormhole contribution in the calculation of $\mathcal{Z}_{\text{AdS}}(\mathcal{M}_1 \sqcup \mathcal{M}_2)$–that is, the partition function of quantum gravity with two asymptotically AdS boundaries, with topologies and conformal metrics specified by $\mathcal{M}_1$ and $\mathcal{M}_2$. According to the holographic principle, we should have

$$\mathcal{Z}_{\text{AdS}}(\mathcal{M}_1 \sqcup \mathcal{M}_2) = \mathcal{Z}_{\text{AdS}}(\mathcal{M}_1) \cdot \mathcal{Z}_{\text{AdS}}(\mathcal{M}_2) \tag{1.2.0}$$

since $\mathcal{Z}_{\text{AdS}}(\mathcal{M}_1 \sqcup \mathcal{M}_2)$ should be equal to the partition function of the dual CFT on $\mathcal{M}_1 \sqcup \mathcal{M}_2$, which is equal to the product of the CFT partition function on $\mathcal{M}_1$ and the CFT partition function on $\mathcal{M}_2$. This property is known as "factorization" of the partition function. The inclusion of wormhole contributions in the gravitational path integral can cause this property to fail. This is due to the presence of wormholes that connect the two asymptotic regions. These contributions are completely absent in the calculation of the single-sided partition functions, $\mathcal{Z}(\mathcal{M}_1)$ and $\mathcal{Z}(\mathcal{M}_2)$, so they cause equation (1.2.1) to fail.

There are many conceivable solutions to this apparent paradox. The most immediate is to simply declare the non-inclusion of wormholes in the gravitational path integral. To be consistent one would likely need to forbid most topologies from contributing to the gravitational path integral, not only the problematic wormholes that connect different asymptotic regions. Even with that in mind, it seems difficult to reconcile a condition of this sort with locality.

Another resolution, advocated in [5], is that wormhole solutions simply do not exist in the relevant theories of gravity with boundary conditions relevant to holography. There are, however, examples of theories that seem otherwise well-defined, that *do* feature such solutions. Two key examples are dilaton gravity in 2d and pure Einstein gravity in 3d, the latter of which is the focus of chapter 3.

Finally, one could imagine that wormhole contributions are present, but that in fully-fledged, UV complete theories of quantum gravity, the resulting non-factorization is cancelled out by additional contributions to the partition function. In that case, the non-factorization would be an artifact of the semi-classical nature of the gravitational path integral. Such a scenario has been explored in, e.g. [6].

1.2.2 Ensembles in Holography

Having given several avenues to escape the problem of wormholes, we now turn to the alternative option. What if wormholes and non-factorization really are features of some theories? Can this be reconciled in some way with the principle of holography, albeit in a modified form? Amazingly, the answer is yes.

In the seminal work of [7], a new type of holographic duality was proposed. This is a duality between quantum gravity–specifically two-dimensional JT gravity–and, rather than a specific boundary theory, an ensemble of quantum mechanical systems. JT gravity is a specific theory of dilaton gravity in two dimensions. In Euclidean signature, it has action

$$S_{\rm JT} = -\frac{S_0}{2\pi}\left(\frac{1}{2}\int_{\mathcal{M}}\sqrt{g}R + \int_{\partial\mathcal{M}}\sqrt{h}K\right) - \left(\frac{1}{2}\int_{\mathcal{M}}\sqrt{g}\phi(R+2) + \int_{\partial\mathcal{M}}\sqrt{h}\phi(K-1)\right) \quad (1.2.0)$$

The partition function of JT gravity with n asymptotic boundaries, including wormhole contributions, was found to be equal to the ensemble average of the product of n quantum-mechanical partition functions.

$$\mathcal{Z}_{\rm JT}(\beta_1,\ldots,\beta_n) = \int d\mu \mathrm{Tr}\left(e^{-\beta_1 H}\right)\cdots\mathrm{Tr}\left(e^{-\beta_n H}\right) \quad (1.2.0)$$

where β_i/ϵ is the regularized length of the ith boundary, and $d\mu$ is a specific measure on the space of Hermitian operators ("Hamiltonians") H. The wormhole contributions now have a clear meaning as moments of the quantum mechanical observables over the ensemble. For example, the two boundary wormhole contribution is

$$\mathcal{Z}_{\rm JT}(\beta_1,\beta_2) - \mathcal{Z}_{\rm JT}(\beta_1)\mathcal{Z}_{\rm JT}(\beta_2) = \mathrm{Cov}_\mu\left(\mathrm{Tr}\left(e^{-\beta_1 H}\right), \mathrm{Tr}\left(e^{-\beta_2 H}\right)\right), \quad (1.2.0)$$

the covariance of the quantum mechanical partition function at inverse temperatures β_1 and β_2 over the ensemble.

This duality is wonderful because it means that while dilaton gravity is not able to reproduce the behavior of a particular unitary quantum mechanical model, it can reproduce the universal–or more precisely, the self-averaging–properties of such models.

A similar duality exists also in higher dimensions. Namely, the duality between "Narain CFT's"–*i.e.* two-dimensional CFT's with $U(1)^c \times U(1)^c$ symmetry–and a somewhat exotic Chern-Simons theory [8, 9]. The partition function of a Narain CFT on a particular two-manifold, $\mathcal{B}$, averaged over the moduli space of Narain CFT's, is equal to the Chern-Simons partition function, summed over handlebodies that "fill in" $\mathcal{B}$,

$$\int d\mu\ \mathcal{Z}_{\mathrm{CFT}_2}(\mathcal{B};\mu) = \sum_{\mathcal{M}\ |\ \partial\mathcal{M}=\mathcal{B}} \mathcal{Z}_{\rm CS}(\mathcal{M}). \quad (1.2.0)$$

This duality also includes "wormholes" in the bulk, in that one needs to sum the Chern-Simons theory calculations over background manifolds in order to match with the corresponding ensemble calculations. If the boundary is disconnected, one will need to include bulk manifolds that connect different boundary components in the sum. However, the bulk theory is very exotic. Is there a similar duality involving boundary theories with less symmetry? One that involves a much simpler gravitational theory?

1.3 Quantum Gravity in AdS_3

Chapter 3 will focus on gravity in three spacetime dimensions. This is a setting in which quantum gravity is a bit more tame, due to the lack of propagating gravitons. A question which has been the center of a lot of research is: what are the limits of the space of quantum gravitational theories in AdS_3? In view of the AdS/CFT correspondence, this can be seen as a question about the space of two-dimensional conformal field theories. For example, what is the largest possible gap between the scaling dimension of the vacuum and the next smallest scaling dimension?

An extreme version of this question is: does pure three-dimensional Einstein gravity exist as a quantum theory? This would be a theory whose lightest state above the vacuum is a black hole. This question was addressed in [10]. Therein, it was found that when computed as an expansion around classical saddlepoints, the partition function of pure gravity in AdS_3 is given by

$$\mathcal{Z}_{\text{MWK}}(\tau,\bar{\tau}) = \sum_{\gamma\in\Gamma_0} \chi_{\text{vac}}(\gamma\cdot\tau)\bar{\chi}_{\text{vac}}(\gamma\cdot\bar{\tau}) \tag{1.3.0}$$

where

$$\chi_{\text{vac}}(\tau) = \frac{e^{-2\pi i\tau\frac{c-1}{24}}}{\eta(\tau)}(1-e^{2\pi i\tau}) \tag{1.3.0}$$

is the vacuum Virasoro character, $\eta(\tau)$ is the Dedekind η function, and $\gamma \in \text{SL}_2\mathbb{Z}$ is an element of the modular group. The group Γ_0 is the subgroup of $\text{SL}_2\mathbb{Z}$ that acts non-trivially on the vacuum character.

This result turns out to be inconsistent with the idea that pure gravity might have a dual CFT description. This is because if one extracts the density of states, $\rho(h,\bar{h})$, using

$$\mathcal{Z}_{\text{MWK}}(\tau,\bar{\tau}) = \int dh d\bar{h}\ \rho(h,\bar{h}) e^{2\pi i\tau\left(h-\frac{c}{24}\right)-2\pi i\bar{\tau}\left(\bar{h}-\frac{\bar{c}}{24}\right)}, \tag{1.3.0}$$

one finds that the density of states is neither discrete nor positive. On the other hand, any compact, unitary CFT has a discrete, positive density of states, with a positive integer number of states at each h, $\bar{h}$.

There have since been many proposals for how to solve this problem. These generally involve adding new contributions to the calculation of [10], which cure some of the problems with the density of states. While some progress has been made curing the negativity problems presented by (1.3), the non-discreteness of the density of states remains a problem. However, with the development of the ensemble-averaged holographic dualities discussed in the previous section, the continuous density of states no longer seems as big of a concern. Perhaps the lack of a discrete spectrum is arising because the dual theory is actually an ensemble of CFT_2's, rather than a specific one!

This idea has been explored in [11]. In particular, in [11] it was found that the Einstein-Hilbert action of certain wormhole solutions in pure gravity with conical defects reproduced the universal formula for OPE coefficients of heavy operators in holographic CFT_2's. In

chapter 3, we will see how this result can be extended to the regime where black holes, rather than conical defects, propagate across a wormhole. This is an important step towards a more complete understanding of how pure gravity in three dimensions relates to universal properties of two-dimensional conformal field theories.

Chapter 2

Geometries for Correlation Functions in General Dimensions

2.1 Introduction

The holographic dual of a CFT correlation function depends qualitatively on the dimensions of the operators involved. Holographic correlators might feature the insertion of light operators dual to particles, *e.g.* Kaluza-Klein modes on AdS, and/or heavier operators. In principle, all light correlators are computed by Witten diagrams. For heavier operators, the correct picture depends on some of the details of the operator. Strings, branes or bricks of branes can all be considered emerging from the insertion points, and each category might come with decorations thereof. Holographic correlators for strings and branes receive the leading order contribution from the action associated to an extended surface in the bulk anchored at the insertion points, as is well established. But when it comes to huge operators, such as large bricks of branes, the bulk geometry itself is deformed. This is a scenario in which much less has been explored. Hence the question we would like to investigate here is: "How do we compute correlators of huge operators from the bulk?"

As a first step, in this chapter we discuss the simplest case of two-point functions for scalar operators, and the construction of the corresponding two-point function geometries. In order to explain what these are we will use the AdS-Schwarzschild black hole in D dimensions as a guiding example.[1] Of course, our main motivation here is to establish a general formalism, which can be applied to more general solutions such as those that are dual to higher point correlation functions [12].

CFT two-point functions are very simple, i.e.

$$\langle O_{\Delta_i}(\vec{x}_1)\, O_{\Delta_j}(\vec{x}_2)\rangle \simeq \frac{\delta_{ij}}{|\vec{x}_1-\vec{x}_2|^{2\Delta_i}}\,. \tag{2.1.0}$$

Our goal, however, is to recover this result from a bulk calculation that involves huge operators. The information that we need to find is the dimension Δ_i of the scalar operators, and

[1] The generalisation to include electric charge and matter will be presented elsewhere [12].

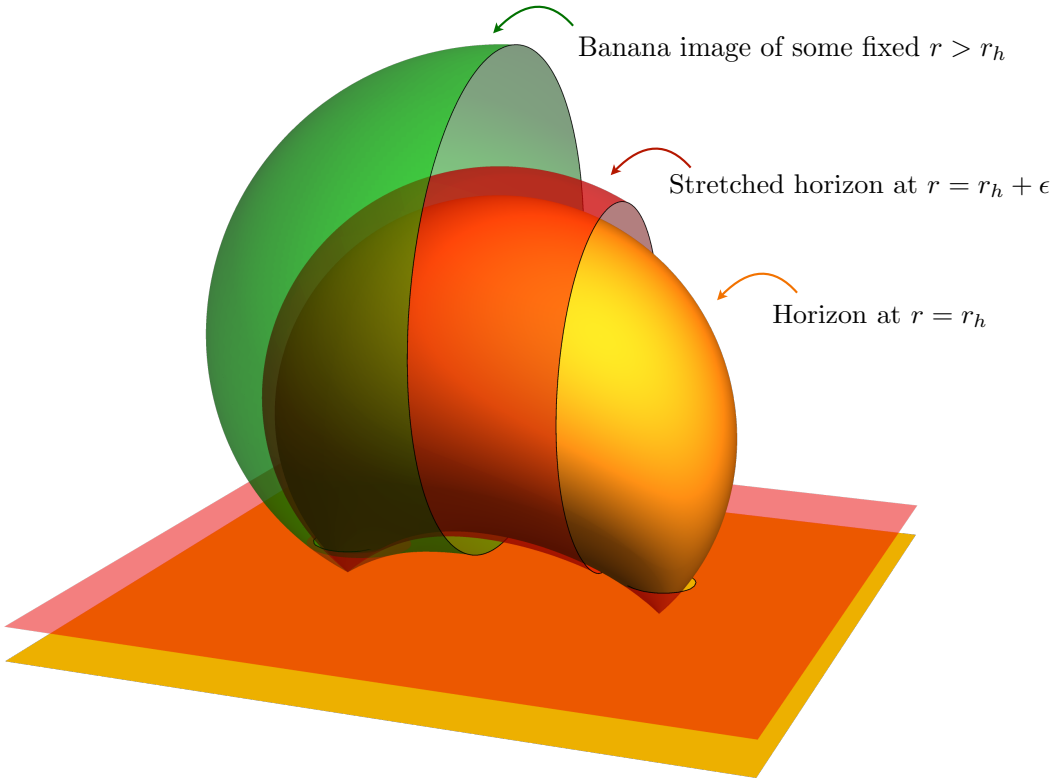

Figure 2.1: The *banana* foliation. (See also figure 2.3.)

the spacetime dependence with respect to their separation $\vec{x}_{12}$. Recall that the spectrum of dimensions of operators in a holographic CFT coincides (up to a shift by the Casimir energy) with the spectrum of energies with respect to global time τ in AdS. Therefore a way to read off Δ is to compute the energy E of the dual operator in a frame where the geometry is asymptotically $\mathbb{R} \times S^{d-1}$. This is true for any operator: light, heavy or huge. Thus in global coordinates, a two-point function geometry is an asymptotically AdS geometry with a backreacted interior which depends on the operator. Using the natural cutoff in these coordinates corresponds to placing the operators at $\tau = \pm\infty$, and one might be satisfied with this.

However, the global AdS perspective is not the end of the story. In this chapter, we will present another computation that is intrinsically Euclidean and such that the operators are inserted at the boundary of AdS in Poincaré coordinates. A similar idea was explored already in the context of classical spinning strings in global AdS in [13]. The strategy there was to embed the surface of the string into Euclidean AdS with Poincaré slices. In these coordinates, the string looks like a fattened geodesic that connects the points at the boundary, where the dual operators are inserted, and its onshell action was shown to compute the corresponding two-point function.

For two-point function geometries, the relationship between global and Poincaré coordinates is a bit more subtle. The reason is that, unlike the case of embedded objects, the metric

itself transforms in a nontrivial way. Nevertheless, we will construct a change of coordinates that maps a geometry with global asymptotics to a geometry with Poincaré asymptotics. We will call this the Global-to-Poincaré (GtP) map. The spacetime we end up with has novel features which we will describe in detail. To start with, we can picture how it looks by visualising the foliation defined by mapping surfaces of constant r in global coordinates into the Poincaré picture. This foliation is composed of "spacetime bananas" that originate from the marked points, *e.g.* see figure 2.1.

The induced metric on the spacetime bananas is what characterises the backreaction of the operators inserted. For gravitational solutions which have a smooth interior, we can follow the foliation to the point where it shrinks to the geodesic connecting the two boundary points. In a neighbourhood of that geodesic, the metric depends on the specifics of the operators inserted, and it will deviate strongly from empty AdS.

When the operator insertions have created a black hole connecting the two insertion points, we can follow the foliation in figure 2.1 only up to the innermost banana which is the GtP image of the black hole horizon at $r = r_h$. As is characteristic of a black hole horizon, the induced geometry on this innermost banana maintains a finite size in the transverse directions (i.e. the horizon area) but has zero length in the longitudinal direction (i.e. the analog of the τ direction). The latter results in a conical singularity on this surface.[2] This zero-length direction goes between the insertion points, passing through the bulk. Therefore, we have to be careful when picturing the horizon as a banana (as in figure 2.1), since the proper length along this banana actually vanishes. For the purpose of visualization, it is useful to think instead of a "stretched horizon", a banana that is some small distance outside of the horizon. This perspective is also closely related to the membrane paradigm [16], which constructs a simplified model to describe the black hole by replacing it with a physical surface (or membrane) at a vanishingly close distance from the event horizon.[3]

At this point, it may beneficial for our reader if we step back to compare our approach to more traditional calculations with Euclidean black holes. First, a comment on nomenclature is that we continue to use "horizon", an intrinsically Lorentzian concept, to refer to the innermost surface in our Euclidean geometry. This is a codimension-two surface since the length along the (Euclidean) "time" direction vanishes, as noted above. Traditionally, one makes the Euclidean time direction periodic and fixes the periodicity to maintain a smooth geometry across this surface. Of course this is the starting point in using Euclidean black hole geometries to study black hole thermodynamics, *e.g.* [17]. In our approach, we are not enforcing any periodicity for the time coordinate. In this regard, our geometries are analogous to "fixed area" states [18, 19], which have recently appeared in discussions of quantum information aspects of holography.[4] In either of these contexts, one is considering an en-

[2]Singularities appearing on a purported horizon while not common are known to arise in a variety of contexts in string theory, *e.g.* see [14, 15]. We adopt the pragmatic point of view of regarding the singularity in our solutions as harmless since they still yield a finite result for the on-shell action, as we will show below.

[3]While this approach is traditionally employed to model the dynamical behaviour of black holes in the context of Lorentzian signature, we may also employ the membrane paradigm in our Euclidean calculations here – see footnote 7.

[4]We note, however, that generally one expects fixed-area states to have a finite conical deficit at the horizon, while in our geometries, the horizon develops an infinite angular excess. That is, in keeping with

semble of high energy states in the boundary CFT while we wish to consider a single state, *i.e.* the state created by the insertion of our huge operator. The latter requires that our Euclidean action includes a boundary contribution, *i.e.* the Gibbons-Hawking-York (GHY) term [17,20], at a stretched horizon to fix the boundary conditions there – again, in contrast to the ensemble calculations.

The importance of the latter is also emphasized by the following holographic considerations: What we want for our geometry is that the onshell action computes a CFT two-point function, rather than say the Gibbs free energy at fixed temperature β^{-1}. Thus, our computation is closely related to a transition amplitude for two states separated by a Euclidean time translation, rather than a trace over an ensemble of states with a thermal circle. Schematically,

$$\langle \mathrm{BH}|e^{-H\delta\tau}|\mathrm{BH}\rangle = e^{-E\delta\tau} \qquad \text{rather than} \qquad Z = \mathrm{tr}(e^{-\beta\hat{H}}) = e^{-\beta E+S}\,. \tag{2.1.0}$$

In both cases, the right-hand side is computed by the onshell action of a gravitational background, and in the transition amplitude, we have roughly $\delta\tau \sim \log|x_{12}|^2$. But for a two-point function, there should be no entropy contribution! We will find that the GHY boundary term on the stretched horizon is crucial to remove the entropy appearing in the calculation of the thermal ensemble. This observation was made previously in [21], which discussed a Euclidean path integral derivation of the transition amplitude in eq. (2.1). Finally, let us also note that one can interpret this new boundary term as the "membrane action" [22] within the framework of the membrane paradigm.

Let us note that semiclassical gravity will not distinguish states that are very close in the spectrum of the boundary theory [23]. Therefore, we should think that our gravitational calculations yield the behaviour for generic scalar states with no charges (*i.e.* vanishing angular momenta and internal charges). However, we contrast this perspective with the recent discussions of averaging in holographic theories, *e.g.* see [11, 24]. For the present purposes, the only relevant "erratic" behaviour in the boundary theory would be in the spectrum of conformal dimensions Δ. But the form of the two-point function (2.1) is completely fixed by conformal invariance for a given Δ. Hence averaging does not play a role here – see further discussion in [12] which examines gravitational calculations of higher point functions for huge operators.

The remainder of this chapter is organised as follows: In section 2.2, we describe the salient aspects of our construction. Specifically, we introduce the GtP change of coordinates and the bananas, then we discuss a version of the onshell action computation, whose immediate aim is to highlight the emergence of nontrivial spacetime dependence, and the crucial role played by the GHY boundary term at the stretched horizon. In section 2.3, we describe further aspects of the two-point function geometry. In particular, we verify the conformal Ward identity from the holographic stress tensor, and we revisit the onshell action computation by discussing the implications of the fact that the Fefferman-Graham coordinates only extend to a finite surface in the bulk, which we call "the wall". In section 2.4, we build on the idea of the horizon as a membrane by showing that – absent fine tuning – geodesics anchored

our discussion of the conformal dimensions and global coordinates, we allow the black holes to "propagate" for an infinite amount to Euclidean time.

at the boundary always remain outside the horizon banana. Then, we compute the action of such geodesics and show in examples that at leading order in the black hole mass, the result is simply the stress tensor conformal block. Finally, we conclude with a discussion of our results and future directions in section 2.5. There, we sketch an outline of our plan to extend our calculations to three- and higher-point geometries, which we will investigate in the future [12].

2.2 The Banana Geometry

In 1916, Schwarzschild discovered the first black hole solution of Einstein gravity. Here we will give it a new outfit, and show how it looks when we think of it as a two-point function geometry. As described in the introduction, from this new point of view, the black hole will look like a spacetime banana.

2.2.1 AdS-Schwarzschild

In global coordinates, the Euclidean metric of the $D = (d+1)$-dimensional AdS-Schwarzschild black hole reads

$$ds^2_{\texttt{global}} = f(r)d\tau^2 + \frac{dr^2}{f(r)} + r^2 d\Omega^2_{d-1} \tag{2.2.0}$$

where the blackening factor is

$$f(r) = 1 + r^2 - \frac{\alpha M}{r^{d-2}}. \tag{2.2.0}$$

Here M is the black hole *mass* (= *energy*) if the parameter α takes the canonical value,

$$\alpha = \frac{16\pi G_{\rm N}}{(d-1)\Omega_{d-1}}\,, \qquad \text{where} \quad \Omega_{d-1} = \texttt{Vol(unit (d-1)-sphere)} = \frac{2\pi^{d/2}}{\Gamma(d/2)} \tag{2.2.0}$$

and $G_{\rm N}$ is Newton's constant in the $(d+1)$-dimensional bulk. In practice, we will set $\alpha = 1$ to avoid cluttering our computations, and spell it out only in the final formulae. Further, we have implicitly set the AdS curvature scale to $L_{AdS} = 1$.

The signature of the black hole can be changed from Euclidean to Lorentzian by taking $\tau = -it$. In either signature, the vector along the time direction is Killing and has norm square proportional to $f(r)$. This norm vanishes at the real value of $r = r_h$ where $f(r_h) = 0$, *i.e.* the Killing vector becomes null in Lorentzian signature and vanishes in Euclidean signature. This value, $r = r_h$, sets the location of the horizon, and it depends on M. Very light black holes with $M \ll 1$ have a very small horizon radius r_h, i.e. they are effectively small excitations in the middle of AdS. Very heavy black holes with $M \gg 1$ have a horizon radius scaling with $M^{1/d}$ and thus occupy most of the AdS spacetime.

Of course, in Lorentzian signature, the horizon $r = r_h$ is the locus where light accumulates from the point of view of an observer at infinity. Free falling observers nevertheless cross the horizon in a finite proper time. On the other hand, as discussed in the introduction,

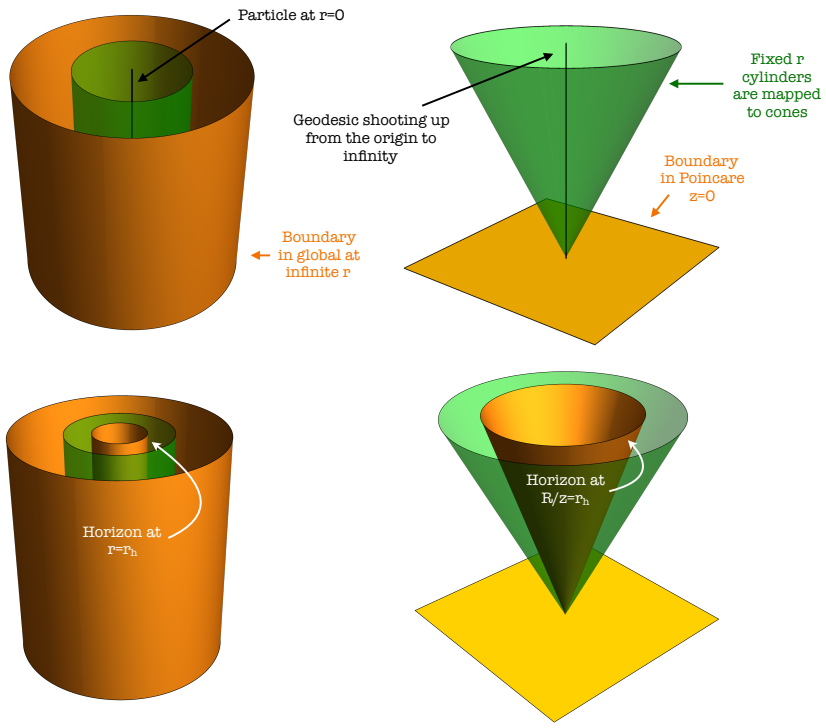

Figure 2.2: Global (**Left**) and Poincaré (**Right**) are related by the map in eq. (2.2.1). The trajectory of a particle at rest in the middle of global AdS is mapped to a geodesic shooting from the origin to infinity in Poincaré AdS, and the $\mathbb{R} \times S^{d-1}$ boundary at $r = \infty$ is mapped to the Poincaré boundary at $\tilde{z} = 0$. Cylinders of varying r that interpolate between the center and the boundary of global AdS correspond to cones in Poincaré coordinates. For black holes, there is an horizon at $r = r_h$ which corresponds to a minimal cone at $R/\tilde{z} = r_h$.

in Euclidean signature, the spacetime ends at the horizon $r = r_h$. There will be a conical singularity at the horizon unless Euclidean time is compactified to a circle, $\tau \sim \tau + \beta$, where the periodicity is given by the inverse Hawking temperature

$$T_{\text{H}} \equiv \beta^{-1} = \frac{f'(r_h)}{4\pi} \,. \tag{2.2.0}$$

Then, the (τ, r) geometry is that of a "cigar" ending at $r = r_h$ (see [25] for a nice review). The horizon area is $A = r_h^{d-1}\Omega_{d-1}$, and it determines the black hole entropy $S = A/4G_{\text{N}}$ in the thermodynamic interpretation of the black hole [17].

What we want for a Euclidean two-point function geometry is a black hole connecting the insertion points at the boundary of AdS in Poincaré coordinates. This picture would match with what we expect for very light black holes behaving as structureless point particles travelling through the AdS vacuum. In that case, the two-point function would be computed by a geodesics anchored at the insertion points.

To match with our expectation, we look for a change of coordinates such that the center

of global AdS, namely $r = 0$ and $-\infty \leq \tau \leq \infty$, is mapped precisely to that geodesic in Poincaré AdS anchored at the insertion points of the two-point function. Further, we require that the $\mathbb{R} \times S^{d-1}$ boundary of global AdS is conformally mapped to the $\mathbb{R}^d$ boundary of Poincaré AdS. With the insertion points at 0 and ∞, we can use $SO(d-1)$ invariance to restrict ourselves to $\tau = \tau(z, R)$ and $r = r(z, R)$ where R is the radial coordinate in the Poincaré boundary. Then, the two conditions above are enough to suggest the change of variables[5]

$$\tau = \frac{1}{2}\log(\tilde{z}^2 + R^2) \qquad ; \qquad r = \frac{R}{\tilde{z}}\,. \tag{2.2.0}$$

Under this map, cylinders of constant radius in global coordinates are mapped to cones in Poincaré coordinates, and translations in global time are mapped to dilations preserving these cones – see Figure 2.2. We call this map the Global to Poincaré (GtP) map.

After the GtP mapping (2.2.1), the black hole metric takes the form

$$ds^2_{cone} = \frac{1}{\tilde{z}^2}\left[\frac{d\tilde{z}^2}{h(\frac{R}{\tilde{z}})} + h(\tfrac{R}{\tilde{z}})\left(dR + \tfrac{R}{\tilde{z}}\,v(\tfrac{R}{\tilde{z}})d\tilde{z}\right)^2 + R^2 d\Omega^2_{d-1}\right], \tag{2.2.0}$$

where

$$h(r) = \frac{1}{f(r)} + \frac{r^2 f(r)}{(1+r^2)^2} \qquad \text{and} \qquad v(r) = \frac{1}{f(r)h(r)}\left[\frac{f(r)^2}{(1+r^2)^2} - 1\right]. \tag{2.2.0}$$

With $M = 0$, we have $f = 1 + r^2$. As a result, one finds $h = 1$ and $v = 0$, and the above metric (2.2.1) reduces to exactly Poincaré AdS.

Finally, we can bring the insertion point at ∞ to a finite distance by a change of coordinates that acts as a special conformal transformation (SCT) on the boundary. Upon introducing Cartesian coordinates $\tilde{x}^i$ to replace the polar coordinates R, Ω_i on the boundary, desired change of coordinates in the bulk is

$$\begin{aligned} \tilde{x}^i \quad &\to x^i = \frac{\tilde{x}^i - b^i\,(\tilde{x}^2 + \tilde{z}^2)}{\widetilde{\Theta}^2} \\ \tilde{z} \quad &\to z = \frac{\tilde{z}}{\widetilde{\Theta}^2} \end{aligned} \qquad \text{with} \quad \widetilde{\Theta}^2 = 1 - 2\,b\cdot\tilde{x} + b^2(\tilde{x}^2 + \tilde{z}^2)\,. \tag{2.2.0}$$

We call the above transformation the SCT mapping. It is useful to recall that the inverse of the SCT mapping with shift parameter b^i is simply another SCT map with shift $-b^i$.

We denote the points at which the operators are inserted as $\vec{x}_{\bullet 1} = 0$ and $\vec{x}_{\bullet 2} = -\frac{b^i}{b^2}$. Without loss of generality, we can choose $\vec{x}_{\bullet 1} - \vec{x}_{\bullet 2}$ to lie along the x^1-axis, *i.e.* $b^i = b\,\delta^{i1}$. Then the geometry maintains a rotational $SO(d-2)$ symmetry in the remaining Cartesian directions. If we denote the radius in these transverse directions as $\rho = (\sum_{i=2}^{d}(x^i)^2)^{1/2}$, then the metric takes the form

$$ds^2_{banana} = N_z^2\,dz^2 + \sum_{a,b=x^1,\,\rho} h_{ab}(dy^a + N_z^a\,dz)(dy^b + N_z^b\,dz) + \frac{\rho^2\,d\Omega^2_{d-2}}{z^2} \tag{2.2.0}$$

[5]It is also possible to deduce this transformation by generalising the argument of [13], in particular, by passing from (τ, r) coordinates to embedding coordinates, and from embedding coordinates to $(\tilde{z}, R)$ in the Poincaré patch. We give the details in appendix A.1.

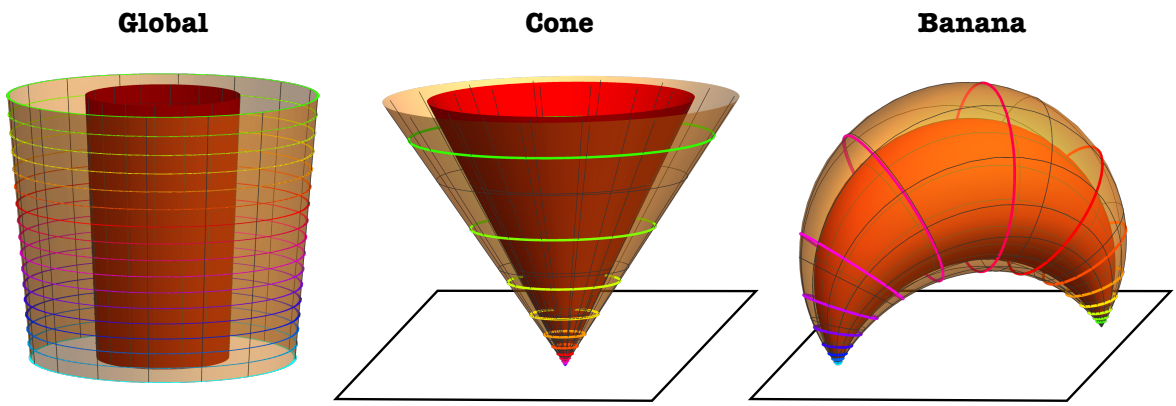

Figure 2.3: Black hole in global AdS (left), as a cone (middle) and a banana (right). The red corresponds to the horizon at $r = r_h$, while the semi-transparent surface corresponds to some constant r surface with $r > r_h$. There is a conical singularity at the horizon, since we did not make τ periodic.

The explicit form of the components is not very illuminating, and hence we omit them here. Of course, the symmetry is enhanced to $SO(d-1)$ with $b \to 0$, since the cone metric (2.2.1) is recovered in this limit.

In figure 2.3, we illustrate the various coordinate transformations. Upon performing the SCT map, the foliation by cones (with $b = 0$) becomes a foliation by bananas (with $b \neq 0$). More precisely, each constant r cylinder in global coordinates is mapped to the banana

$$r^2 = \Theta^2 \left(\frac{x^2}{z^2} + 1 \right) - 1 \qquad \text{with} \quad \Theta^2 = 1 + 2\, b \cdot x + b^2 (x^2 + z^2) \tag{2.2.0}$$

Solving this equation for z gives two positive components $z_\pm(r) \geq 0$, distinguished by the sign of a square root – see figure 2.4 and also eq. (2.2.2). The z_- component has the shape of a pair of pants, while the z_+ component is a cap. In the limit $b \to 0$, the former transitions to the cone surfaces and z_+ goes off to infinity.

Of course, the induced metric on each banana is the same as that of a surface of constant r in global coordinates, even if the metric looks initially more complicated. For example, restricting to a cone $\tilde{z} = \frac{R}{r}$ with a fixed value $r \in \mathbb{R}$ in eq. (2.2.1), a direct computation yields

$$ds^2_{\text{cone}}\big|_{\tilde{z}=\frac{R}{r}} = f(r)\, \frac{dR^2}{R^2} + r^2 d\Omega^2_{d-1}\,. \tag{2.2.0}$$

Further, eq. (2.2.1) yields $\frac{dR}{R} = d\tau$ with fixed r, and hence eq. (2.2.1) reduces to precisely the same induced metric as in global coordinates (2.2.1) with fixed r.

Although the induced metric on the bananas is the same as in global coordinates, the main purpose of the GtP map is to give us a Poincaré boundary, which allows us to study the backreaction of the operators along slices of constant z, *i.e.* the bulk evolution picture.

The surface $z = \epsilon$ is also a simple cut-off surface[6] for computing the onshell action, which is ultimately what we want to compute to match with a CFT two-point function. The main novelty here is that the $z = \epsilon$ surface contains points which are both far and close to the operator insertions, *i.e.* far and close to the black hole horizon. Thus the pre-image of $z = \epsilon$ in global coordinates is a surface that explores the space from near the asymptotic boundary to deep into the bulk, and therefore the corresponding boundary conditions probes properties of the geometry that are usually viewed as distinct, *i.e.* near infinity and in the interior. While this distinction will be formalised in section 2.3 where we discuss the Fefferman-Graham patch, we first need to understand how to deal with the horizon.

As mentioned in the introduction, traditionally Euclidean black holes appear as the bulk saddle point describing an ensemble of high energy states in the boundary CFT. In contrast, we wish to consider a single unique state, *i.e.* the state created by the insertion of our huge operator. For this purpose, we introduce a stretched horizon at $r = r_h(1 + \epsilon')$. away from the horizon. Then to fix the boundary conditions at the horizon, we introduce Gibbons-Hawking-York (GHY) term [17, 20] on the stretched horizon and then take the limit $\epsilon' \to 0$.[7]

In sum, the total onshell action for our two-point function black hole is

$$I_{\boxed{\bullet\bullet}} = I_{bulk} \; + \; I_{boundary} \; + \; I_{ct} \tag{2.2.0}$$

where the first term is the Einstein-Hilbert bulk action (with a negative cosmological constant). The boundary action is comprised of two GHY terms, one on the asymptotic boundary and the other on the stretched horizon, *i.e.*

$$I_{boundary} = I_{GHY}(\partial_{AdS}) + I_{GHY}(\text{stretch})\,. \tag{2.2.0}$$

Finally, there are the boundary counterterms I_{ct} which are evaluated on the asymptotic boundary, *e.g.* see [26–31]. In the next section, we discuss the precise definition of all of these terms I_{bulk}, $I_{boundary}$ and I_{ct}, and further we will compute their values.

2.2.2 CFT two-point function from gravity: the onshell action

The goal of this section is to evaluate the gravitational action $I_{\boxed{\bullet\bullet}}$ for the banana geometry and show that it reproduces a scalar two-point CFT correlator. Of course, given eq. (2.1), we know what to expect:

$$I_{\boxed{\bullet\bullet}} = \Delta \, \log|\vec{x}_{\bullet 1} - \vec{x}_{\bullet 2}|^2 \; + \; \texttt{distance-independent constant} \tag{2.2.0}$$

so that

$$\langle O(\vec{x}_{\bullet 1}) O(\vec{x}_{\bullet 2})\rangle = e^{-I_{\boxed{\bullet\bullet}}} \simeq \frac{1}{|\vec{x}_{\bullet 1} - \vec{x}_{\bullet 2}|^{2\Delta}}\,. \tag{2.2.0}$$

[6] This is a slightly unconventional choice here since the metric (2.2.1) is not in the standard Fefferman-Graham gauge – see eq. (2.3) below.

[7] As noted above, we might alternatively consider our calculation within the framework of the membrane paradigm [16], where the stretched horizon corresponds to a physical membrane. In order to describe this membrane, one needs introduce an action as described in [22]. The interested reader is referred there for its derivation but here, we simply note that onshell, this membrane action reduces to a GHY term.

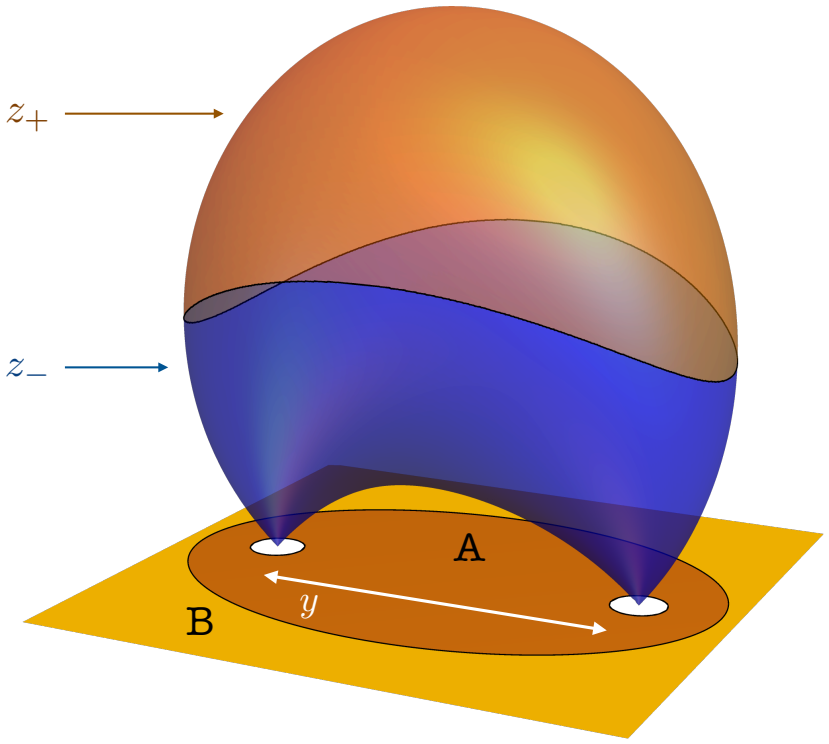

Figure 2.4: The two solutions $z_\pm$ of the banana equation (2.2.1). We denote the (boundary) distance between the insertion points as $|\vec{x}_{\bullet 1} - \vec{x}_{\bullet 2}| = y = \frac{1}{b}$. The z_- component has the shape of a pair of pants, while z_+ is a cap. For $r = r_h$, we denote the inside and outside of the ellipse below the stretched horizon as A and B, respectively.

We will focus first on reproducing the spacetime dependence as function of Δ. We will also comment on the overall normalisation, which was omitted in eq. (2.2.2).

As pointed out already in (2.2.1), there are three contributions to the total action, which come from: *bulk*, *boundaries* and *counterterms*,

$$I_{\boxed{\bullet\bullet}} = I_{bulk} \ + I_{GHY}(\partial_{AdS}) + I_{GHY}(\text{stretch}) + \ I_{ct} \tag{2.2.0}$$

We will analyse each of them in turn.

The bulk action

The Einstein-Hilbert action is

$$I_{bulk} = -\frac{1}{16\pi G_{\rm N}} \int d^d x\, dz\, \sqrt{g} \left(R + \frac{d(d-1)}{L^2_{AdS}} \right) . \tag{2.2.0}$$

Here and below, we are implicitly working with the metric (2.2.1) using the coordinates introduced by the SCT mapping (2.2.1). Then upon using the Einstein equations[8] and

[8]We use $R_{\mu\nu} = -d\, g_{\mu\nu}$ after setting $L_{AdS} = 1$. Further, with the coordinates introduced by the SCT map (2.2.1), we have $\sqrt{g}\, dz\, d^d x = \frac{1}{z^{d+1}}\, dz\, d^d x$, just as in empty AdS.

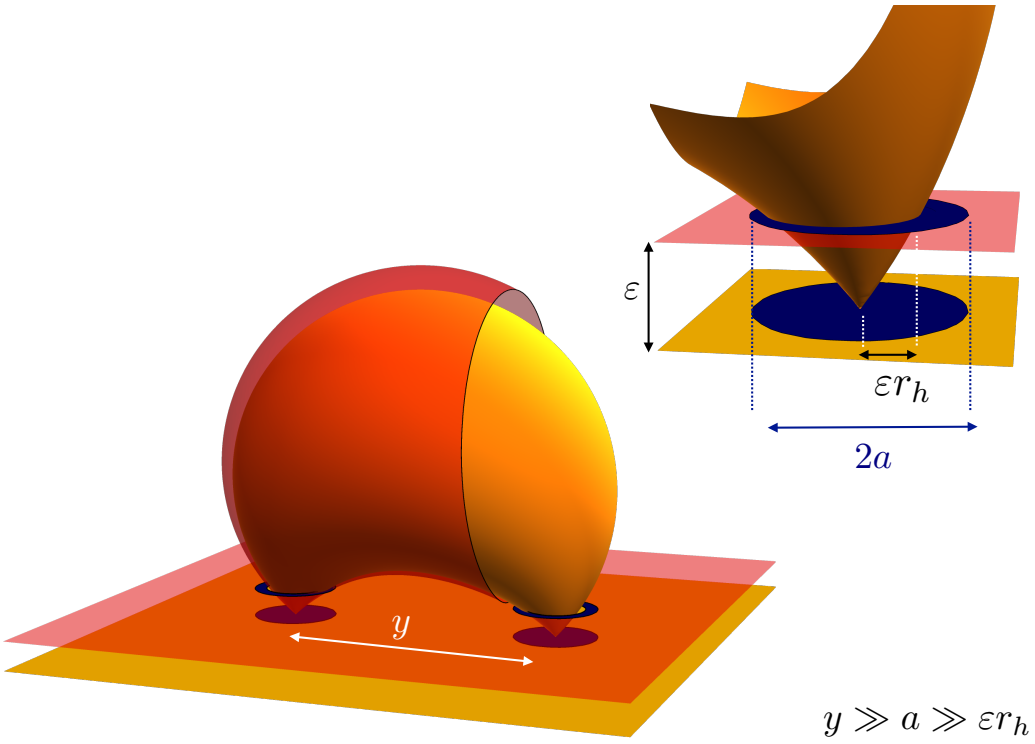

Figure 2.5: To regulate the onshell action, we introduce a cut-off surface at $z = \epsilon$ near the asymptotic boundary and a stretched horizon at $r = r_h(1 + \epsilon')$. These two surfaces intersect and effectively excise a disk of radius $r_h\epsilon$ to leading order in ϵ, close to the insertion points. To compute the boundary integrals, we will excise a larger disk of radius a, much smaller than the separation between the insertions $y = \frac{1}{b}$, but much larger than ϵr_h. We will show that this scheme reproduces the expected spacetime dependence $y^{-2\Delta}$ of a two-point function, up to a distance-independent constant. .

carrying out the dz integration for $z \geq \epsilon$, we find

$$I_{bulk} = \frac{1}{8\pi G_{\rm N}} \int_A d^d x \left[\frac{1}{z_+(r_h)^d} - \frac{1}{z_-(r_h)^d} \right] + \frac{1}{8\pi G_{\rm N}} \int_{A\cup B} d^d x \, \frac{1}{\epsilon^d} \tag{2.2.0}$$

where the domain of integration A is the ellipse given by projecting the banana describing the horizon into the boundary coordinates – see figure 2.4 and eq. (2.2.2). B is the domain outside this ellipse and hence, the second term, which is the usual divergence of the AdS volume, is integrated over the entire AdS boundary.

The first term consists of the boundary contributions coming from where the z integration reaches the banana at the (stretched) horizon,[9] and $z_\pm(r_h)$ are the two components of this

[9]Here and for some quantities below, the distinction between horizon and stretched horizon does not matter. That is, we do not encounter any divergences if we evaluate these quantities on the stretched horizon and take then the limit $\epsilon' \to 0$. Hence we can evaluate them directly at $r = r_h$.

banana described below eq. (2.2.1). Substituting $r = r_h$ into eq. (2.2.1), we find

$$z_{\pm}(r_h) = \left[\frac{r_h^2}{2b^2} - x^1 \left(x^1 + \frac{1}{b}\right) - \rho^2 \pm \frac{r_h}{b} \sqrt{\frac{r_h^2}{4b^2} - x^1 \left(x^1 + \frac{1}{b}\right) - \rho^2 \left(1 + \frac{1}{r_h^2}\right)} \right]^{\frac{1}{2}}, \tag{2.2.0}$$

as depicted in figure 2.4. The ellipse dividing the domains A and B corresponds to the vanishing locus of the square root in the above expression. Hence A is given by the inequality,[10]

$$x^1 \left(x^1 + \frac{1}{b}\right) + \rho^2 \left(1 + \frac{1}{r_h^2}\right) \leq \frac{r_h^2}{4b^2} \tag{2.2.0}$$

where as discussed below eq. (2.2.1), we have placed the two insertion points on the x^1-axis at $x^1 = 0$ and $-1/b$.

The bulk construction with the stretched horizon implies that we should also excise a small disk around each insertion point from the inner domain A for the term involving $z_-(r_h)$ – see figure 2.5. As we shall see, this feature of the computation is precisely the reason why the first contribution in eq. (2.2.2) is nonstandard and interesting to evaluate.

Let us examine how the z_- component reaches the insertion points, by zooming there with a small δ expansion, $(x^1, \rho) \to \delta\,(x^1, \rho)$ and $(x^1, \rho) \to (-\frac{1}{b}, 0) + \delta\,(x^1, \rho)$. We find

$$\frac{1}{z_-(r_h)^d} = r_h^d \underbrace{\frac{1}{((x^1)^2 + \rho^2)^{d/2}\,((1 + bx^1)^2 + b^2\rho^2)^{d/2}}}_{f_{2pt}} + \mathcal{D}(x_1, x_2, r_h; b) \tag{2.2.0}$$

where the difference function $\mathcal{D}$ vanishes when $b = 0$. The first term in its most general form is given by

$$f_{2pt} = \frac{|\vec{x}_{\bullet 1} - \vec{x}_{\bullet 2}|^d}{|\vec{x} - \vec{x}_{\bullet 1}|^d\,|\vec{x} - \vec{x}_{\bullet 2}|^d}. \tag{2.2.0}$$

i.e. a simple function of distances. The integral of f_{2pt} in A diverges logarithmically,[11] while instead the reminder $\mathcal{D}$ is integrable in A. On the other hand, f_{2pt} is integrable at infinity, and thus in B. Therefore, by adding and subtracting f_{2pt} in B, we can write the bulk action as

$$I_{bulk} = \frac{1}{8\pi G_{\rm N}} \int_{A\cup B} d^d x \left[\frac{1}{\epsilon^d} - r_h^d\, f_{2pt}(x) \right] + \mathcal{N}_{bulk}$$

where we defined the constant

$$\mathcal{N}_{bulk} = \frac{1}{8\pi G_{\rm N}} \int_B d^d x\; r_h^d\, f_{2pt} + \frac{1}{8\pi G_{\rm N}} \int_A d^d x \left[\frac{1}{z_+(r_h)^d} - \mathcal{D} \right]. \tag{2.2.0}$$

We emphasize that $\mathcal{N}_{bulk}$ is a constant independent of the seperation $|\vec{x}_{\bullet 1} - \vec{x}_{\bullet 2}| = 1/b$. Indeed, if we rescale the coordinates, say $(x^1, \rho) \to (x^1/b, \rho/b)$, the dependence on the

[10] Recall that $\rho^2 = \sum_{i=2}^d (x^i)^2$.

[11] For example, in the cone coordinates (with $b = 0$), we have $\int d^d x\, f_{2pt} = \int \frac{dR}{R}\, d\Omega_{d-1}$ and the radial integral over R would yield a logarithmic divergence.

separation factors out completely from $z_\pm$ in eq. (2.2.2) and from f_{2pt} and $\mathcal{D}$ in eq. (2.2.2). Further, this overall factor cancels precisely that coming from the measure d^dx in the two integrals comprising $\mathcal{N}_{bulk}$ in eq. (2.2.2). Similarly, the b dependence also scales out of the ellipse separating A and B, *e.g.* see eq. (2.2.2). Finally, since there is no divergence in $\mathcal{D}$ near the insertion points, we can close the disks opened in A. Hence we conclude that $\mathcal{N}_{bulk}$ is completely independent of the separation between insertion points, and in fact eq. (2.2.2) yields a finite constant depending only on r_h in the $\epsilon \to 0$ limit.

The contribution coming from the first term in eq. (2.2.2) is different because f_{2pt} yields a logarithmic divergence, and so it is really crucial to excise a disk of radius a around each of the insertion points. Thus, although the dependence on $|\vec{x}_{\bullet 1} - \vec{x}_{\bullet 2}|$ can be scaled away between the integrand and the measure, as above, this rescaling changes the domain of integration. Hence the integral *does* depend on the distance.

The asymptotic boundary action

The action has two contributions on the asymptotic AdS boundary. The first is the GHY term[12]

$$I_{GHY}(\partial_{AdS}) = \frac{1}{8\pi G_{\rm N}} \int_\partial d^dx \sqrt{h}\, K_{\partial_{AdS}} \qquad \text{with} \quad K_{\partial_{AdS}} = -\nabla_\mu \frac{N_z^\mu}{|N_z|} \tag{2.2.0}$$

and the second, the counterterm action[13]

$$I_{ct} = \frac{1}{8\pi G_{\rm N}} \int_\partial d^dx\, \sqrt{h} \left((d-1) + \frac{1}{2(d-2)}\, \mathcal{R}[h] + \cdots \right). \tag{2.2.0}$$

Here we are using the boundary metric h_{ij} at $z = \epsilon$ and the outward-pointing unit normal vector $N_z^\mu = (-1, N_z^i)$ in the banana metric. The quantities N_z^i here and N_z in eq. (2.2.2) correspond to those appearing in the metric (2.2.1).

As already mentioned, we find points that are both far and close to the horizon on the $z = \epsilon$ cut-off. For example, in the cone coordinates (2.2.1), on the cut-off surface $z = \epsilon$, we can approach $R = r_h\epsilon$ where the blackening factor vanishes, or we can consider large R where the metric is Poincaré AdS at leading order in ϵ. The behavior of the metric h_{ij} as $\epsilon \to 0$, as well as that of N_z^i, depends on this distinction. To properly disentangle these two regions, we introduce Fefferman-Graham coordinates in section 2.3, and here we adopt a simpler strategy instead. Our approach is to choose the radius a of the disks that we excise from A so that the expansion of h_{ij} and N_z^i, in $z = \epsilon$ with $\vec{x}$ fixed, is valid.[14] This is illustrated in figure 2.5.

[12] Recall that for any vector V^μ, the divergence $\nabla_\mu V^\mu = \frac{1}{\sqrt{g}}\, \partial_\mu(\sqrt{g}\, V^\mu)$. Further, $\sqrt{g}$ coincides with that in empty AdS space, as noted in footnote 8.

[13] The "$\cdots$" contain terms whose number and form depend on the number of bulk dimensions. Note that we are following the approach of [26] where the counterterms are expressed in terms of the induced metric on the asymptotic boundary.

[14] Our strategy will work here because we are studying a solution of the vacuum Einstein equations, and the powers of the z expansion have the same gap as the FG expansion.

Given the approximation $|\vec{x}_{\bullet 1}-\vec{x}_{\bullet 2}| \gg a \gg \epsilon r_h$, the various quantities entering I_{GHY} and I_{ct} automatically have an expansion in $z/|\vec{x}-\vec{x}_{\bullet 1}||\vec{x}-\vec{x}_{\bullet 2}|$ because this is the expansion of the SCT map, when we go from the expansion in z/R of the cone to the banana coordinates. For example, we find

$$d^d x\sqrt{h} = \frac{1}{z^d}\left[1-\frac{\alpha M}{2}\frac{z^d}{((x^1)^2+\rho^2)^{\frac{d}{2}}((1+bx^1)^2+b^2\rho^2)^{\frac{d}{2}}}+\dots\right]dx^1\rho^{d-2}d\rho\, d\Omega_{d-2} \qquad (2.2.0)$$

Then, at leading order $K_{\partial_{AdS}} = -d + O(z^{d+1})$ and the counterterms involving the boundary curvature are suppressed because of the flat metric on the asymptotic boundary. Combining the asymptotic boundary contributions with the bulk action (2.2.2), we find[15]

$$I_{bulk} + I_{GHY}(\partial_{AdS}) + I_{ct} \simeq \frac{(\alpha M - 2r_h^d)}{16\pi G_{\rm N}}\int_{\boxed{\bullet\bullet}} d^d x\, f_{2pt}\,, \qquad (2.2.0)$$

up to the constant term $\mathcal{N}_{bulk}$. The domain of integration is the entire boundary minus the small disks around the insertion points, which we denote $\boxed{\bullet\bullet} = A\cup B -$ disks.

The integral of f_{2pt} can be performed by introducing bipolar coordinates.[16] Let us simply quote the final result,

$$\int_{\boxed{\bullet\bullet}} d^d x\, f_{2pt} = \Omega_{d-1}\log\frac{|\vec{x}_{\bullet 1}-\vec{x}_{\bullet 2}|^2}{a^2} \qquad (2.2.0)$$

The overall coefficient in eq. (2.2.2) then becomes

$$\frac{\Omega_{d-1}}{16\pi G_{\rm N}}\left(\alpha M - 2r_h^d\right) = M - S\,T_H = F_{\rm Gibbs} \qquad (2.2.0)$$

where

$$E = \frac{\Omega_{d-1}(d-1)\alpha M}{16\pi G_{\rm N}} = M\,, \qquad S = \frac{\Omega_{d-1}r_h^{d-1}}{4G_{\rm N}}\,, \qquad T_H = \frac{f'(r_h)}{4\pi} \qquad (2.2.0)$$

with the blackening factor $f(r)$ and the coefficient α given in eqs. (2.2.1) and (2.2.1), respectively.[17] Therefore,

$$I_{bulk} + I_{GHY}(\partial_{AdS}) + I_{ct} = (M - S\,T_H)\,\log\frac{|\vec{x}_{\bullet 1}-\vec{x}_{\bullet 2}|^2}{a^2} + \mathcal{N}_{bulk}\,. \qquad (2.2.0)$$

[15] At an intermediate step, we have

$$I_{bulk}+I_{GHY}(\partial_{AdS})+I_{ct} \simeq \frac{1}{8\pi G_{\rm N}}\int d^d x\Big[\underbrace{\frac{1}{\epsilon^d} - r_h^d\, f_{2pt}(x)}_{I_{bulk}} + \underbrace{\left(-\frac{d}{\epsilon^d}+\frac{dM}{2}f_{2pt}\right)}_{I_{GHY}} + \underbrace{\left(\frac{(d-1)}{\epsilon^d}-\frac{(d-1)M}{2}f_{2pt}\right)}_{I_{ct}}\Big]$$

[16] Use

$$x^1 = \frac{T(1+T\cos\sigma)}{b(1+T^2+2T\cos\sigma)} \qquad \text{and} \qquad \rho = \frac{T\sin\sigma}{b(1+T^2+2T\cos\sigma)}$$

where $\sigma\in[0,\pi]$ for $d>2$. For $T\to 0$, we encircle $\vec{x}_{\bullet 1}=0$, while for $T\to\infty$, we encircle $\vec{x}_{\bullet 2} = -\frac{1}{b}\,\hat{x}^1$.

[17] We will also find $E=M$ by evaluating the holographic stress tensor in section 2.3.1.

We have nearly reproduced the desired CFT spacetime dependence, since we have a logarithm coming from f_{2pt}. However, the prefactor for this logarithm is the Gibbs free energy, similarly to what we would have expected had we done the computation in global AdS – but for a possible Casimir energy. However, as discussed in eq. (2.2.2), we expect the prefactor to the CFT dimension $\Delta = M$. That is, we would like to subtract the entropy contribution in eq. (2.2.2). In the following subsection, we will see that the GHY contribution on the stretched horizon does precisely this. This confirms that this surface term is precisely what is needed to fix the calculation to that of a single operator inserted at the asymptotic AdS boundary.

The stretched horizon action

Recall that we introduced a final boundary at the stretched horizon $r = r_h(1+\epsilon')$ and supplemented the action with a GHY term there, namely

$$I_{GHY}(\text{stretch}) = \frac{1}{8\pi G_{\text{N}}}\int_{\partial} d^d x \lim_{\epsilon'\to 0}\sqrt{\sigma}\, K_{\text{stretch}} \qquad \text{with} \quad K_{\text{stretch}} = -\nabla_\mu \frac{V^\mu}{|V|} \tag{2.2.0}$$

where the extrinsic curvature K is now determined by the divergence of a vector V^μ orthogonal to the stretched horizon, and σ is the determinant of the induced metric on the stretched horizon.

We can find V^μ by considering the image of ∂_r through the GtP and SCT transformations. This gives

$$\frac{V_\mu}{|V|} = -\frac{1}{\sqrt{f(r)}}\,\partial_\mu r(\vec{x}, z) \tag{2.2.0}$$

where $r(\vec{x}, z)$ in eq. (2.2.1). Simplifying the divergence as in footnote 12, and further using $f(r_h) = 0$ with $f'(r_h) = 4\pi T_H$, we arrive at

$$K_{\text{stretch}} = \frac{2\pi T_H}{\sqrt{f(r)}}\,. \tag{2.2.0}$$

On the other hand, if we only had the banana metric (2.2.1) (*i.e.* we did not know the transformations from the global coordinates and the relation $r_h = r(z, \vec{x})$), we could obtain the same result by looking at the vector orthogonal to the Killing flow in $(\vec{x}, z)$ coordinates to construct V^μ.[18]

To complete $I_{GHY}(\text{stretch})$, we need to compute the determinant of the induced metric, which we find takes the form

$$d^d x\,\sqrt{\sigma} = \frac{\rho^{d-2}\, d\Omega_{d-1}}{z^{d-2}}\,\frac{\sqrt{f(r)}dx^1\, d\rho}{z^2 r_h} \times \left(1 + \tilde{\mathcal{D}}(x_1, x_2, r_h; b)\right)\Big|_{z=z_\pm} \tag{2.2.0}$$

[18] In the cone coordinates, this is again very straightforward since $SO(d-1)$ symmetry reduces the problem to the (z, R) plane with Killing vector $\nabla_{\{\mu}\mathscr{K}_{\nu\}} = 0$ given by $\mathscr{K} = z\partial_z + R\partial_R$. In this case, we can also appreciate a nontrivial features of the cut-off surface $z = \epsilon$, by noting from our expressions in eqs. (2.2.1)-(2.2.1) that as we approach the horizon the other vector $N_z^\mu = (-1, N_z^i)$ becomes aligned with the Killing vector.

where the difference function $\tilde{\mathcal{D}}$ vanishes exactly for $b = 0$, and for $b \neq 0$ vanishes linearly when we expand around the insertion points. As we did before, we now specialize to the $z = z_-$ component of the stretched horizon, and extract the logarithmic form. This is again singled out by z_-^d in the denominator of eq. (2.2.2), which similarly to eq. (2.2.2) leads to $r_h^d\, f_{2pt}$ in the domain A. The overall power of r_h is then $r_h^{d-1} = 4G_{\rm N}\, S/\Omega_{d-1}$. Finally, by adding and subtracting f_{2pt}, we conclude that

$$I_{GHY}(\text{stretch}) = S\, T_H\, \log \frac{|\vec{x}_{\bullet 1} - \vec{x}_{\bullet 2}|^2}{a^2} + \mathcal{N}_{\text{stretch}}\,. \tag{2.2.0}$$

With the same argument as for $\mathcal{N}_{bulk}$. we can show that $\mathcal{N}_{\text{stretch}}$ is a constant that does not dependent on the separation between insertion points.

CFT from gravity

Combining eqs. (2.2.2) and (2.2.2) for the total onshell action, our final result reads

$$I_{\boxed{\bullet\bullet}} = M \log \frac{|\vec{x}_{\bullet 1} - \vec{x}_{\bullet 2}|^2}{a^2} + \mathcal{N} \tag{2.2.0}$$

where $M = \Delta$ and $\mathcal{N} = \mathcal{N}_{bulk} + \mathcal{N}_{\text{stretch}}$. It follows that

$$\langle O(\vec{x}_{\bullet 1}) O(\vec{x}_{\bullet 2})\rangle = e^{-I_{\boxed{\bullet\bullet}}} \simeq \frac{1}{|\vec{x}_{\bullet 1} - \vec{x}_{\bullet 2}|^{2\Delta}}\,, \tag{2.2.0}$$

as promised. In sum, taking into account the backreaction from the insertion of two huge operators, the gravitational action, including a GHY term at the horizon, yields to the desired CFT two-point function (2.2.2).

A posteriori, we find that the onshell action in the two-point function geometry gives a result which is consistent with the following sequence of operations,

$$Z = \text{tr}(e^{-\beta \hat{H}}) = e^{-\beta F_{\text{Gibbs}}} \;\to e^{-F_{\text{Gibbs}}\delta\tau} \to e^{-E\delta\tau} \to e^{-\Delta\delta\tau}\,. \tag{2.2.0}$$

Starting from the thermal partition function, which computes $F_{\text{Gibbs}} = E - S\, T_H$, we open up the thermal circle β to an interval of length $\delta\tau$. This gives $e^{-F_{\text{Gibbs}}\delta\tau}$ where now the endpoints play the role of the operator insertions, and induce a conical singularity in the bulk. To account for the latter, we include the GHY term at the stretched horizon, and this changes F_{Gibbs} into E. Up to this point, the CFT has S^{d-1} as its spacial slice and E includes also Casimir energies in even d. By performing a Weyl transformation, we put the CFT on $\mathbb{R}^d$. This changes the AdS cut-off and yields the final "dilatation amplitude", $e^{-\Delta\delta\tau}$.[19] The actual computation which we performed shows how the $\log|\vec{x}_{\bullet 1} - \vec{x}_{\bullet 2}|$ dependence comes about and in particular the importance of excising small disks around the operators.

We also have the normalization $\mathcal{N}$. It can be written down by following carefully the various steps above. Still, on its own it can always be absorbed in the definition of the

[19] Time-like amplitudes of CFT states in holography can also be investigate using the formalism of [32]. It would be interesting to relate this with our approach.

operator. Physical quantities involve ratios, such as three-point couplings divided by two-point function normalizations. Then it is crucial to make sure that once we attack higher-point correlation functions, we compute them with the same scheme we are using for the two-point function. This is one of the motivations for the explorations that follow.

2.3 Fefferman-Graham Coordinates

In this section, we explore further aspects of the banana geometry. In particular, we will introduce Fefferman-Graham coordinates, verify that the holographic stress tensor satisfies the conformal Ward Identity, and discuss a nonperturbative feature of the Fefferman-Graham patch, which we call *the wall*. With these insights, we will then revisit the notion of the cut-off surface at the boundary of AdS with marked points, and the computation of the onshell action as a proper surface integral.

Let us begin by recalling that Fefferman-Graham (FG) coordinates are defined by [33,34]

$$ds^2_{FG} = \frac{d\mathbf{z}^2}{\mathbf{z}^2} + \mathbf{h}_{ij}(\mathbf{z},\vec{\mathbf{x}})\, d\mathbf{x}^i\, d\mathbf{x}^j\,. \tag{2.3.0}$$

The banana metric (2.2.1) is *not* in this gauge, but can be brought to this form by a change of variables $z = z(\mathbf{z},\vec{\mathbf{x}})$, $x^i = x^i(\mathbf{z},\vec{\mathbf{x}})$, which is uniquely specified by requiring absence of mixed terms $d\mathbf{z}\, d\vec{\mathbf{x}}$ and that $g_{\mathbf{zz}} = 1/\mathbf{z}^2$ is fixed. In this gauge, $\mathbf{h}_{ij}(\mathbf{z},\vec{\mathbf{x}})$ provides neatly the holographic evolution of the boundary metric, where the latter is defined as the leading non-normalisable mode in the small $\mathbf{z}$ expansion. In our case, since we are studying a vacuum solution with a flat Poincaré boundary, we will have

$$\mathbf{h}_{ij} = \frac{1}{\mathbf{z}^2}\left(\delta_{ij} + \frac{2}{d}\,\mathbf{t}_{ij}\,\mathbf{z}^d + \cdots\right) \tag{2.3.0}$$

with $\mathbf{t}_{ij}$ traceless. Higher order terms are fixed once $\mathbf{t}_{ij}$ is given. Standard holographic renormalization methods, *e.g.* [27, 28] show that $\mathbf{t}_{ij}$ is the (expectation value of the) stress tensor in the boundary CFT.

In order to generate FG coordinates, we can start from the small $\mathbf{z}$ expansion. For the banana on the line (2.2.1), the FG gauge takes the form

$$ds^2_{FG} = \frac{d\mathbf{z}^2}{\mathbf{z}^2} + \sum_{a,b=\mathbf{x}^1,\boldsymbol{\rho}} \mathbf{h}_{ab} d\mathbf{y}^a d\mathbf{y}^b + \mathbf{h}_{\Omega\Omega} d\Omega^2_{d-2} \tag{2.3.0}$$

with metric components depending on the three variables $\mathbf{z}$, $\mathbf{x}^1$ and $\boldsymbol{\rho} = (\sum_{i=2}^d (\mathbf{x}^i)^2)^{1/2}$, in addition to M and b. Resumming in three-variables is a hard problem, in general. An exception is AdS_3 where the series truncates, and we rediscover a result from Bañados [35]

$$\begin{aligned} ds^2 &= d\mathrm{AdS}_3{}^2 + \left[\mathbf{t}\,(d\mathbf{y}^1 + i d\mathbf{y}^2)^2 + \text{c.c.}\right] + \mathbf{z}^2\,|\mathbf{t}|^2((d\mathbf{y}^1)^2 + (d\mathbf{y}^2)^2) \\ &\text{where} \qquad \mathbf{t} = -\frac{M}{4(\mathbf{y}^1 + i\mathbf{y}^2)(1 + b(\mathbf{y}^1 + i\mathbf{y}^2))}\,. \end{aligned} \tag{2.3.1}$$

In the special case of the cone, $b = 0$, the coordinates $\mathbf{x}^1$ and $\boldsymbol{\rho}$ combine together to restore $SO(d-1)$ symmetry, and this allows us to find

$$ds^2_{FG} = \frac{1}{\mathbf{z}^2}\left[d\mathbf{z}^2 + \frac{(1-\frac{M\mathbf{z}^d}{4\mathbf{R}^d})^2}{(1+\frac{M\mathbf{z}^d}{4\mathbf{R}^d})^{\frac{2(d-2)}{d}}}d\mathbf{R}^2 + (1+\tfrac{M\mathbf{z}^d}{4\mathbf{R}^d})^{\frac{4}{d}}\mathbf{R}^2 d\Omega^2_{d-1}\right] \tag{2.3.0}$$

with the change of variables from GtP cone to FG cone given by

$$\frac{R}{z} = \frac{\mathbf{R}}{\mathbf{z}}\left(1+\frac{M}{4}\frac{\mathbf{z}^d}{\mathbf{R}^d}\right)^{\frac{2}{d}} \qquad ; \qquad R^2+z^2 = \mathbf{R}^2\exp\left[\int_0^{\frac{\mathbf{z}}{\mathbf{R}}}\frac{2xdx}{k(x)}\right] \tag{2.3.0}$$

where $k(x) = x^2 + (1-\frac{M}{4}x^d)^2/(1+\frac{M}{4}x^d)^{\frac{2(d-2)}{d}}$.[20]

For the FG cone, $SO(d-1)$ symmetry implies that the image of a cylinder of radius $r = R/z$ in global, is again a cone. However, the FG banana looks different. For example, in AdS_3 and AdS_5, we have[21]

$$r^2_{AdS_3} = \frac{\tilde{\mathbf{R}}^2}{\mathbf{z}^2} + \frac{M}{2} + \frac{M}{4}\left[\frac{2b(\mathbf{x}^1(1+b\mathbf{x}^1)-b\boldsymbol{\rho}^2)\mathbf{z}^2}{\mathbf{R}^2\mathbf{R}_b^2} + \frac{M\mathbf{z}^2}{4\mathbf{R}^2\mathbf{R}_b^2}\right]$$

$$r^2_{AdS_5} = \frac{\tilde{\mathbf{R}}^2}{\mathbf{z}^2} + \frac{M\mathbf{z}^2}{4\mathbf{R}^2\mathbf{R}_b^2} - \frac{M}{2}\left[1 - \frac{b\,\mathbf{z}^2(\tilde{\mathbf{x}}^1 - b\,\mathbf{z}^2)}{\mathbf{R}^2\mathbf{R}_b^2} - \frac{(\tilde{\mathbf{R}}^2 - 2b\,\tilde{\mathbf{x}}^1\,\mathbf{z}^2)}{b\,\boldsymbol{\rho}\,\mathbf{z}^2}\tan^{-1}\left[\frac{b\,\boldsymbol{\rho}\,\mathbf{z}^2}{\tilde{\mathbf{R}}^2 - b\,\tilde{\mathbf{x}}^1\,\mathbf{z}^2}\right]\right] + O(M^2)$$

where $\tilde{\mathbf{R}}^2 = (\tilde{\mathbf{x}}^1)^2 + \boldsymbol{\rho}^2$ with $\tilde{\mathbf{x}}^1 = \mathbf{x}^1 + b\,(\mathbf{R}^2+\mathbf{z}^2)$, $\mathbf{R}^2 = (\mathbf{x}^1)^2+\boldsymbol{\rho}^2$ and $\mathbf{R}_b^2 = (1+b\mathbf{x}^1)^2 + b^2\,\boldsymbol{\rho}^2$.

The functional differences between a FG banana and a GtP banana (2.2.1) have a simple explanation: The GtP transformation is designed to foliate empty AdS, and knows nothing about the actual black hole metric. For example, it is M independent. On the other hand, FG coordinates by construction are sensitive to the black hole geometry, thus foliate the space accordingly. There is however a limitation: the FG patch is not expected to cover the entire black hole geometry. This statement is simple to understand: since the small $\mathbf{z}$ expansion is fully determined by the knowledge of the boundary metric and boundary stress tensor $\mathbf{t}_{ij}$, there is no freedom left to impose other boundary conditions, such as regularity conditions at the horizon. This means that the FG patch must breakdown at some surface where the Jacobian of the coordinate transformation from global to FG vanishes. We will refer to this surface as *the wall*. In practise, the wall encloses the horizon at a finite distance, and there is no way to access the horizon from the FG patch (on a real slice).[22]

In $\mathbf{x}, \mathbf{z}$ coordinates, the wall coincides with the surface where $\det \mathbf{h}_{ab} = 0$. This can be seen by examining the measure for the FG metric (2.3),

$$\frac{\sqrt{\mathbf{h}}}{\mathbf{z}} = \sqrt{g(\vec{\mathbf{x}},\mathbf{z})\,\mathrm{Jac}^2(\vec{\mathbf{x}},\mathbf{z})} \tag{2.3.-1}$$

[20] See also [36, 37] where similar metrics appear.

[21] Note that when $M = 0$, we recover the SCT map in the first term. On the other hand, with the limit $b \to 0$, we recover our previous formula (2.3).

[22] See [38] for a discussion about the radius of convergence in asymptotically AdS black holes in global coordinates.

and further we have $g(\vec{\mathbf{x}}, \mathbf{z}) = \sqrt{g(r)} = r^{d-1} > 0$ for the black hole metric (2.2.1). In the FG cone coordinates, the wall is itself a cone given by

$$\mathbf{R} = \left(\frac{M}{4}\right)^{\frac{1}{d}} \mathbf{z} \tag{2.3.-1}$$

corresponding to $r_{wall} = M^{\frac{1}{d}}$. As expected, $r_{wall} > r_h$. Note however that in general, the wall does not have to be a FG banana, nor the minimum in $\mathbf{z}$ of $r(\vec{\mathbf{x}}, \mathbf{z})$ for fixed $\vec{\mathbf{x}}$. For example in AdS_3, the wall is given by

$$\left((\mathbf{x}^1)^2 + \boldsymbol{\rho}^2\right)\left((1 + b\mathbf{x}^1)^2 + \boldsymbol{\rho}^2\right) = \frac{M}{4}\,\mathbf{z}^2\,, \tag{2.3.-1}$$

which is not comparable with eq. (2.3).

Even so, the wall and GtP bananas both originate from the insertion points at the AdS boundary, where $\mathbf{z} = z = 0$ and $\vec{\mathbf{x}} = \vec{x}$. The novelty is what happens with respect to the cut-off, $\mathbf{z} = \boldsymbol{\epsilon}$ versus $z = \epsilon$. In fact, when we look at $\mathbf{z} = \boldsymbol{\epsilon}$ in the two-point function geometry with coordinates $z, \vec{x}$, this surface cannot get arbitrarily close to the horizon, but intersects and stops at the preimage of the wall. This intersection is well defined and brings us to an important consideration: Imagine we want to construct a black hole numerically, in global coordinates. We are used to specify a boundary condition at infinity and a boundary condition in the interior. However, in the two-point function geometry, all of the boundary conditions are specified on $z = \epsilon$, and of course, they are distinct depending on whether we stay far or close to the operators. This distinction is quantified by the wall between the FG patch and the rest of the geometry. In this sense, the usual notion of bulk evolution is modified in an interesting way.

2.3.1 Holographic stress tensor

To compute expectation values in the holographic CFT, the small $\mathbf{z}$ expansion of the FG metric is all we need, and this is straightforward to obtain even in the banana geometry. The computation of the holographic stress tensors that follows is an example. Nicely enough, for the cone coordinates, we can check all the various steps directly with pencil and paper.

Using the definition of the holographic stress tensor given in [27, 28], we have

$$\langle T_{ij}(\vec{\mathbf{x}})\rangle_{\boxed{\bullet\bullet}} = \frac{1}{8\pi G_{\mathrm{N}}} \lim_{\boldsymbol{\epsilon}\to 0} \frac{1}{\boldsymbol{\epsilon}^{d-2}} \left[\mathcal{K}_{ij} - \mathcal{K}\mathbf{h}_{ij} + \frac{2}{\sqrt{\mathbf{h}}}\frac{\delta I_{ct}}{\delta \mathbf{h}^{ij}}\right]_{\mathbf{z}=\boldsymbol{\epsilon}} \qquad \text{with} \quad \mathcal{K}_{ij} = \tfrac{1}{2}\mathbf{z}\,\partial_{\mathbf{z}}\mathbf{h}_{ij} \tag{2.3.-1}$$

and where, as in (2.2.2), the counterterm action is

$$I_{ct} = \int_{\mathbf{z}=\boldsymbol{\epsilon}} d^d\mathbf{x}\,\sqrt{\mathbf{h}}\left((d-1) + \frac{1}{2(d-2)}\,\mathcal{R}[\mathbf{h}] + \cdots\right). \tag{2.3.-1}$$

Individual contributions in $\langle T_{ij}\rangle_{\boxed{\bullet\bullet}}$ are divergent, but the combined sum in eq. (2.3.1) is finite. For a flat boundary, only the first term in eq. (2.2.2) is needed to resolve the divergence. Note

that had we done the computation in global coordinates, using FG coordinates with $\mathbb{R}\times S^{d-1}$ asymptotics, all counterterms would have contributed to the final result, *e.g.* see [26,30]. So even though we started from the very same AdS-Schwarzschild black hole, the details of the $\langle T_{ij}\rangle_{\boxed{\bullet\bullet}}$ computation are quite different. For example, we will not be sensitive to Casimir energies of the S^{d-1}, and moreover, the spacetime dependence of $\langle T_{ij}\rangle_{\boxed{\bullet\bullet}}$ is quite more interesting.

With the insertion points $\vec{\mathbf{x}}_{\bullet 1}$ and $\vec{\mathbf{x}}_{\bullet 2}$, the final result is

$$\langle T_{ij}(\vec{\mathbf{x}})\rangle_{\boxed{\bullet\bullet}} = \mathbf{t}_{ij}(\vec{\mathbf{x}}) = \frac{d\,M}{(d-1)\Omega_{d-1}}\,\frac{|\vec{\mathbf{x}}_{\bullet 1}-\vec{\mathbf{x}}_{\bullet 2}|^d}{|\vec{\mathbf{x}}-\vec{\mathbf{x}}_{\bullet 1}|^d|\vec{\mathbf{x}}-\vec{\mathbf{x}}_{\bullet 2}|^d}\,\lambda_{ij}(\vec{\mathbf{x}};\vec{\mathbf{x}}_{\bullet 1},\vec{\mathbf{x}}_{\bullet 2}) \tag{2.3.-1}$$

where again $\Omega_{d-1}=2\pi^{\frac{d}{2}}/\Gamma[\frac{d}{2}]$, and the traceless tensor λ_{ij} is given by

$$\lambda_{ij}(\vec{\mathbf{x}};\vec{\mathbf{x}}_{\bullet 1},\vec{\mathbf{x}}_{\bullet 2}) = -u_iu_j+\frac{\delta_{ij}}{d} \qquad \text{with}\quad u_i = \frac{|\vec{\mathbf{x}}-\vec{\mathbf{x}}_{\bullet 1}|\,|\vec{\mathbf{x}}-\vec{\mathbf{x}}_{\bullet 2}|}{|\vec{\mathbf{x}}_{\bullet 1}-\vec{\mathbf{x}}_{\bullet 2}|}\left[\frac{(\vec{\mathbf{x}}-\vec{\mathbf{x}}_{\bullet 1})_i}{|\vec{\mathbf{x}}-\vec{\mathbf{x}}_{\bullet 1}|^2}-\frac{(\vec{\mathbf{x}}-\vec{\mathbf{x}}_{\bullet 2})_i}{|\vec{\mathbf{x}}-\vec{\mathbf{x}}_{\bullet 2}|^2}\right].$$

Now interpreting eq. (2.3.1) as

$$\langle T_{ij}(\vec{\mathbf{x}})\rangle_{\boxed{\bullet\bullet}} = \frac{\langle T_{ij}(\vec{\mathbf{x}})\,O(\vec{x}_{\bullet 1})\,O(\vec{x}_{\bullet 2})\rangle}{\langle O(\vec{x}_{\bullet 1})\,O(\vec{x}_{\bullet 2})\rangle}\,, \tag{2.3.-1}$$

we see that this expression precisely reproduces the conformally invariant three-point function of the energy momentum tensor and two scalar operators [39–42] with

$$\Delta = M\,. \tag{2.3.-1}$$

This is a simple yet very important consistency check for our two-point function geometries! Moreover, it gives us an independent derivation of the relation between the conformal dimension and the mass of the black hole, which we used in the onshell action computation.

2.3.2 The bulk, the total derivative and the cut-off

We now want to comment on the onshell action. The idea is to divide the geometry into a FG patch where the cut-off surface lives, and a global patch close to the horizon where the stretched horizon lives. This organization is conceptually helpful because, as we saw in section 2.2.2, both contributions are crucial in order to obtain the expected CFT dependence on the dimension $\Delta = M$. The approach described in the following sections is not restricted to the Schwarzschild black hole but also generalizes to charged black holes in AdS [12].

Our starting point is the observation that when the bulk action in global coordinates can be written onshell as a total derivative, we can apply the GtP transformation directly on the integrand. So let us assume that the onshell action in global reads

$$I_{\bigcirc} = \int d\Omega_{d-1}\int d\tau\int dr\times\frac{d}{dr}\mathcal{A}(r) \tag{2.3.-1}$$

for some function $\mathcal{A}(r)$. For the AdS-Schwarzschild geometry, this is [30][23]

$$\mathcal{A}(r) = -2r^{d-2} + 2r^{d-2} f(r) = 2r^d - 2M \tag{2.3.-1}$$

Going through the GtP map (2.2.1) and the SCT map (2.2.1) to reach the banana geometry (2.2.1) with the insertion points on a line, we find:

$$\begin{aligned} I_{\boxed{\bullet\bullet}} &= \int d\Omega_{d-1} \int dR\, d\tilde{z} \times \left[-\frac{R}{R^2+\tilde{z}^2}\partial_{\tilde{z}} + \frac{\tilde{z}}{R^2+\tilde{z}^2}\partial_R \right] \mathcal{A}\big(r = \tfrac{R}{\tilde{z}}\big) \\ &= \int d\Omega_{d-2} \int d\rho\, dx^1\, dz \times \sum_{i=z,x^1,\rho} u_i\, \partial_i \mathcal{A}\big(r(z,\vec{x})\big) \quad \text{with} \quad u_i = -\frac{1}{d-2}\frac{\rho^{d-2}}{z^{d+1}} \frac{\partial_i r^{2-d}}{(\frac{x^2}{z^2}+1)\frac{\Theta^2}{z^2}} \end{aligned}$$

where $r(z,\vec{x}) = \sqrt{\Theta^2\left(\frac{x^2}{z^2}+1\right)-1}$ and $\Theta^2 = 1 + 2\,b\cdot x + b^2(x^2+z^2)$ with $x^2 = (x^1)^2 + \rho^2$, as given in eq. (2.2.1). Note that the dot product here is taken using δ_{ij}. Of course, the second expression reduces to the first one when $b = 0$. Then, it is simple to check, and perhaps expected, that the vector u^i is divergence free.[24] Thus we can evaluate the onshell action by using the divergence theorem, reducing it to a surface integral, namely

$$I_{\boxed{\bullet\bullet}} = \int d\sigma\, \frac{\vec{u}\cdot\vec{n}}{|\vec{n}|}\, \mathcal{A}\big(r(z,\vec{x})\big) \tag{2.3.-2}$$

where $\vec{n}$ is an outward-pointing normal to the integration surface σ. For the cone, this is just a line integral in the $(\tilde{z}, R)$ plane.

The choice of integration surface is crucial. For example, in the cone we could pick the union of the two cones corresponding to $\frac{R}{z} = r_\infty$ with a large $r_\infty \to \infty$ for the asymptotic AdS cut-off, and $\frac{R}{z} = r_h(1+\epsilon')$, for the stretched horizon. By computing the onshell action between these surfaces, we would actually be repeating the same computation as in global coordinates.[25] This is *not* the computation which we want for the two-point function. Rather, we want to compute the onshell action with a cut-off at $\mathbf{z} = \boldsymbol{\epsilon}$ in the FG patch.

In the following, we describe the computation of $I_{\boxed{\bullet\bullet}}$ with the appropriate boundary surface σ. We will distinguish the three boundary components as: the asymptotic cut-off surface described by coordinates $\vec{c} = (x^1(\mathbf{z}=\boldsymbol{\epsilon},\vec{\mathbf{x}}), \rho(\mathbf{z}=\boldsymbol{\epsilon},\vec{\mathbf{x}}), z(\mathbf{z}=\boldsymbol{\epsilon},\vec{\mathbf{x}}))$; the banana corresponding to the stretched horizon; and two pieces of connecting tissue between the previous components, one for each of the insertion points.

The asymptotic cut-off

The asymptotic cut-off surface $\mathbf{z} = \boldsymbol{\epsilon}$ is described by $\vec{c} = (x^1(\boldsymbol{\epsilon},\vec{\mathbf{x}}), \rho(\boldsymbol{\epsilon},\vec{\mathbf{x}}), z(\boldsymbol{\epsilon},\vec{\mathbf{x}}))$, in terms of FG coordinates. From our discussion about the FG patch in the previous section, we know

[23] In fact, for all $SO(d-1)$ symmetric and static backgrounds, which solve for Einstein gravity coupled to a general (two-derivative) action of scalar and vector fields, one can cast $\mathcal{A}(r)$ as a particular functional of the (time and radius) components of the metric [30].

[24] Note also that $\sum_i \partial_i r \partial_i r = (\frac{R^2}{z^2}+1)\frac{\Theta^2}{z^2}$.

[25] The way terms combine together is slightly different, but we checked that we do get the same result as in global coordinates. In particular, we find a Casimir energy contribution for even d.

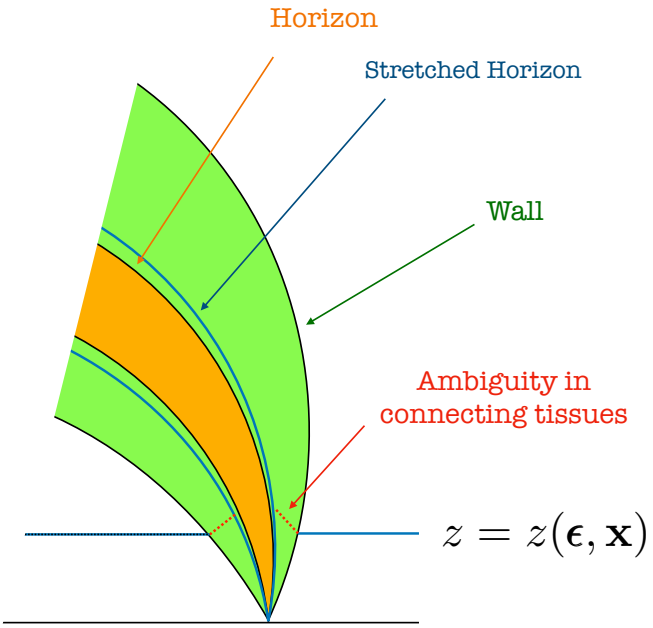

Figure 2.6: A section of the banana geometry to illustrate the integration surface σ. The cut-off surface $z = (\mathbf{z}, \mathbf{x}), x = (\mathbf{z}, \mathbf{x})$ can be extended up to the preimage of the wall, the choice of connecting tissues from there to the stretched horizon results in a choice of normalisation.

that the integration over $\vec{\mathbf{x}}$ can be extended at most up to the intersection of $\mathbf{z} = \boldsymbol{\epsilon}$ and the wall – see figure 2.6. This observation explains more precisely what happened in section 2.2.2 when we introduced a large enough radius a for the disks encircling the insertion points in figure 2.5. We understand now that the minimum value that a can take is the preimage of $\vec{\mathbf{x}}$ on the wall at $\mathbf{z} = \boldsymbol{\epsilon}$.

In the cone, the surface integral on $\vec{c} = (R(\boldsymbol{\epsilon}, \mathbf{R}), z(\boldsymbol{\epsilon}, \mathbf{R}))$ is very explicit, since we know the change of variables (2.3). We find

$$\mathcal{A}_{cone}(\boldsymbol{\epsilon}, \mathbf{R}) = \frac{2\mathbf{R}^d}{\boldsymbol{\epsilon}^d} - M + \frac{M^2}{4^2}\frac{\boldsymbol{\epsilon}^d}{\mathbf{R}^d} \tag{2.3.-2}$$

Then, the normal vector $\vec{n}$ is a rotation of $\partial_{\mathbf{R}}\vec{c}$, and the very definition of the surface integral cancels $|\vec{n}|$, so the measure of the integral becomes

$$\int_{\mathbf{z}=\boldsymbol{\epsilon}} d\sigma \frac{\vec{u}\cdot\vec{n}}{|\vec{n}|} = \int \frac{d\mathbf{R}}{\mathbf{R}}\left(1 - \frac{\boldsymbol{\epsilon}^2}{\mathbf{R}^2}\frac{1}{k(\frac{\boldsymbol{\epsilon}}{\mathbf{R}})}\right) = \int \frac{d\mathbf{R}}{\mathbf{R}}\left(\frac{1}{(1+\frac{\boldsymbol{\epsilon}^2}{\mathbf{R}^2})} - \frac{d-1}{d}M\frac{\boldsymbol{\epsilon}^{d+2}}{\mathbf{R}^{d+2}} + \dots\right). \tag{2.3.-2}$$

The whole $k(x)$ is given in eq. (2.3). When taking the $\boldsymbol{\epsilon} \to 0$ limit, we have to be careful in isolating the AdS contribution in $\vec{u}\cdot\vec{n}$ from the rest because $\mathcal{A}_{cone}$ itself comes with a Laurent series in $\boldsymbol{\epsilon}$. What we want to ensure is that the corrections to AdS proportional to M do not interfere with the structure of $\mathcal{A}_{cone}$ as a series in $\boldsymbol{\epsilon}$. This implies that we have

to resum the AdS contribution in $\boldsymbol{\epsilon}$ before taking the limit to zero. This is what we made explicit on the right-hand side of eq. (2.3.2).

The GHY and counterterm contributions at the asymptotic boundary can by definition be evaluated in the FG patch directly. Putting all of these together cancels the usual UV divergence from AdS and a finite result remains,

$$\lim_{\boldsymbol{\epsilon}\to 0}\frac{1}{16\pi G_{\rm N}}\int_{\mathbf{z}=\boldsymbol{\epsilon}} d\sigma\,\frac{\vec{u}\cdot\vec{n}}{|\vec{n}|}\mathcal{A}(r)+I_{GHY}(\partial_{AdS})+I_{ct}=-\frac{M}{16\pi G_{\rm N}}\int_{\mathbf{R}_\star}^{1/\mathbf{R}_\star}\frac{d\mathbf{R}}{\mathbf{R}}\,. \tag{2.3.-2}$$

We can take any $\mathbf{R}_\star \geq \left[\frac{M}{4}\right]^{\frac{1}{d}}\boldsymbol{\epsilon}$, where the limit is the value fixed by the wall. It is worth mentioning that in the cone coordinates, we can compute the onshell action directly by evaluating $\sqrt{\det g_{FG}}$, from $\mathbf{z}=\boldsymbol{\epsilon}$ to the $\mathbf{z}=$ wall. Since we know the preimage, *i.e.* $r_{wall}=M^{\frac{1}{d}}$, we can then check this result against the surface integral done with $\mathcal{A}$. We find perfect agreement, as it should. In passing, we also notice that $\mathcal{A}(r_{wall})=0$.

We now repeat the cut-off surface integration for the banana. This time we do not have the full change of variables, however, we can proceed by using the series expansion in $\mathbf{z}$. The measure factor can be found to generalize the right-hand side of eq. (2.3.2) into[26]

$$\vec{u}\cdot\vec{n}\big|_{\mathbf{z}=\boldsymbol{\epsilon}}=\frac{\boldsymbol{\rho}^{d-2}}{\tilde{\mathbf{R}}^{\frac{d}{2}}}\,\frac{\boldsymbol{\rho}^2+\tilde{\mathbf{x}}^1(\tilde{\mathbf{x}}^1-2b\boldsymbol{\epsilon}^2)}{(\mathbf{R}^2+\boldsymbol{\epsilon}^2)\,\Theta^2(\mathbf{x}^1,\boldsymbol{\rho},\boldsymbol{\epsilon})}+MO(\boldsymbol{\epsilon}^{d+1}) \tag{2.3.-2}$$

where $\mathbf{R}^2=\boldsymbol{\rho}^2+(\mathbf{x}^1)^2$, $\tilde{\mathbf{R}}^2=\boldsymbol{\rho}^2+(\tilde{\mathbf{x}}^1)^2$, and $\tilde{\mathbf{x}}^1=\mathbf{x}^1+b\,(\mathbf{R}^2+\mathbf{z}^2)$. Then $\mathcal{A}_{banana}=\frac{2\tilde{\mathbf{R}}^d}{\boldsymbol{\epsilon}^d}-M+O(Mb\boldsymbol{\epsilon}^d,M^2\boldsymbol{\epsilon}^d)$. It follows again that

$$\begin{aligned}\lim_{\boldsymbol{\epsilon}\to 0}\frac{1}{16\pi G_{\rm N}}\int_{\mathbf{z}=\boldsymbol{\epsilon}} d\sigma\,\frac{\vec{u}\cdot\vec{n}}{|\vec{n}|}\mathcal{A}(r)+I_{GHY}(\partial_{AdS})+I_{ct} \qquad (2.3.-1)\\ =-\frac{M}{16\pi G_{\rm N}}\int_{\boxed{\bullet\bullet}}\frac{\boldsymbol{\rho}^{d-2}\,d\boldsymbol{\rho}\,d\mathbf{x}^1 d\Omega_{d-2}}{((\mathbf{x}^1)^2+\boldsymbol{\rho}^2)^{d/2}\,((1+b\mathbf{x}^1)^2+\boldsymbol{\rho}^2)^{d/2}}\,,\end{aligned}$$

where in the remaining integral, we recognise the expression for f_{2pt} familiar from section 2.2.2, *e.g.* compare with eq. (2.2.2).

From cut-off to stretched horizon

At this point, we must consider the two components of the integration surface σ comprising connecting tissue extending between the asymptotic cut-off surface and the stretched horizon – see figure 2.6. The simplest choice is to go straight into the bulk. Other choices are possible, for example, we can use them to match the $z=\epsilon$ surface *close* to the insertion points. Compared to computations usually done for probe objects, the freedom in cutting the geometry passed the FG wall is something new. To see why consider a geodesic connecting the insertion points. The length of such a geodesic, *i.e.* $(\mathbf{z}(s),\mathbf{x}(s))=\ell\,(\sin s,\cos s)$ with $s\in(0,\pi)$, computes the two-point function. The ambient space is just empty AdS and

[26] To compute $\vec{u}\cdot\vec{n}$, we observe that $\vec{n}=-\partial_{\mathbf{z}}+MO(\mathbf{z}^{d+1})$, thus we replace the coordinate dependence of u^z with bold font variables, and check that the actual FG expansion only modifies this by terms $MO(\mathbf{z}^{d+1})$.

the cut-off is $\mathbf{z} = \boldsymbol{\epsilon}$, to be understood physically as a UV cut-off or lattice spacing. The range of integration is read off from the equation $\mathbf{z}(s) = \boldsymbol{\epsilon}$. Equally, we can parametrise the integration with respect to the $\mathbf{x}$ coordinate. Note at this point, the obvious fact that empty AdS is already in the FG gauge. In particular, there is no extra space which corresponds to integrating over the two connecting tissues between the cut-off and the horizon. It is also clear now that the role of the connecting tissues is simply to change the normalization of the operators, since different tissues yield different normalization constants to the final action.

Stretched horizon

Finally, the stretched horizon contribution is the surface integral on $\vec{c} = (x^1, \rho, z = z(x^1, \rho))$, where $z = z(x^1, \rho)$ solves the equation $r(z, \vec{x}) = r_h(1 + \epsilon')$ as we did in (2.2.2). The normal vector $\vec{n}$ is the cross product $\partial_{x^1}\vec{c} \times \partial_\rho \vec{c}$, and of course, it becomes proportional to $\partial_i r(z, \vec{x})$. Then, similarly to what we did in section 2.2.2, we look at $z = z_-(x^1, \rho)$, and we extract the logarithmic form close to the insertion points. The relevant integral is

$$I_{hor} = -\frac{1}{16\pi G_{\text{N}}} \int_A \frac{\rho^{d-2} d\rho\, dx^1\, d\Omega_{d-2}}{\tilde{R}_-^{d-1}} \frac{b^2(1 + r_h^2)\mathcal{A}(r_h)}{(z_+^2 - z_-^2)(R^2 + z_-^2)((1 + bx^1)^2 + b^2\rho^2 + b^2 z_-^2)} \tag{2.3.-2}$$

where $\tilde{R}_- = \tilde{R}(x^1, \rho, z = z_-(x^1, \rho))$. Close to the insertion points, the logarithmic form in eq. (2.3.2) is

$$I_{hor} = -\frac{\mathcal{A}(r_h)}{16\pi G_{\text{N}}} \int_A \frac{\rho^{d-2} d\rho\, dx^1\, d\Omega_{d-2}}{((x^1)^2 + \rho^2)^{d/2}((1 + bx^1)^2 + b^2\rho^2)^{d/2}} + \cdots, \tag{2.3.-2}$$

where again we recognize appearance of f_{2pt}. The rest of the terms denoted by the ellipsis are again free of divergences and will only contribute to the normalization.

The onshell action revisited

At this point, we can assemble again the total onshell action,

$$I_{\boxed{\bullet\bullet}} = I_{bulk} \; + I_{GHY}(\partial_{AdS}) + I_{GHY}(\text{stretch}) + \; I_{ct} \tag{2.3.-2}$$

where the contribution in I_{bulk} coming from the asymptotic boundary (*i.e.* $\mathbf{z} = \boldsymbol{\epsilon}$) is given in eq. (2.3.-1), and the contribution from the stretched horizon is given in eqs. (2.3.2) and (2.3.2). Moreover, we have argued that the boundary components connecting the cut-off surface at the asymptotic boundary and at the stretched horizon only contribute to the overall normalization of the two-point function. To finalize, we need to include the GHY term at the stretched horizon, but this is the same as (2.2.2). Therefore, by mechanically substituting in all of the contributions, we establish the same result which we found in section 2.2.2 for the CFT two-point function,

$$I_{\boxed{\bullet\bullet}} = \Delta \int_{\boxed{\bullet\bullet}} d^d x\, f_{2pt} \; + \mathcal{N}. \tag{2.3.-2}$$

where $\Delta = M$ for the operators, and as we understood the normalization depends on the choice of connecting tissues.

A bonus of our discussion here, compared to that of section 2.2.2, is that by rewriting the bulk contribution to the onshell action as a manifest surface integral (*i.e.* the integrand became a total derivative), we could make precise the FG renormalization scheme for the cut-off. Another great advantage of working with a total derivative will be the following observation, or "how to compute the total action without really trying".

Given an ansatz for a gravitational background in global coordinates, we can recast Einstein's equation as the equation of motion from an effective Lagrangian. With the latter, we look for a conserved (and finite) Noether charge $\mathcal{Q}(r)$ corresponding to a scaling symmetry [43, 44] in this effective Lagrangian. Since this Noether charge is conserved, it must be a constant satisfying $\partial_r \mathcal{Q}(r) = 0$. For the AdS-Schwarzschild in (2.2.1), this procedure yields

$$\mathcal{Q}(r) = -\tfrac{1}{2} r^{d-1} f'(r) + r^{d-2} f(r) - r^{d-2} = -\tfrac{d}{2} M \,. \tag{2.3.-2}$$

We note that the middle expression above applies for a general ansatz of the form given in eq. (2.2.1) (*i.e.* without specifying the specific solution for $f(r)$), while the final constant proportional to M comes from substituting in eq. (2.2.1).

The utility of the Noether charge is to relate the boundary contributions to the onshell action and the stretched horizon contribution. To see this, we first replace $r^{d-1} f'(r)$ term (*i.e.* the first contribution in the middle expression above) with the GHY term on a surface of constant r in global coordinates, namely

$$\mathcal{G} \equiv 2\sqrt{f(r)} r^{d-2} K = r^{d-1} f'(r) + 2(d-1) r^{d-2} f(r) \,. \tag{2.3.-2}$$

where the extrinsic curvature is $K = r^{-d+2} \partial_r (r^{d-2} \sqrt{f(r)})$. Similarly, we replace the r^{d-2} term (*i.e.* the third contribution in the middle expression in eq. (2.3.2)) using $\mathcal{A}(r)$ in eq. (2.3.2). Thus we arrive at the following expression for the Noether charge

$$\mathcal{Q}(r) = -\tfrac{1}{2} \mathcal{G}(r) + \tfrac{1}{2} \mathcal{A}(r) + (d-1) r^{d-2} f(r) \,. \tag{2.3.-2}$$

As our notation indicates, we may evaluate the Noether charge at any radius and so it is interesting to evaluate the above at the horizon $r = r_h$. There the last term vanishes since $f(r_h) = 0$, and we are left with the first two. In this form, we don't have to know the exact gravity solution, but only read off how the constant Noether charge is related to quantities which we need to evaluate at the horizon. In particular, we have the surface term coming from the radial integral in bulk action and the GHY term on the stretched horizon. That is, we may use eq. (2.3.2) to re-express the surface term in eq. (2.3.2) along with the GHY term on the stretched horizon in terms of the Noether charge, as desired. Hence combining these contributions with the expression in eq. (2.3.-1), the onshell action becomes

$$\begin{aligned} I_{\boxed{\bullet\bullet}} &= I_{bulk} \; + I_{GHY}(\partial_{AdS}) + I_{GHY}(\text{stretch}) + \; I_{ct} \\ &= \frac{1}{16\pi G_{\rm N}} \Big[- M - 2 \lim_{r\to\infty} \mathcal{Q}(r) \Big] \int_{\boxed{\bullet\bullet}} d^d x \, f_{2pt} \; + \; \mathcal{N} \,. \end{aligned}$$

Then the integral can be evaluated as in eq. (2.2.2), and after restoring the mass normalization α given by eq. (2.2.1), we recover

$$I_{\boxed{\bullet\bullet}} = \Delta \log \frac{|\vec{x}_{\bullet 1} - \vec{x}_{\bullet 2}|^2}{a^2} + \mathcal{N} \tag{2.3.-2}$$

using $\Delta = M$. Hence we have again demonstrated our claim of deriving the two-point function correlator for huge operators from gravity.

2.4 Geodesics in the black hole two-point function geometry

As we have been discussing, the insertion of huge operators results in backreaction on the AdS geometry, and we found that our two-point function geometry simply corresponds to a Euclidean black hole presented in a somewhat unusual way. In this section, we study both qualitatively and quantitatively how the motion of geodesics that shoot in from the asymptotic boundary of AdS is affected by the presence on the Euclidean black hole. These geodesics would correspond to the insertion of additional light operators and so this is a first step towards investigating higher point functions with our geometric approach. We note that heavy-light four-point correlators were studied previously with geodesics propagating in a global black hole background by [45]- [46].

Figure 2.7 illustrates a variety of geodesics originating from points on the asymptotic boundary, with a given velocity. A prominent feature of the plot is that the geodesics shown there do not reach the horizon. In fact, the only geodesics that collide with the horizon are finely tuned. The latter is clearly understood by considering the metric (2.2.1) in global coordinates. In this setting, it is straightforward to show that the only geodesics reaching $r = r_h$ must have a vanishing velocity in the τ direction. Further, the angular momentum can not be very large (*i.e.* $|\mathcal{J}| \leq r_h$).

We can also use geodesics to provide probes for a four-point function of two light particles of dimension m in the presence of two maximally heavy operators of dimension M, *i.e.* the black hole banana. This correlator is obtained by evaluating

$$S(M) = m \int ds \sqrt{g_{\mu\nu}[M]\, \dot{x}^\mu(s)\, \dot{x}^\nu(s)} \tag{2.4.0}$$

where now the geodesic $x^\mu(s)$, differently from what we did above, has boundary conditions such that it approaches the two insertions points at the regulated boundary, namely $z = \epsilon$ for $\vec{x}_{\bullet 1}$ and $\vec{x}_{\bullet 2}$. By conformal invariance we can arrange the external points as in figure 2.8. Thus, the correlator is more precisely given by

$$\langle \phi_H(0)\phi_L(1)\phi_L(x)\phi_H(\infty)\rangle = e^{-(S(M)-S(0))} \tag{2.4.0}$$

where the right-hand side is finite in ϵ after subtracting the AdS value.

The computation of $x^\mu(s)$ and the action S are described in appendix A.2. In the $M \to 0$ limit, the result simplifies significantly. For example, in $\mathrm{AdS}_5/\mathrm{CFT}_4$, we find

$$S(M) - S(0) = \tfrac{1}{4} mM \times (x-1)(\bar{x}-1) \times \frac{h(x) - h(\bar{x})}{x - \bar{x}} + O(M^2)\,, \tag{2.4.0}$$

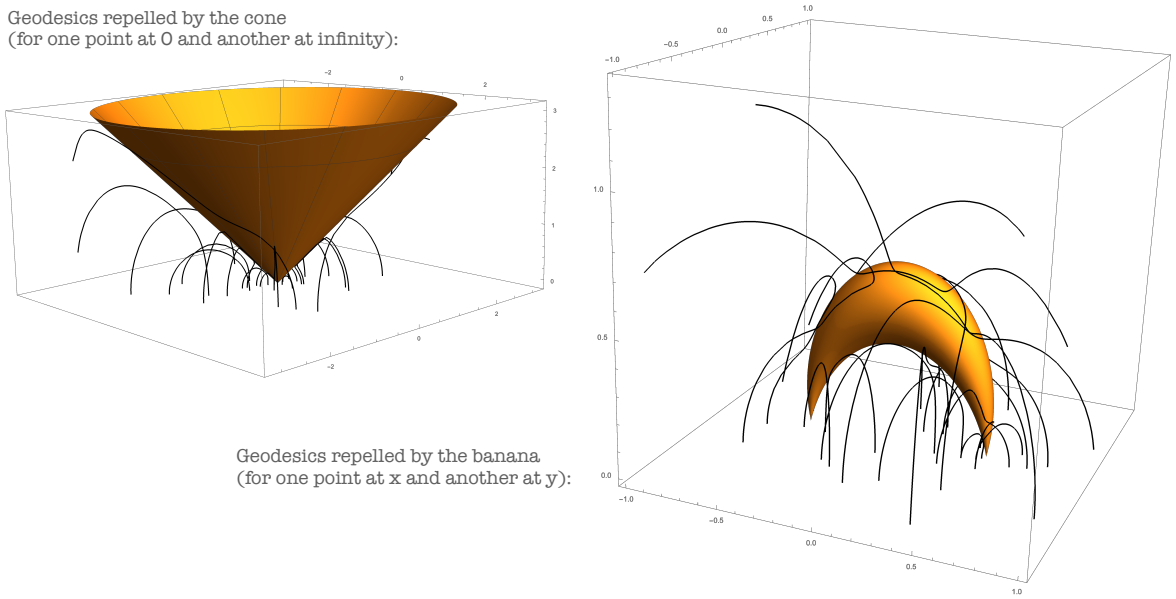

Figure 2.7: Geodesics moving in the black hole background when the stretched horizon is a cone (**left**) and when it is a banana (**right**). Unless finely tuned, geodesics do not collide with the horizon.

where

$$h(x) = \frac{6}{x-1} - \frac{(x^2+4x+1)\log(x)}{(x-1)^2} \tag{2.4.0}$$

Quite nicely, the right hand side of (2.4) coincides *precisely* with the t-channel conformal block for dimension $\Delta = 4$ and spin $J = 2$ in four spacetime dimensions,[27]

$$\log \frac{\langle \phi_H(0)\phi_L(1)\phi_L(x)\phi_H(\infty)\rangle}{\langle \phi_H(\infty)\phi_H(0)\rangle\langle \phi_L(x)\phi_L(1)\rangle} = \frac{mM}{120}\mathcal{F}(4,2,1-x,1-\bar{x}) + O(M^2) \tag{2.4.1}$$

This is the expected result for a graviton exchange dual to the stress-tensor! In the AdS_3, the action can be computed without expanding at small M and the result reads

$$S(M) - S(0) = -m\log\left((1-M)\frac{z(1-w)^{\frac{1}{2}-\frac{1}{2\sqrt{1-M}}}\bar{z}(1-\bar{w})^{\frac{1}{2}-\frac{1}{2\sqrt{1-M}}}}{w\bar{w}}\right) \tag{2.4.1}$$

where $1-w = (1-z)^{\sqrt{1-M}}$. This is nothing but the (logarithm of) the semiclassical heavy-light limit of the Virasoro block, as discussed in [47].

Similar conclusions can be obtained in other dimensions. In appendix A.2 we also discuss aspects of the conformal block decomposition, and how it depends on M. Our computation

[27] The four-dimensional blocks read

$$\mathcal{F}(\Delta, J, x, \bar{x}) = \frac{x\bar{x}}{x-\bar{x}}(h_{\frac{\Delta+l}{2}}(x)h_{\frac{\Delta-l-2}{2}}(\bar{x}) - (x \leftrightarrow \bar{x}))\,, \qquad h_\lambda(x) = x^\lambda {}_2F_1(\lambda,\lambda,2\lambda,x)\,. \tag{2.4.1}$$

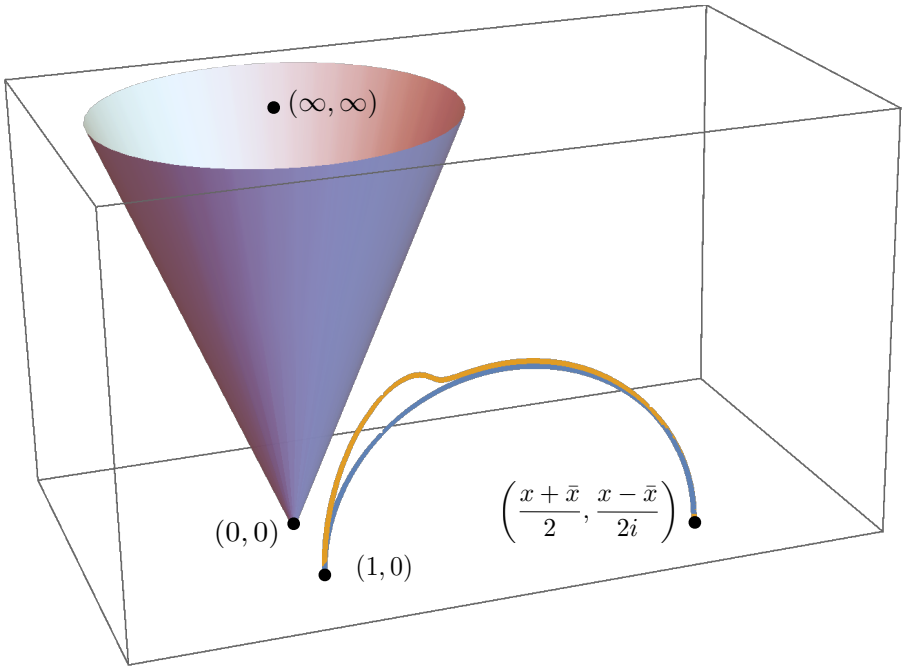

Figure 2.8: Geodesic slightly deformed by a small black hole cone. The reduced four point function is the difference between the length of the geodesic without the cone (in blue) and the geodesic deformed by the cone (in orange). Here for concreteness we plotted a case where $(x,\bar{x}) = (7/6+7i/2, 7/6-7i/2)$ and $M = 1/5$.

fits very well with the known results about the block expansion of HHLL correlators with respect to properties of OPE coefficients, *e.g.* see [45]- [48], and of geodesic Witten diagrams [49].

2.5 Discussion

Euclidean correlation functions of very heavy operators have so far been largely unexplored in AdS/CFT. These are dual to full-fledged backreacted geometries with disturbances of the metric running all the way to marked points on the Poincaré boundary of AdS. Each one of such points corresponds to the insertion of a huge operator which spreads out in the bulk and changes the AdS geometry in some way.

In this chapter, we studied two-point function geometries, and showed that the geometry is nicely understood in terms of a banana foliation, with the tips of the bananas anchored at the insertion points. For smooth geometries, we can shrink the bananas to the geodesic connecting the insertion points. For black holes instead, we can follow the bananas but only up to the location of the stretched horizon. When the black hole is super light, this stretched horizon is approximately occupying the space of a geodesic, on the other hand, when the black hole is very massive it occupies a lot of the AdS space. In all cases, we demonstrated that the onshell action of these two-point black holes reproduces the CFT result for two-point functions (2.1). In particular, the renormalized onshell action has nontrivial

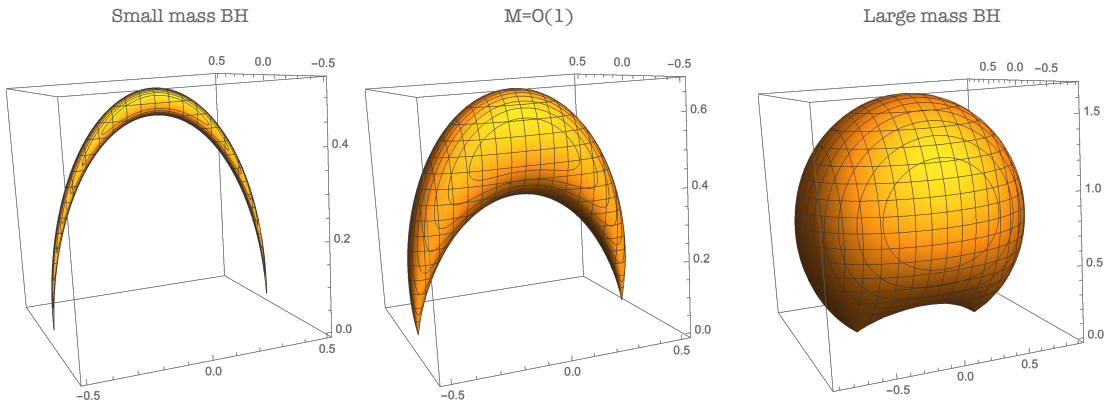

Figure 2.9: Thin bananas are effectively geodesics. Fat bananas occupy a lot of space.

spacetime dependence, coming from a logarithmic form at the marked points, and matches the dependence on the dimension $\Delta = M$ as a consequence of a crucial interplay between the boundary contribution at the AdS cut-off, and the boundary term at the stretched horizon.

For holographic two-point functions in AdS, we believe we have unveiled a pretty complete picture. The bananas are a special foliation of global AdS, which we obtained from the GtP map, and therefore this map provides a solution generating technique from global AdS geometries to two-point function geometries. It applies to all consistent truncations ansatz in string theory [12], thus AdS bubbles [50,51], charged clouds [52], and more generally, electric solutions of $\mathcal{N} = 2$ gauged SUGRA with spherically symmetric matter distributions. But there are also gravity solutions which are not consistent truncation ansatz, with interesting topology changes. A well known example are the Lin-Lunin-Maldacena geometries [53] describing all maximally heavy half-BPS operators in $\mathcal{N} = 4$ super Yang-Mills. It would be interesting to generalize our results to this case too, especially in the light of the crucial interplay between bulk and boundary contributions that yield in the end the correct two-point function.

Our main motivation for this work, though, was to set up the formalism in general, and apply it to higher point correlation functions. Something preliminary we can say about these is the following. We can always solve the FG form of a given multipoint geometry in a series expansion, once we know the expectation value of the stress-tensor. For example, for three-operators we would find,

$$ds^2\Big|_{FG} = \frac{d\mathbf{z}^2 + d\vec{\mathbf{x}}^2}{\mathbf{z}^2} + \ldots + \mathbf{z}^d \frac{\langle T_{ij}(\mathbf{x}) O_\Delta(\mathbf{x}_1) O_\Delta(\mathbf{x}_2) O_\Delta(\mathbf{x}_3)\rangle}{\langle O_\Delta(\mathbf{x}_1) O_\Delta(\mathbf{x}_2) O_\Delta(\mathbf{x}_3)\rangle} + \ldots \tag{2.5.0}$$

with the higher order contributions (in $\mathbf{z}$) determined by Einstein's equations. However, as we showed in this chapter, already for the two points the black hole geometry is a completion of the FG patch, and in particular the horizon lies beyond the wall where $\det g_{FG} = 0$. Once again, the information from the stretched horizon was crucial in order to recover the CFT result as function of $\Delta = M$. So, here comes the question. For three- and higher point functions, what lies behind this wall?

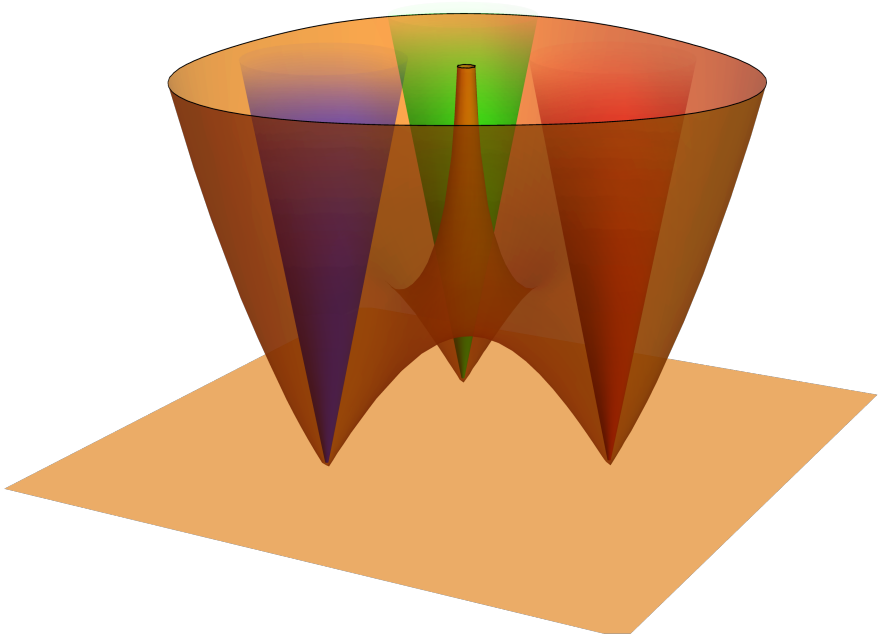

Figure 2.10: The $\det(g_{\texttt{Banados}}) = 0$ surface in the three point function case, with $d = 2$. The horizons (depicted in RGB), begin as cones. What fate awaits them far beyond the wall?

Do Euclidean three- and higher point functions of huge operators have anything to do with physics of black holes merging? How sensitive are these geometries to the microscopic details of the operators? How would firewalls or fuzzballs manifest themselves? Do averages play any role in these correlators in lower dimensions? What about in higher dimensions?

This would be a good point to stop, but we cannot resist ourselves from adding two more small comments.

2.5.1 Comment 1: Three Dimensions

Three dimensions is a great laboratory for developing intuition. In fact, in three dimensions, the exact FG metric was found by Bañados [35] and simply reads

$$ds^2 = dAdS_3 + T(\mathbf{x})d\mathbf{x}^2 + \bar{T}(\bar{\mathbf{x}})d\bar{\mathbf{x}}^2 + \mathbf{z}^2 T(\mathbf{x})\bar{T}(\bar{\mathbf{x}})d\mathbf{x}d\bar{\mathbf{x}} \tag{2.5.0}$$

where T ($\bar{T}$) are the (anti)holomorphic boundary stress tensor. For example, for a scalar three-point function, we have

$$T(\mathbf{x}) = -\frac{1}{(\mathbf{x}-x_1)(\mathbf{x}-x_2)(\mathbf{x}-x_3)} \sum_{i\neq j\neq k} \frac{M_i x_{ij} x_{ik}}{4(\mathbf{x}-x_i)} \qquad ; \qquad \bar{T}(\bar{\mathbf{x}}) = T(\bar{\mathbf{x}}) \tag{2.5.0}$$

With this assignment, ds^2 in eq. (2.5.1) describes the three-point function geometry for three black holes in $\text{AdS}_3/\text{CFT}_2$ of masses M_1, M_2, M_3 inserted at locations x_1, x_2, x_3. As in the two-point function case, this metric has a wall beyond which we need better coordinates to figure out what the geometry does. This wall is much richer than in the two-point function

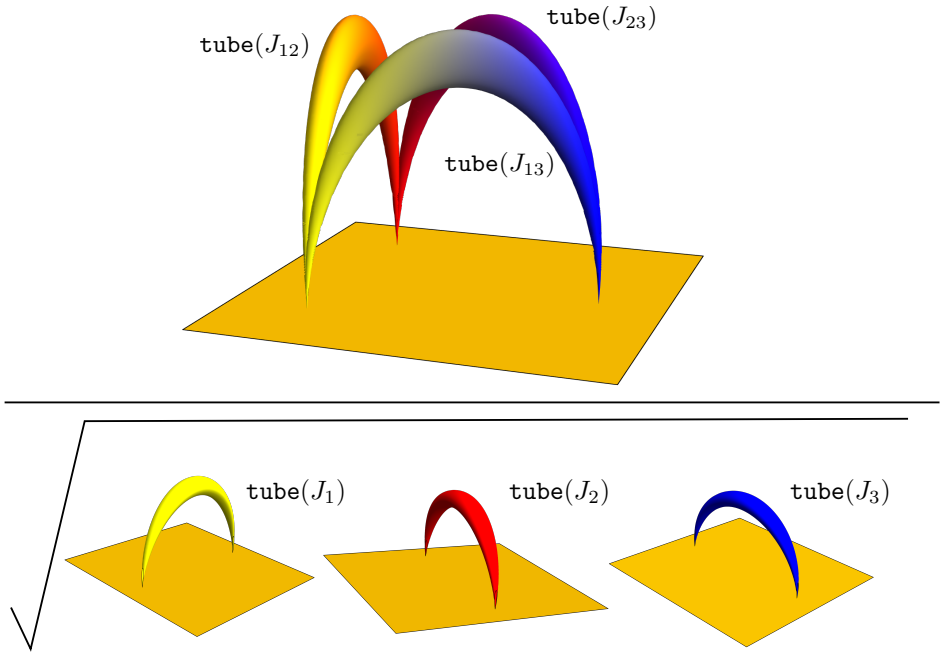

Figure 2.11: A suggestive explanation for a result like (2.5.2), where the geometry is foliated by conifolds shooting out of the insertion points like pairwise two-point function geometries.

case – see figure 2.10. What lies behind this wall? What is the full three-point function geometry and what is the corresponding structure constant in the dual field theory? This challenge is the subject of the next chapter.

2.5.2 Comment 2: LLM Three-Point Functions

What about higher dimensions? What about three-point function geometries in $\mathcal{N} = 4$ SYM? – or other maximally symmetric theories in various dimensions?

In global $AdS_5 \times S^5$ the most general half-BPS geometries are LLM geometries [53] (see also [54] for a nice review and for the holographic renormalization aspects of these geometries). In $\mathcal{N} = 4$ SYM, they correspond to operators in the Schur basis [55] of the form

$$\mathcal{O} \propto \chi_{\underline{\lambda}}(y \cdot \phi) \tag{2.5.0}$$

with Young diagram $\underline{\lambda}$ of $O(N^2)$ boxes. The vector y is a six dimensional null vector picking up a particular combination of the six scalars ϕ^I of the gauge theory. While it would be fascinating to construct general three-point functions of the operators (2.5.2) from group theory alone, one might start wondering if are there any hints or expectations that would help our intuition? Well, as we discuss below, there are some.

A three-point function,

$$\langle \mathcal{O}_1 \mathcal{O}_2 \mathcal{O}_3 \rangle = \prod_{i<j} \left(\frac{y_i \cdot y_j}{(x_i - x_j)^2} \right)^{J_{ij}} C_{\underline{\lambda}_1, \underline{\lambda}_2, \underline{\lambda}_3} \,, \tag{2.5.0}$$

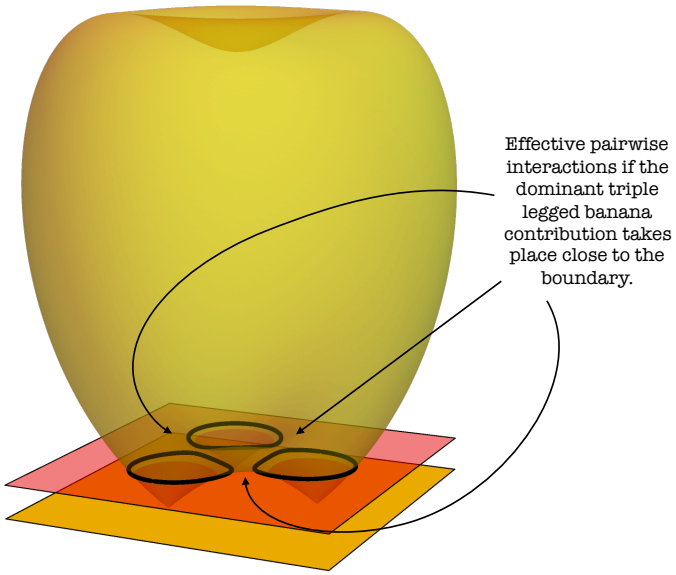

Figure 2.12: Another scenario where operators in the bulk merge, but the dominant contribution to the action is effectively pairwise because the geometry change is huge.

depends on a fixed kinematical factor, built out of the J_{ij}, *i.e.* the number of propagators between operators i and j,

$$J_{12} = \frac{J_1 + J_2 - J_3}{2}\,, \qquad J_{13} = \frac{J_1 + J_3 - J_2}{2}\,, \qquad J_{23} = \frac{J_3 + J_2 - J_1}{2}\,, \tag{2.5.0}$$

and by the structure constant C, which here is coupling independent, and therefore it can be computed in free $\mathcal{N} = 4$ SYM by Wick contractions. Computing C is thus a well-posed but not trivial combinatorial problem for any triplet $\underline{\lambda}_{i=1,2,3}$.

It would be great to solve this problem completely, or at least for operators with very large Young diagrams.[28] In a simple instance, *i.e.* when the operators are fully symmetric labelled by a Young diagram with a single row of J boxes, we did manage to find the solution (see appendix A.3 for details)

$$\tilde{C}^{\texttt{symmetric}}_{J_1 J_2 J_3} \equiv \frac{{}_3F_2(-J_{12}, -J_{13}, -J_{23}; 1, 1-N-\frac{J_1+J_2+J_3}{2}; 1)(N)_{\frac{J_1+J_2+J_3}{2}}}{(-)^{\frac{J_1+J_2+J_3}{2}}\sqrt{(-N-J_1+1)_{J_1}(-N-J_2+1)_{J_2}(-N-J_3+1)_{J_3}}}\,. \tag{2.5.0}$$

The $\tilde{C}$ is normalised by two-point functions, and the hypergeomtric function ${}_3F_2$ accounts for genuine interactions among the three operators; when the $J_{i=1,2,3} \in \mathbb{N}$ it evaluates to a non trivial polynomial of N. In the limit when $J_i = N^2 j_i$ the result simplifies to:

$$\log \tilde{C}^{\texttt{symmetric}}_{J_1 J_2 J_3} \simeq -N^2\Big[\sum_{ij} \texttt{tube}(j_{ij}) - \tfrac{1}{2}\sum_{i} \texttt{tube}(j_i)\Big] \qquad \text{with} \quad \texttt{tube}(j) = j\log j\,. \tag{2.5.0}$$

[28] Everything we discuss in this section should have a nice embedding in twisted holography [56–58] which would be fascinating to work out.

Even though $\tilde{C}^{\texttt{symmetric}}_{J_1J_2J_3}$ is telling us something only about the limit of a regular geometry, where each individual operator is dual to a thin ring that is taken off to infinity with respect to the $AdS_5\times S^5$ droplet [54], the expression we got is quite suggestive.

In fact, we can rewrite the asymptotics as

$$\lim_{N\gg 1} \underbrace{\frac{J_1!J_2!J_3!}{(\frac{J_1+J_2-J_3}{2})!(\frac{J_1+J_3-J_2}{2})!(\frac{J_2+J_3-J_1}{2})!}}_{\#\,\texttt{Wick contractions at 3pt}} \times \underbrace{\frac{1}{\sqrt{J_1!J_2!J_3!}}}_{\texttt{2pt normalisation}} \simeq e^{N^2\left[\frac{1}{2}\sum_i j_i\log j_i - \sum_{ij} j_{ij}\log j_{ij})\right]} \quad (2.5.0)$$

showing that it coincides with the leading asymptotics of the number of Wick contractions for three-points, when $J_i = N^2 j_i$, divided by two-point normalizations. In other words, we get a purely combinatorial result. Note now that a LLM operator generically involves multi-particle states and that the `tube` function is the building block for the two-point function normalization. So what if when $J \gg N$ the operator $\mathcal{O}$ breaks apart and the bulk geometry is foliated as in figure 2.11? with conifold geometries emerging from the insertion points?

Another scenario, which was inspired to us by a beautiful talk of David Simmons-Duffin at KITP in January 2023, is represented in figure 2.12 – see [59]. There we imagine that each operator shoots from the boundary a huge geometry change, like the fat bananas in the figure, so that interactions among the three operators are effectively pairwise. This scenario could also reproduce something like eq. (2.5.2).

We look forward to continuing to explore huge correlators, from the boundary, as well as from the bulk.

Chapter 3

Correlations Functions of Heavy Operators in $\mathbf{AdS}_3/\mathbf{CFT}_2$

3.1 Introduction

In chapter 2, we initiated the study of holographic correlation functions in $\mathrm{AdS}_{d+1}/\mathrm{CFT}_d$ that involve huge operators at the insertion points. By "huge", we mean operators of very large conformal dimension, such that their dual description is heavy enough to backreact and change the bulk geometry (*i.e.* $\Delta \sim L_{\mathrm{AdS}}^{d-1}/G_{\mathrm{N}}$). For two-point functions, the new backreacted geometries were referred to as "spacetime bananas", and to illustrate their features, we discussed heavy scalar operators that create an AdS-Schwarzschild black hole in the bulk. Inspired by this two-point function construction, one of the goals we envisioned in [1] was to understand what geometries describe three- and higher point functions for huge operators. In this chapter, we address this program for asymptotically AdS_3 spacetimes. By taking advantage of the simplicity of pure three-dimensional Einstein gravity, we will construct the geometries dual to huge three-point functions and establish a general formalism of "domes and doors" which could be applied in the future to higher multipoint correlators.

As discussed in chapter 2, the backreaction of the dual operators on the bulk geometry induces an expectation value for the boundary stress tensor [60], which is interpreted as

$$\langle\, T_{ij}(\vec{\mathbf{x}})\,\rangle = \frac{\left\langle T_{ij}(\vec{\mathbf{x}}) \prod_{k=1}^{n} O_{\Delta_k}(\vec{x}_k)\right\rangle}{\left\langle \prod_{i=k}^{n} O_{\Delta_k}(\vec{x}_k)\right\rangle}\,. \tag{3.1.0}$$

That is, the boundary expectation value corresponds to the stress tensor induced by the insertion of the various huge operators in the correlation function. We make use of this general result with two simplifications in the present work: First, we set the boundary dimension $d = 2$, *i.e.* we examine holographic correlations functions for asymptotically AdS_3 geometries. Second, we examine the correlation function of three huge scalar operators, *i.e.* $n = 3$. Let us add that for the most part, our calculations are done in Euclidean signature.[1]

[1] We will consider adding a Lorentzian component to the geometry in section 3.3.2.

It will be convenient to parameterize the conformal dimensions of the three heavy scalar primary operators as $\Delta_j = \frac{c}{12} M_j$, where $c = 3L_{\text{AdS}}/2G_{\text{N}}$ is the central charge in the boundary CFT_2. Now taking the two-dimensional boundary geometry to be the plane,[2] we insert these operators at locations z_j and eq. (3.1) yields

$$\langle T_{zz}(z)\rangle = \frac{c}{24}\,\frac{1}{(z-z_1)(z-z_2)(z-z_3)}\sum_i \frac{M_i \prod_{j\neq i}(z_i - z_j)}{z - z_i} \tag{3.1.0}$$

for the holomorphic component of the stress tensor. Of course, the anti-holomorphic stress tensor has an identical expectation value with $z \to \bar{z}$.

In passing, we note that for any (order one) value of the M_j, the insertion of these boundary operators will result in a deformed bulk geometry. However, there are two distinct regimes: for $M_j > 1$, the operators are dual to black holes while for $M_j < 1$, they describe conical defects in the bulk. For the most part, we focus on the black hole regime. However, we return to consider defect geometries in section 3.6.

Now combining data of the flat metric for the CFT_2 background and the expectation value of the stress tensor, we have sufficient boundary conditions to solve for the bulk geometry in a Fefferman-Graham (FG) expansion [61]. A remarkable fact about three-dimensional gravity is that the FG expansion of the metric sourced by (3.1) truncates at a finite order. The resulting metric was studied by Bañados [35],

$$ds^2 = \frac{dy^2 + dz d\bar{z}}{y^2} + L(z)dz^2 + \bar{L}(\bar{z})d\bar{z}^2 + y^2 L(z)\bar{L}(\bar{z})dzd\bar{z} \tag{3.1.0}$$

where $\langle T_{zz}(z)\rangle = -\frac{c}{6}L(z)$ and $\langle T_{\mathbf{zz}}(\mathbf{z})\rangle = -\frac{c}{6}\bar{L}(\mathbf{z})$. This metric is a solution to Einstein's equations for any L and $\bar{L}$. The simplicity of the FG expansion, which truncates at order y^2, can be seen as a reflection of the lack of propagating degrees of freedom in three-dimensional Einstein gravity.

Simple as it may appear, the Bañados metric (3.1) with stress tensor (3.1) contains a great deal of interesting physics. First of all, the coordinates in this metric do not cover the full space: there is a coordinate singularity where $\det(g) = 0$, which we call the "wall", and is depicted in figure 3.1. The presence of a wall is a generic feature of the Bañados metric (3.1). For example, there is also a wall for the two-point function geometry, as noted in chapter 2. However, as we saw in that chapter, for the two-point correlator the geometry beyond the wall is easily revealed by a coordinate transformation to the more familiar AdS-Schwarzschild black hole. For the three-point correlator (3.1), the extension is not immediate and needs to be constructed. This will be one of the main goals of this chapter.

One approach of constructing the complete three-point function geometry is to exploit the fact that all solutions in three-dimensional Einstein gravity with negative cosmological constant are locally isometric to AdS_3. That is, all solutions can be cast as AdS_3 with identifications. To find the required identifications, we will start from the beautiful analysis done by Roberts [62] – see Appendix B.1 for a review – where it was shown that the change

[2] Here z is the usual complex coordinate on the plane.

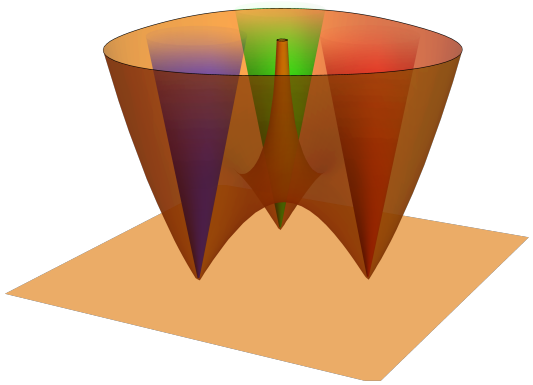

Figure 3.1: The $\det(g) = 0$ wall for the three-point geometry, with the horizons hidden within.

of coordinates

$$\left(Y, Z, \bar{Z}\right) = \left(0, f, \bar{f}\right) + \frac{y}{f'\bar{f}' + y^2\, f''\,\bar{f}''/4}\left((f'\bar{f}')^{3/2}, -y(f')^2\bar{f}''/2, -y(\bar{f}')^2 f''/2\right) \tag{3.1.0}$$

maps the solution with the Bañados metric (3.1) into Euclidean AdS_3 in Poincaré coordinates,

$$ds^2_{AdS_3} = \frac{dY^2 + dZd\bar{Z}}{Y^2}\,. \tag{3.1.0}$$

This map is determined in terms of two boundary functions $f(z)$ and $\bar{f}(\bar{z})$, and the Schwarzian derivatives of these determine $L(z)$ and $\bar{L}(\bar{z})$,

$$L(z) = -\tfrac{1}{2}\{f, z\} \qquad ; \qquad \bar{L}(\bar{z}) = -\tfrac{1}{2}\{\bar{f}, \bar{z}\}. \tag{3.1.0}$$

Thus, from (3.1), we will be able to understand what identifications of AdS_3 are needed in order to construct the three-point geometry, and in particular, the extension beyond the wall.

Considering the two-point function geometry as an example, one can represent the Euclidean BTZ black hole in terms of AdS_3 with identifications – see figure 3.2. On the boundary, one finds a torus described by identifying (up to a Weyl rescaling) a pair of circles in the $(Z, \bar{Z})$-plane. Extending the identification into the bulk, these circles become the asymptotic boundaries of two domes, which are identified in the AdS_3 bulk. Now, the angular direction in the $(Z, \bar{Z})$-plane represents the Euclidean time direction. In the standard approach of black hole thermodynamics, an angular periodicity of 2π is imposed, which results in a smooth geometry in the bulk, *i.e.* the usual hyperbolic solid torus considered in *e.g.* [10, 63, 64]. However, for the two-point correlator, as argued in chapter 2, we need to decompactify the Euclidean time direction and introduce instead a branch cut in the $(Z, \bar{Z})$-plane – the purple line in figure 3.2(a). The figure then represents one sheet of an infinite cylindrical covering geometry. In the bulk, this cut extends to a two-dimensional surface, which we denote as the "door" – the purple surface in figure 3.2(b). The door reaches up to the conical singularity at the horizon (the vertical, dashed line). As on the boundary, there is now an infinite sequence

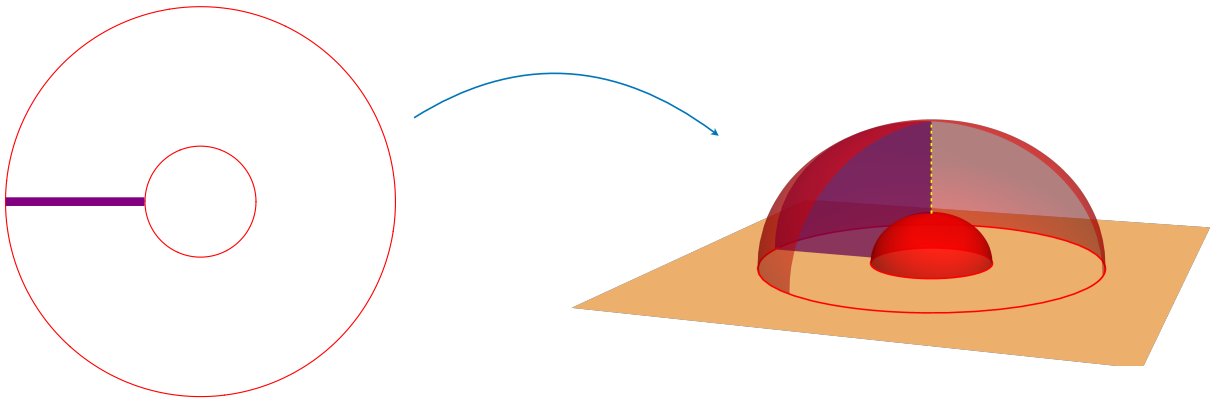

(a) Starting from Bañados, we find identifications at the boundary.

(b) Extending the identifications into the bulk, they become domes.

Figure 3.2: Representing the Euclidean BTZ black hole in terms of AdS_3 with identifications. On the boundary shown in panel (a), one finds a torus where the two circles are identified. Extending the identification into the bulk, these circles become the asymptotic boundaries of the domes shown in panel (b).

of identical sheets in the bulk. Approaching one of the black hole operator insertions means circling around the geometry and going through the door infinitely many times.

Explaining the corresponding picture for the three-point function is the first key result of this chapter. The second will be reproducing the universal formula for the OPE structure constant in the regime of huge operators, as predicted in [65] (see also [66–68]). This universal OPE formula is related to the structure constants of Liouville theory, expressed by the DOZZ formula [69–71] (see also [72]). As we will see, the holographic renormalization of the geometries dual to correlation functions of heavy operators involves classical solutions of the Liouville equations. It is through this connection that we find the anticipated universal expression for the OPE coefficients.

The remainder of the chapter is organized as follows: In section 3.2 we examine description of the two-point function geometry in terms of "domes and doors", in more detail. Of course, this is simply a new perspective of the same geometry that we discussed in chapter 2. This discussion is a warm up to familiarize the reader with this new description, which we then apply to describe the the three point function geometry in section 3.3. For three black hole operators, we will see that the extension of the Bañados metric involves a single room with three doors, and six infinite sequences of rooms with one door each. In section 3.4, we explain a connection between these three-dimensional solutions and classical solutions in Liouville theory. Then, in section 3.5, we exploit this connection to evaluate the onshell action of these geometries. In agreement with predictions from the modular bootstrap [65], we will reproduce the expected classical limit of the Liouville three-point function. As noted above, there are two regimes for the conformal dimensions, producing either black holes or conical defects in the bulk. In section 3.6, we discuss the latter. Although the defect geometries are considerably different, *e.g.* see figure 3.17, we show that the domes-and-doors

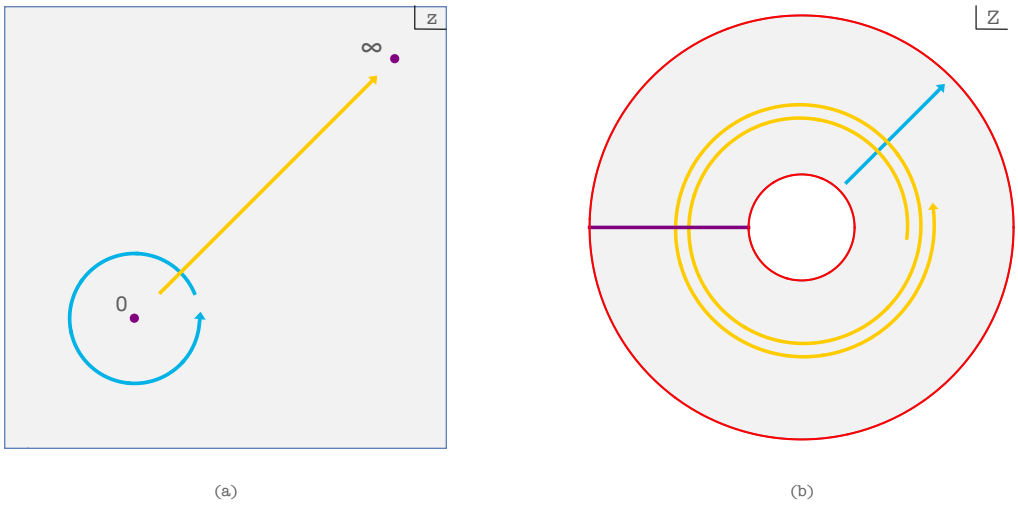

(a) (b)

Figure 3.3: The map $z \to Z = z^{iR_h}$ swaps dilatations and rotations in the two planes. The identification $z = e^{2\pi i} z$ restricts the region of interest in the $(Z, \bar{Z})$-plane to an annulus. Moving along an arbitrary ray in the $(z, \mathbf{z})$-plane, from 0 and ∞, translates into the need for an infinite covering of this annulus in the $(Z, \bar{Z})$-plane. Hence, we introduce a branch cut represented by the purple line on the right. Passing through this cut infinitely many times in the clockwise/anti-clockwise direction means asymptotically approaching the origin/infinity in the $(z, \mathbf{z})$-plane, where the two insertions lie.

framework smoothly interpolates from black holes to the defect geometries studied in [11,73]. We conclude by listing some open problems and musing about some higher dimensional speculations in section 3.7.

3.2 Two-point Function. The Banana is a Door.

The two-point function case is given by the Bañados metric (3.1) with[3]

$$L(z) = -\frac{M(z_1 - z_2)^2}{4(z - z_1)^2(z - z_2)^2}\,. \tag{3.2.0}$$

Here (and henceforth in this chapter) we are setting $\bar{L} = L$ as is the case for spinless objects. This geometry also arises in the study of the entanglement properties of the state prepared by one of the heavy operators acting on the vacuum, see [74].

As already highlighted in chapter 2, the Bañados metric only describes the two-point geometry in a coordinate patch which extends from the asymptotic AdS boundary (at small

[3]The resulting Bañados metric coincides with the cone metric considered in chapter 2 for three dimensions, namely

$$ds^2 = \frac{1}{\mathbf{y}^2}\left[d\mathbf{y}^2 + (1 - \tfrac{M\mathbf{y}^2}{4\mathbf{R}^2})^2 d\mathbf{R}^2 + (1 + \tfrac{M\mathbf{y}^2}{4\mathbf{R}^2})^2 \mathbf{R}^2 d\theta^2\right]$$

where we introduced polar coordinates on the z plane, $z = \mathbf{R}e^{i\theta}$.

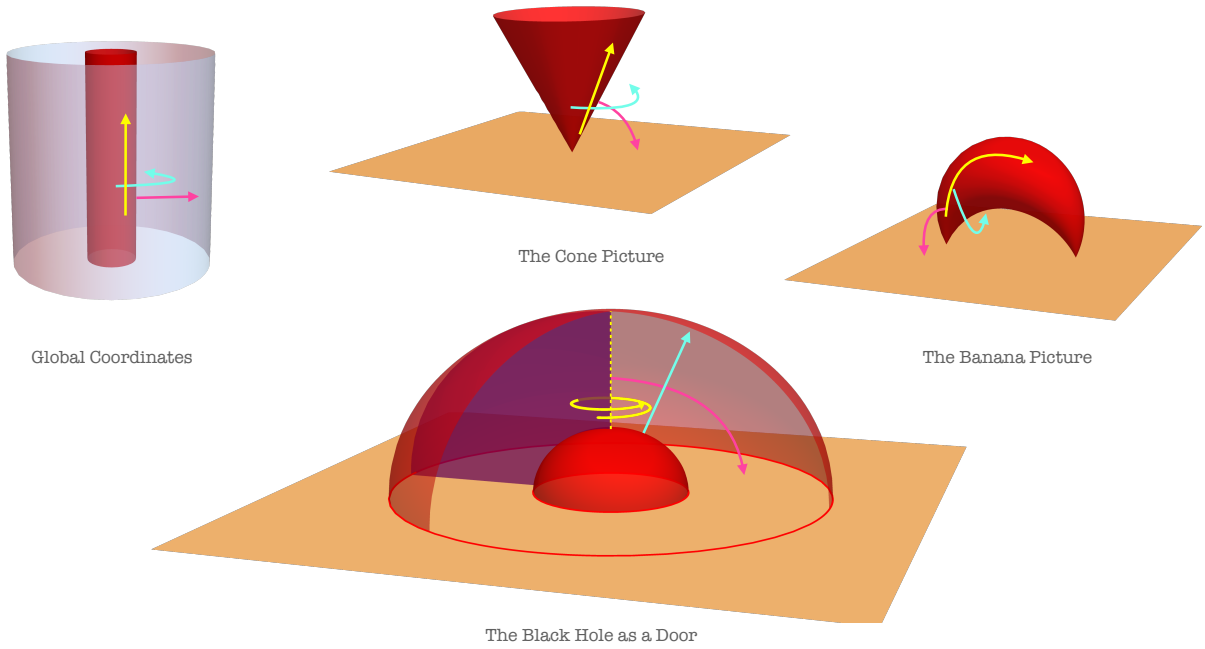

Figure 3.4: In the bottom panel, the two-point function geometry is shown as an infinite branched cover of the solid torus usually used to describe the Euclidean BTZ black hole. To represent the covering space, we introduce a branch cut or "door", shown in purple. Passing through the door, leads to an identical copy of the solid torus. The top three panels show the geometry adapted to three different coordinate systems considered in chapter 2 The far left panel shows the directions for the Euclidean time (yellow), radius (red) and angle (green) in global coordinates. The corresponding directions are shown in the other panels for other coordinate systems. In the dome-and-door illustration, the Euclidean time direction corresponds to angular rotations in the $(Z, \bar{Z})$-plane. Hence, approaching one of the operator insertions corresponds to rotating infinitely many times in one direction or the other. The axis of this rotation is the horizon (the vertical yellow dashed line).

y) up to where $\det(g) = 0$, *i.e.* the surface

$$y^4 L(z)\bar{L}(\bar{z}) = 1\,. \tag{3.2.0}$$

Note that when the boundary stress tensor has poles, as it always does when there are local operator insertions in the CFT_2, this surface will extend all the way to the conformal boundary at $y = 0$.

As noted in the introduction, we can extend beyond the wall by finding the identifications needed to construct the full geometry as a quotient of Euclidean AdS_3. These identifications can be read off from the Roberts map (3.1) by noting that the boundary $y = 0$ and $(z, \bar{z})$ is mapped into the boundary $Y = 0$ with $(Z, \bar{Z}) = (f(z), \bar{f}(\bar{z}))$. Hence these two functions have a clean geometrical interpretation as describing how the two boundary geometries map into one another. Similar considerations can be drawn for a neighbourhood of the boundary, where the Roberts map is well-defined.

For a two-point function in the black hole regime (*i.e.* with $M > 1$), with the insertion

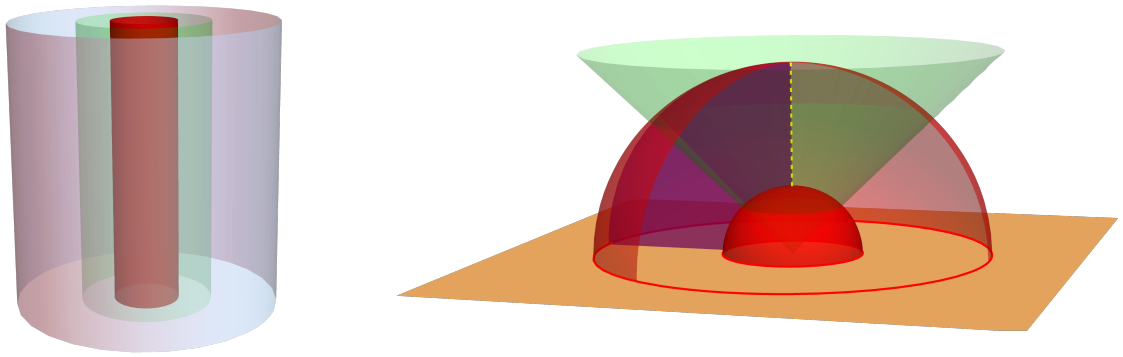

(a) Global Coordinates

(b) Black Hole as a Door

Figure 3.5: In the Bañados patch, the horizon is hidden behind the $\det(g)$ wall (in green). In global coordinates in panel (a), the horizon is at $r = R_h = \sqrt{M-1}$ while the wall sits at $r = \sqrt{M} > R_h$. Under the Roberts map, the $\det(g)$ wall is mapped to a cone shown in panel (b).

points at zero and infinity, eq. (3.2) reduces to $L(z) = -\frac{M}{4z^2}$ and $\bar{L}(\bar{z}) = -\frac{M}{4\mathbf{z}^2}$, and we find

$$f_{\text{BH}}(z) = z^{iR_h} \quad ; \quad \bar{f}_{\text{BH}}(\bar{z}) = \bar{z}^{-iR_h} \quad ; \quad R_h = \sqrt{M-1} \in \mathbb{R}^+ \,. \tag{3.2.0}$$

Recall that $R_h = \sqrt{M-1}$ would correspond to the horizon radius of the black hole in global coordinates. Note that f_{BH} and $\bar{f}_{\text{BH}}$ are conjugates of each other, and so the Roberts map sends the Bañados patch into the real Euclidean AdS_3. Because the exponents are purely imaginary, we see that travelling along a ray from the origin to infinity in the z plane will correspond to rotating infinitely many times in the $(Z, \bar{Z})$-plane around the origin. That is, on the boundary, eq. (3.2) yields

$$z = e^{\tau + i\phi} \quad \longrightarrow \quad Z = e^{iR_h\tau - R_h\phi} \tag{3.2.0}$$

Hence going to $z = 0$ at fixed ϕ corresponds to $\tau \to -\infty$, which corresponds to an infinite number of clockwise rotations at fixed radius in the the $(Z, \bar{Z})$-plane, and similarly for $z \to \infty$. In order to cover the two-point function geometry we need to cover the $(Z, \bar{Z})$-plane infinitely many times as we go around the origin. To connect all these infinitely many (in this case) identical sheets, we add a branch cut anchored at the origin and extending out along the negative real axis (*i.e.* $\phi = \pi$). Crossing the cut allows one to move from one sheet to another on the boundary.

Conversely, rotating around the $(z, \bar{z}) = (0, 0)$ point corresponds to travelling along a ray in the $(Z, \bar{Z})$-plane. Under a 2π rotation in the z plane, we find $\sqrt{Z\bar{Z}} \to \sqrt{Z\bar{Z}}e^{2\pi R_h}$. Hence we can restrict region of interest in the $(Z, \bar{Z})$ plane to an annulus between two radii, R_1 and $R_2 = R_1 e^{2\pi R_h}$, which are identified. Any choice of R_1 is as good as any other since this is just a choice of origin for the polar angle in the $(z, \bar{z})$-plane. All in all, we end up with the geometry described in figure 3.3.

The boundary identifications and branch cuts in the $(Z, \bar{Z})$-plane extend into the bulk, as shown in the bottom panel of figure 3.4. Extending the cut to a two-dimensional surface in

the bulk leads to our notion of a "door" (shown in purple). Note that in the bulk, the branch cut is also bounded by the axis of rotation, *i.e.* the vertical line $Z = 0 = \bar{Z}$. In passing through the door, one moves from one sheet to another in the bulk. Similarly, the boundary annulus is promoted to the bulk region between a pair of concentric domes. These domes are identified and so upon passing through the outer dome, one emerges again into the same region from the inner dome. The black hole horizon is the geodesic line $(Z, \bar{Z}) = 0$ that travels vertically between the domes, and as noted above, it serves as part of the doorframe.

As emphasized in figure 3.4, the dome-and-door construction is simply an alternative description of the geometry studied in chapter 2. In particular, we can write the change of variables from empty AdS_3 in eq. (3.1) to the "cone" metric, by composing the known change of variables to the BTZ black hole [75], namely

$$Y = \frac{R_h}{r} e^{R_h \phi} \quad ; \quad Z = \sqrt{1 - \frac{R_h^2}{r^2}}\, e^{R_h(\phi + i\tau)} \quad ; \quad \bar{Z} = \sqrt{1 - \frac{R_h^2}{r^2}}\, e^{R_h(\phi - i\tau)}\,, \tag{3.2.0}$$

with the Global-to-Poincare map introduced in chapter 2. The "banana" geometry is then obtained by a change of coordinates that acts as a special conformal transformation on the boundary.

Let us add that in the dome-and-door construction, we could use isometries of AdS_3 to obtain an infinite family of equivalent pictures where the boundary circles are no longer concentric – see details in appendix B.1. In this case, the horizon becomes a semicircular geodesic between the domes. The door again extends between the domes, and from the asymptotic boundary to the horizon. These different realizations of the two-point function geometry will make an appearance in the following section.

To summarize, we note that the Bañados coordinates break down at the wall (3.2). For the two-point geometry, this becomes the cone shown in green in figure 3.5(b). This cone corresponds to a cylinder in the global coordinates describing the BTZ black hole, which hides the horizon behind it, as depicted in figure 3.5(a). By mapping the Bañados patch isometrically into Euclidean AdS_3, we found a simple construction of the solution using identifications along spherical domes plus a door extending between them. This geometry can be readily extended beyond the wall (*i.e.* the green cone) to get the complete geometry depicted in figure 3.5(b). In this complete geometry, the horizon is the vertical geodesic going from the tip of the inner dome to the tip of the outer dome. As discussed in the introduction, were it not for the door, this geometry would be the well-known story for how to construct Euclidean AdS-Schwarzschild in three dimensions as a quotient of Euclidean AdS_3.

3.3 The 3pt Function Wormhole. A Room with Three Doors.

Having reviewed the two-point function geometry as AdS_3 with identifications, we are ready to discuss the three-point function geometry. Recall that the corresponding expectation value of the stress tensor is given by (3.1), namely

$$L(z) = -\frac{1}{(z - z_1)(z - z_2)(z - z_3)} \sum_i \frac{M_i \prod_{j \neq i} z_{ij}}{4(z - z_i)} \tag{3.3.0}$$

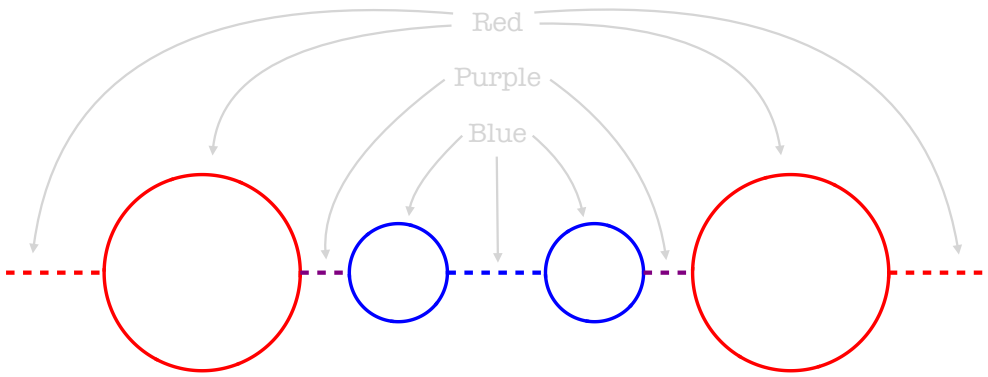

Figure 3.6: The identifications (solid lines) at the boundary of the three-point function geometry. Gluing the circles that share a color creates a genus-two surface. The boundary of the three-point function geometry involves a covering of this surface with infinitely many sheets. To pass between these sheets we introduced a series of branch cuts along the real axis (dashed lines).

with $z_{ij} = z_i - z_j$. Assuming the operators are inserted at $z_1 = 0$, $z_2 = \infty$ and $z_3 = 1$ for convenience, a particular $f(z)$ that solves the Schwarzian equation (3.1) for $L(z)$ in (3.3), and determines the Roberts map (3.1), is [4]

$$f_{\mathtt{3pt}}(z) = i\mathcal{N} z^{iR_1} \frac{{}_2F_1\left(\frac{1}{2} + i\frac{R_1-R_2-R_3}{2}, \frac{1}{2} + i\frac{R_1+R_2-R_3}{2}; 1 + iR_1; z\right)}{{}_2F_1\left(\frac{1}{2} - i\frac{R_1-R_2+R_3}{2}, \frac{1}{2} - i\frac{R_1+R_2+R_3}{2}; 1 - iR_1; z\right)} \,. \tag{3.3.0}$$

Then, we pick $\bar{f}_{\mathtt{3pt}}$ to be the complex conjugate of $f_{\mathtt{3pt}}$, so that eq. (3.1) is real. We have introduced $R_i = \sqrt{M_i - 1} \in \mathbb{R}^+$, which correspond to the horizon radii for the dual black holes.

The function $f_{\mathtt{3pt}}(z)$, also known as the *Schwarz triangle function*, has branch points at the locations of the operator insertions. We can choose the branch cuts to run from 0 to ∞ along the negative real z axis, and from 1 to ∞ along the positive real axis. With this choice, we can then investigate the images of each side of these branch cuts, which is a pair of circles, and start building up our three-point function geometry.

In order to describe our geometry in a simple way, we will consider the setup of figure 3.6. For this figure we have used the isometries of Euclidean AdS_3 to put the circles defining the identifications on the boundary into a standard configuration, where they are aligned symmetrically along the real axis.[5] The color code indicates which circles are to be glued to one another. Performing these identifications produces a genus-2 surface. However, just

[4] Here $\mathcal{N}^2 = \frac{\Gamma^2(-iR_1)}{\Gamma^2(+iR_1)} \frac{\gamma\left(\frac{1+i(R_1+R_2+R_3)}{2}\right)\gamma\left(\frac{1+i(R_1-R_2+R_3)}{2}\right)}{\gamma\left(\frac{1-i(R_1+R_2-R_3)}{2}\right)\gamma\left(\frac{1-i(R_1-R_2-R_3)}{2}\right)}$, where $\gamma(x) = \Gamma(1-x)/\Gamma(x)$. Different solutions to the Schwarzian equation are related to each other by Möbius transformations of f, as described in appendix B.1. We have made a specific choice here (particularly, for the phase described by $\mathcal{N}$), so that the monodromy of $f_{\mathtt{3pt}}$ around the operator insertion at z=1 acts as an isometry of the hyperbolic plane, *e.g.* see [76]. This choice will ensure that it yields a smooth, single-valued solution to the Liouville equation in section 3.4.

[5] This requires composing $f_{\mathtt{3pt}}(z)$ with a Möbius transformation of the AdS_3 boundary – see appendix B.1.

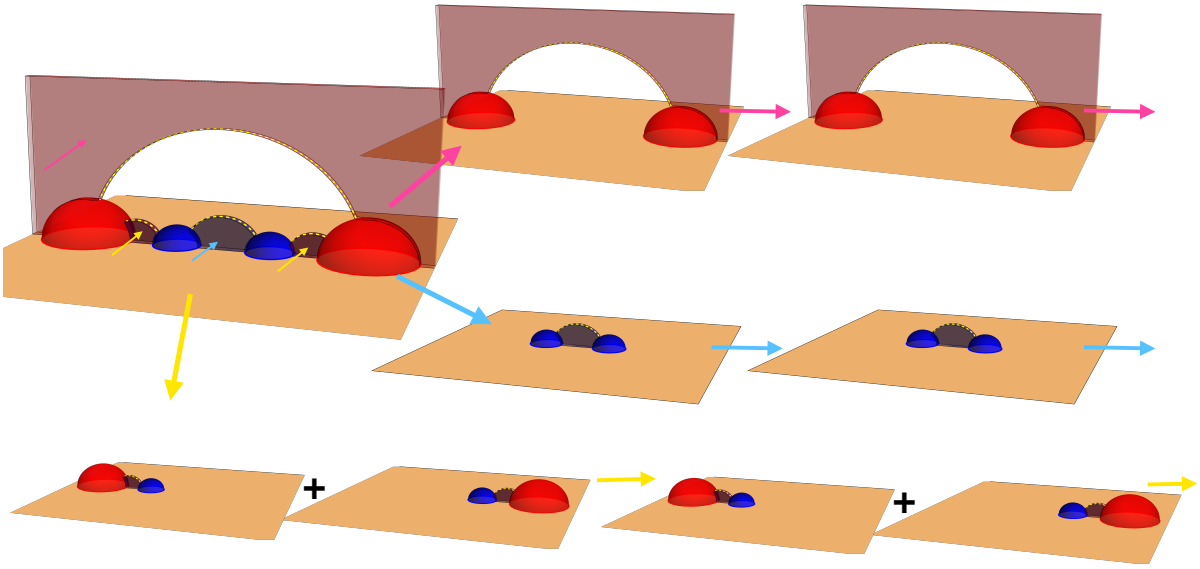

Figure 3.7: The three-point function geometry consists of a central room with all of the domes present and three doors anchored to the three horizons. Passing through any of these leads to an infinite sequence of rooms with fewer domes. One of the doors (shown in purple) is split into two pieces that are glued together by the domes. This splitting continues as we travel down the corresponding infinite sequence of rooms.

as in the two-point function geometry, approaching one of the operator insertions translates into rotating infinitely many times around these circles. The corresponding branch cuts are drawn as dashed lines along the real axis in the figure.[6] To have a concrete realization in mind, let us say that crossing the red cut infinitely many times leads to the operator at z_1, while crossing the purple door leads to the operator at z_2, and crossing the blue door leads to the operator at z_3. Recall that passing through each branch cut leads to a new sheet on the boundary. The crucial novelty compared to the two-point function case is to realize that on each of these other sheets, we encounter only a subset of circles. This can be understood by noting that only one of the branch cuts is visible in a domain close to a given operator. Further, let us note that since the cuts cover the entire real axis (between the circles), it is impossible to find a path (in the boundary) which would take us from the bottom of the figure to the top side.

When we extend the boundary identifications into the bulk, each pair of boundary circles extends to a pair of domes which are identified in the bulk. Further, there are three (closed) geodesics connecting the domes, which we refer to as the three horizons. The three boundary cuts now extend to three doors in the bulk, each of which stretch from the asymptotic boundary to the corresponding horizon. If it were not for the doors, this would be the familiar genus-2 handlebody solution, encountered in *e.g.* [63, 77, 78].

[6] Note that the purple cut which extends between the red and blue circles has two components that are glued into a single cut by the quotient.

3.3.1 Appearance of a Wormhole

From our discussion so far, we have found that the three-point function geometry consists of a junction of "chambers" – see figure 3.7. There is a single central chamber, which is special because all of the domes and doors appear there. For each of the three horizons, there is a door and passing from the central chamber through one of the doors leads to a "leg", which is sequence of new chambers, each of which is isometric to the two-point function geometry. That is, in each of the leg chambers, we see only a subset of the domes and a single door, exactly what is needed to construct the two-point geometry discussed in the previous section. So the most surprising aspect of our dome-and-door construction is that when we take into account that we can leave the central chamber through either side of the door, there are in total *six* "legs". But the two-point function discussion suggests that each leg corresponds to an operator insertion, so we would have expected only three!

The resolution to this "puzzle" is found by reconsidering the boundary of the geometry. As we pointed out above, the presence of the branch cuts along the real axis (in figure 3.6) splits the boundary of the central chamber into two disconnected pieces. That is, if we start near the bottom of the figure we can only access three of the legs since we can only pass through the cuts from below. However, as shown in figure 3.7, we can start from one side of the boundary and reach the other by following a path through the bulk that passes through the gap between the three horizons. Any curve going from one side of a given door to the other necessarily leaves the boundary and crosses through the bulk. So we see that the three-point function geometry is not a single sided geometry but rather a Euclidean *wormhole* with two asymptotic regions!

Hence the central chamber plays a special role in connecting the two asymptotic boundaries of the wormhole. In this context, the "convex hull" bounded by the three horizons on the surface $Z = \bar{Z}$ becomes the mouth of the wormhole, *i.e.* the extremal surface at the center of the wormhole. A convenient set of coordinates to describe the wormhole metric is given the following "book page" ansatz [26, 79],

$$ds^2 = d\rho^2 + \cosh^2\rho \; d\Sigma^2 \tag{3.3.0}$$

where the metric $d\Sigma^2(w, \bar{w})$ has constant negative curvature. The two asymptotic AdS_3 boundaries are reached with $\rho \to \pm\infty$. As we explained above, they are separated by the doors. It will be the purpose of section 3.4 to describe $d\Sigma^2$ for the three-point function geometry.

It should be noted at this point that semiclassical gravity will not distinguish CFT states whose dimensions are very close in the spectrum [23]. As a result, in the limit of large central charge, we should expect holographic CFT observables to show an "erratic" behaviour coming from averaging over states in a narrow band of the conformal dimensions $\Delta_j = \frac{c}{12} M_j$. While for the two-point function geometry averaging does not play a role, for the three-point function geometry that we just constructed, the appearance of a wormhole connecting two asymptotic AdS boundaries suggests a different conclusion. Multi-boundary Euclidean geometries have recently been the subject of many interesting developments, see *e.g.* [7, 11, 24, 79–82], and at least in some cases can be understood holographically as contributing to the moments of CFT observables averaged over appropriately defined *ensembles* of CFT's.

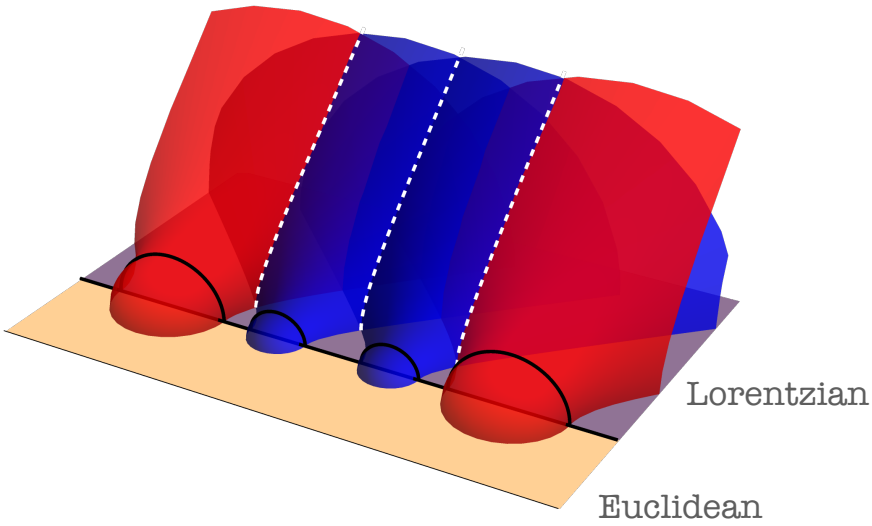

Figure 3.8: A Lorentzian cap is obtained by Wick rotating $\rho \to it$. The domes in the Euclidean part of the geometry, become hyperboloids in Lorentzian signature. The black hole singularities are the result of the intersections of the hyperboloids, which we represent here as a white dashed lines. Note that there is another singularity 'at infinity' where the two red hyperboloids intersect. Further, there is a single asymptotic region between the red and blue hyperboloids, which is split into two pieces in the diagram. (This is analogous to the splitting of the purple door in figure 3.7.)

This suggests that rather than calculating the value of a specific three-point function, the geometry we have constructed here should be interpreted as a contribution to the *variance* of the three-point function over some ensemble of CFT_2's.

3.3.2 A Lorentzian Alternative

We would like to note that there is another approach to extending our dome-and-door construction away from the boundary that results in a single-sided solution. This requires us to continue the geometry to Lorentzian signature at the mouth of the wormhole, and the effect is to remove one of the two asymptotic boundaries.[7] This can be achieved by Wick rotating the book-page metric (3.3.1) at $\rho = 0$. With $\rho \to it$, the metric takes a cosmological Friedmann–Robertson–Walker form,

$$ds^2 = -dt^2 + \cos^2 t \; d\Sigma^2 \,. \tag{3.3.0}$$

If we continue the entire geometry beyond $t = 0$, the Lorentzian geometry corresponds to (the future half of) a three-sided black hole geometry, *e.g.* see [78, 83–85]. The Euclidean domes that define the identification are analytically continued into hyperboloids in the Lorentzian geometry. There are three exterior regions, each of which is isometric to the BTZ black hole exterior, and there is non-trivial spacetime region hidden behind the horizons. For our purposes, we only perform the Wick rotation at the mouth of the wormhole, and so

[7] We thank Juan Maldacena for bringing this possibility to our attention.

the Lorentzian geometry only includes a portion of this region hidden behind the horizons. While this leaves our construction with some ambiguity (see further discussion in section 3.5), this is sufficient to remove access to the second asymptotic boundary.

Let us foreshadow the result of computing the action of these geometries in section 3.5, to understand better the relationship between the wormhole and the single-sided, partially Lorentzian solutions. Since we are dividing the Euclidean wormhole geometry in half, the contribution of the Euclidean portion of the single-sided geometry is exactly half the action of the wormhole. Further, the action of the Lorentzian region is imaginary and so just contributes a phase to the three-point function. Overall, we will find

$$I_{\text{single-sided}} = \frac{1}{2} I_{\text{wormhole}} + i \sum_i f(i) \,, \tag{3.3.0}$$

where it is a nontrivial result that the imaginary term takes the form of the sum shown above. This form allows the corresponding phases to be absorbed into the definition of the operators.

3.4 Relationship with Liouville Theory

We have described the three-point geometry with a variety of different coordinate systems and metrics. In particular, we first considered the Bañados form (3.1), then we used identifications within Poincaré coordinates (3.1) to construct the full bulk geometry, and we connected these two descriptions. Above, we also introduced the "book page" ansatz (3.3.1). The primary motivation for the latter there was that it facilitates the Lorentzian construction described in section 3.3.2. Here, we reconsider the book-page metric and introduce a description of the three-point geometry in terms of a Liouville field [63, 86], which will be convenient to compute the on-shell action in the next section 3.5, since as it will turn out, the on-shell action reproduces a universal formula [65] for the OPE structure constants expressed as the classical limit of the DOZZ formula [69–71].

Recall the book-page metric (3.3.1) takes the form [26, 79]

$$ds^2 = d\rho^2 + \cosh^2\rho \; d\Sigma^2 \,, \tag{3.4.0}$$

where $d\Sigma^2$ describes a slice of the geometry with constant negative curvature, *i.e.* the book page. Irrespective of the details of these slices, the metric (3.4) is a solution of the three-dimensional Einstein equations with a negative cosmological constant.

It is useful to see the book-page description of empty AdS_3, which is simply an AdS_2 foliation. Consider AdS_3 described by Bañados metric (3.1) with $L(z) = 0 = \bar{L}(\bar{z})$ or the Poincaré metric (3.1), the change of variables to eq. (3.4) is

$$y = Y = \frac{w_1}{\cosh\rho} \qquad \text{and} \qquad z = Z = w_1 \tanh(\rho) + i w_2 \,, \tag{3.4.0}$$

with $w = w_1 + i w_2$. Eq. (3.4) then yields

$$ds^2 = d\rho^2 + \cosh^2\rho \; \frac{4\, dw\, d\bar{w}}{(w+\bar{w})^2} \,. \tag{3.4.0}$$

Note that fixing w_1 and w_2 to be constants, the paths described by ρ running over its full range are semicircular geodesics anchored at the boundary at $z = Z = \pm w_1 + i w_2$. As noted previously, we reach the asymptotic boundary (*i.e.* $y = 0 = Y$) with $\rho \to \pm\infty$. However, we can also reach the boundary on any fixed-ρ slice by taking $w_1 = \mathrm{Re}(w) \to 0$. That is, all of the book pages (*i.e.* two-dimensional slices) meet the asymptotic boundary along the imaginary axis, $\mathrm{Re}(z) = 0 = \mathrm{Re}(Z)$.[8]

Clearly in the above example, where Σ is noncompact, the corresponding solution (3.4) has a single asymptotic region. More generally, the solutions (3.4) have two separate boundaries at $\rho \to \pm\infty$. This is clear when Σ is a compact (negatively-curved) surface, which yields a two-sided wormhole where the two asymptotic regions have the topology of Σ [79].

While it is straightforward to extend the ansatz (3.4) to any number of dimensions [26,79], there is a particular result which is special to three bulk dimensions. In particular with $d = 2$, we observe that the line element $d\Sigma^2$ can be described by a field $\varphi(w, \bar{w})$ that satisfies the classical Liouville equation with a negative cosmological constant. That is,

$$d\Sigma^2 = e^{\varphi(w,\bar{w})}\, dw\, d\bar{w} \qquad \text{where} \quad \partial\bar{\partial}\,\varphi(w,\bar{w}) = \frac{1}{2} e^{\varphi(w,\bar{w})}\,. \tag{3.4.0}$$

This allows us to describe our multi-point geometries for huge operators in terms of solutions of the Liouville equation. To proceed, we only need to determine the appropriate Liouville solution. This can be done by working out locally the change of coordinates to the asymptotic FG patch. This change of coordinates involves the three functions $\rho = \rho(y, z, \bar{z})$, $w = w(y, z, \bar{z})$ and $\bar{w} = \bar{w}(y, z, \bar{z})$, such that in a small y expansion the book page metric is brought into the Bañados form with given $L(z), \bar{L}(\bar{z})$. This then yields the relation between the Liouville field $\varphi(z, \bar{z})$ and the profile of the stress tensor $L(z), \bar{L}(\bar{z})$. The first few terms of the FG expansion are

$$\rho = -\log(y/2) + \tfrac{1}{2}\varphi(z,\bar{z}) + \frac{y^2}{4}\,\partial\varphi(z,\bar{z})\,\bar{\partial}\varphi(z,\bar{z}) + \cdots\,,$$

$$w = z - \frac{y^2}{2}\,\partial\varphi(z,\bar{z}) + \cdots\,, \qquad \bar{w} = \bar{z} - \frac{y^2}{2}\,\bar{\partial}\varphi(z,\bar{z}) + \cdots\,.$$

Note that the above change of variables is an infinite expansion in y, but once we substitute into the metric, the metric truncates at order y^2 giving the Bañados metric. Then, the relation between the Liouville field $\varphi(z, \bar{z})$ and the stress tensor $L(z), \bar{L}(\bar{z})$ is[9]

$$\begin{aligned} L(z) &= \frac{1}{4}(\partial\varphi(z,\bar{z}))^2 - \frac{1}{2}\,\partial^2\varphi(z,\bar{z})\,, \\ \bar{L}(\mathbf{z}) &= \frac{1}{4}(\bar{\partial}\varphi(z,\bar{z}))^2 - \frac{1}{2}\,\bar{\partial}^2\varphi(z,\bar{z})\,. \end{aligned} \tag{3.4.1}$$

[8] Hence, we see the complete "book" of the book-page ansatz (3.4). The front and back covers of the book lie flat on the asymptotic boundary $y = 0$, and are reached with $\rho \to \pm\infty$, respectively. Of course, the two-dimensional AdS_2 slices foliating the bulk geometry correspond to the book pages. Lastly, these pages all meet at the spine of the book at $y = 0$, $\Re(z) = 0$, which is reached with $w_1 \to 0$.

[9] It is straightforward to confirm that these expression yield $\bar{\partial}L = 0 = \partial\bar{L}$, as desired, using the Liouville equation of motion (3.4).

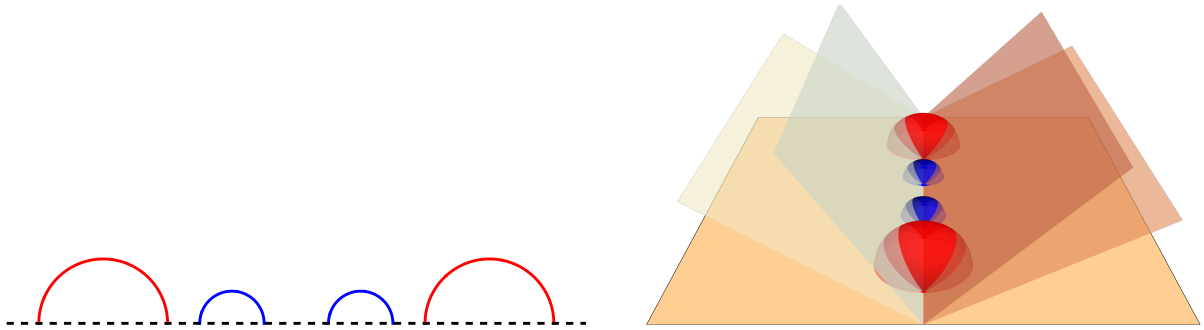

(a) A quotient of the upper half plane defining a hyperbolic surface.

(b) The corresponding hyperbolic 3-manifold, constructed using the Maldacena-Maoz ansatz.

Figure 3.9: The hyperbolic genus-two handlebody as a Maldacena-Maoz wormhole

The general solution to the Liouville equation (3.4) can be parameterized by a holomorphic and an anti-holomorphic function, f and $\bar{f}$, with

$$\varphi(z,\bar{z}) = \ln\left(\frac{4\,\partial f\,\bar{\partial}\bar{f}}{\left(f+\bar{f}\right)^2}\right) \tag{3.4.0}$$

Substituting this expression into eq. (3.4.1), we find

$$L(z) = -\tfrac{1}{2}\{f,z\} \qquad ; \qquad \bar{L}(\bar{z}) = -\tfrac{1}{2}\{\bar{f},\bar{z}\} \tag{3.4.0}$$

Hence, we have recovered the Schwarzian equations (3.1) appearing in the discussion of the Roberts map. That is, $f(z)$ and $\bar{f}(\bar{z})$ in eq. (3.4) are the same functions appearing in the Roberts change of variables (3.1) from Euclidean AdS_3 to the Bañados metric – see also Appendix B.1.

Next, we describe features of the Liouville field for the two- and three-point functions in detail.

The Black Hole Two-Point Function

The Liouville field for the two-point function with black hole insertions at 0 and ∞ follows straightforwardly by substituting f_{BH} and $\bar{f}_{\text{BH}}$ from eq. (2.3.-1) into eq. (3.4). This yields

$$e^{\varphi_{2pt}} = \frac{R_h^2}{w\bar{w}\,\cos^2\left(R_h \ln(\sqrt{w\bar{w}})\right)} \tag{3.4.0}$$

where $R_h = \sqrt{M-1}$ and recall that $M \geq 1$ for the black hole operators.

Note that $e^{\varphi_{2pt}}$ diverges at concentric rings where the denominator vanishes, *i.e.* $w\bar{w} = e^{n\pi/R_h}$ where n is an integer. Scaling $w \to e^{\pi/R_h}w$ leaves the metric (3.4) invariant. Hence book pages are equally well described by allowing $w, \bar{w}$ to run over any one of the anuli between consecutive divergences. Further, following the discussion of the AdS_3 metric (3.4), the divergences correspond to locations where the book pages reach the asymptotic boundary.

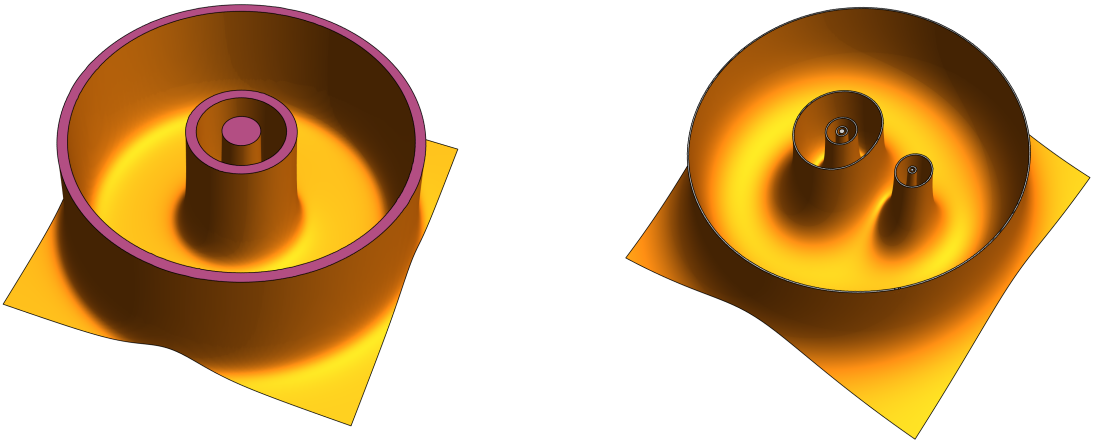

(a) The Liouville solution related to the black hole 2pt function.

(b) The Liouville solution related to the black hole 3pt function.

Figure 3.10: $e^{\varphi(z,\bar{z})}$ for the Liouville solutions relevant to **(a)** the black hole two-point function and **(b)** the black hole three-point function. Around each operator insertion there is an infinite sequence of singularities along closed contours (shown in purple). These singularities correspond to the location of the doors in the full three-dimensional geometries. Between each of these singularities is a closed geodesic, corresponding to the black hole horizon. In the three-point function, there is a single special region which is bounded by three singularity contours rather than only two. This special chamber also contains three closed geodesics rather than just one.

Hence the book pages reach infinity on two periodically identified intervals, see figure 3.9 (b).

At the boundary, we find from (3.4) that $w = z$ so we can borrow our discussion around (3.2) to infer what the singularities of $\varphi_{2pt}(w, \bar{w})$ represent in the dome-and-door construction. In fact, it follows from that discussion that as move from one operator insertion at $w = 0$ to the other operator insertion at $w = \infty$, we should cross the base of a door infinitely many times, thus the singularities represent precisely the base of the door.

The Liouville Solution with Three Operator Insertions

For the black hole three-point function with insertion points at 0, 1 and ∞, a solution to the relevant Schwarzian equation (3.1) is the Schwarz triangle function given in eq. (3.3). We can simply plug this Schwarzian solution into eq. (3.4) to read off the Liouville solution.

The result was described in [76]. It has three sets of concentric singularities, each of which accumulates towards one of the operator insertions. The annuli between the singular rings correspond to book pages describing the leg regions, discussed in section 3.3. These book pages are analogous to those found above for the two-point function, and each has two independent boundary regions, corresponding to the singularities in the Liouville field defining the boundaries of the annulus. As with the two-point function solution above, there is a scaling symmetry which ensures that all of these annuli describe the same book-page

geometry.

There is also a special region that is bounded by three singular contours, one from each of the three families accumulating toward the operator insertions – see figure 3.10(b). Of course, this special region describes the book page for the central chamber appearing in the dome-and-door construction.

3.5 The Action

We now proceed to evaluate the action for the three-point function geometry discussed in the previous section.

The gravitational action is given by

$$I = -\frac{1}{16\pi G_{\rm N}}\int_{\mathcal{M}} d\rho\, d^2z\sqrt{g}(R-\Lambda) + \frac{1}{8\pi G_{\rm N}}\int_{\partial\mathcal{M}} d^2z\sqrt{h}K + \frac{1}{8\pi G_{\rm N}}\int_{\partial\mathcal{M}} d^2z\sqrt{h} \tag{3.5.0}$$

where the last term is the counterterm on the asymptotic boundary. Recall we set $L_{\rm AdS}=1$ and hence $\Lambda=-2$. Then, using Einstein's equations, we have $R=-6$. Furthermore, the extrinsic curvature of the asymptotic cutoff surface is given by $K=-2+O(\epsilon^3)$. Therefore, combining the bulk term with the asymptotic boundary contributions in the above action, we find

$$I = \frac{1}{4\pi G_{\rm N}}\int_{\mathcal{M}} d\rho\, d^2z\sqrt{g} - \frac{1}{8\pi G_{\rm N}}\int_{\partial\mathcal{M}} d^2z\sqrt{h} = \frac{1}{4\pi G_{\rm N}}\left(V-\frac{1}{2}A\right) \tag{3.5.0}$$

where V and A are the bulk volume and asymptotic boundary area, respectively. In addition to the contributions (3.5), the action (3.5) includes a Gibbons-Hawking-York (GHY) term on the stretched horizons. So the total action is simply given by

$$I = \frac{1}{4\pi G_{\rm N}}\left(V-\frac{1}{2}A\right) + \frac{1}{8\pi G_{\rm N}}\int_{\rm horizon}\sqrt{h}K\,. \tag{3.5.0}$$

We will need to regulate the volume of the wormhole geometry in order to obtain a finite value for the action. The correct cutoff is determined by first introducing a "naïve" cutoff at surfaces of constant $\rho=\pm\ln(2/\epsilon)$, and then shifting the cutoff to its correct location. Since we are hoping to obtain a result consistent with a three-point function in a CFT_2 in flat space, we would like the metric on the cutoff surface to have the form

$$ds^2_{\rm physical} = \frac{dzd\bar{z}}{\epsilon^2} + O(\epsilon^0). \tag{3.5.0}$$

Note that the naïve surface of constant ρ is not the physical cutoff we are interested in. For instance, it is negatively curved, since the metric on the surface is

$$ds^2_{\rm naïve} = \frac{\left(1+\frac{1}{4}\epsilon^2\right)^2}{\epsilon^2}e^{\varphi(z,\bar{z})}dzd\bar{z}. \tag{3.5.0}$$

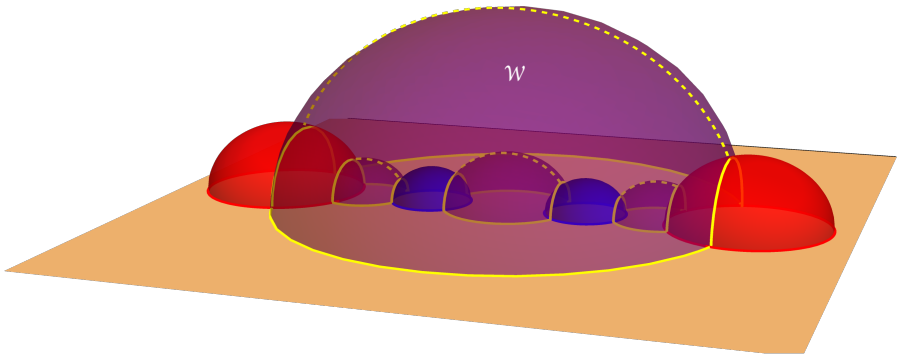

Figure 3.11: The central region $\mathcal{W}$ is defined by first considering the region in $z, \bar{z}$ between the three horizons, shown as dashed yellow lines, on the vertical $\rho = 0$ plane. The extension of this region for all ρ is shown here in purple. Passing out of this region through any of the purple walls allows one to approach one of the doors.

The correct boundary metric can be obtained by shifting the cutoff by an amount proportional to $\varphi(z, \bar{z})$,

$$\rho_* = \pm \ln\left(\frac{2}{\epsilon}\right) \mp \frac{\varphi(z, \bar{z})}{2} \tag{3.5.0}$$

This cutoff cannot be used everywhere, because as explained above the corresponding classical Liouville solution $\varphi(z, \bar{z})$ is singular. This corresponds directly to the fact that the surface of constant ρ fails to serve as a cutoff at all in cases involving black hole operators, since in such a case all of the constant ρ surfaces reach all the way to the conformal boundary. Hence, we will need to modify the regularization scheme in the region near where these singularities occur.

In [76, 87], a prescription for calculating the Liouville action in the presence of three hyperbolic singularities was introduced. That prescription involves splitting the z plane into a central region, where the Liouville solution is regular, and several "leg" regions, where the Liouville solution has singularities. In the leg regions, the Liouville solution is then replaced by a carefully chosen solution to the *Laplace* equation. Inspired by this calculation, we will divide our three-dimensional geometry into a central region and several legs. In the central region, we will find the physical cutoff using the same method that works for the cases involving only conical defects – see section 3.6 below. In each of the legs, we will need to find a new regularization procedure with different "naïve" cutoffs and shifts to obtain the full physical cutoff.

To describe the regions more precisely, recall the structure of the metric $e^{\varphi} dz d\bar{z}$ – see figure 3.10 (b). This metric is singular at concentric rings surrounding each operator. Between each pair of singularities, there is a closed geodesic corresponding to the horizon of the black hole created by the operator. In the three point function case, there are three series of concentric rings where the metric is singular (one for each operator). The three series of concentric singularities are joined by a special "central chamber", which is the unique domain in $z, \bar{z}$ that is bounded by three singularities rather than only two. In this central chamber, there are three closed geodesics (one for each operator), instead of just one. This corresponds directly

to the central chamber in the three-dimensional geometry discussed previously, where one can see all three of the horizons (and all three doors). The central region $\mathcal{W}$ is the region in the $(z, \mathbf{z})$-plane that lies between these three closed geodesics, *i.e.* the three horizons.

Recall from section 3.3.2 that if we continue to Lorentzian signature with $\rho = it$, we get a spacetime with three asymptotically AdS boundaries, *e.g.* see [78, 83–85]. An observer near any of the three asymptotic boundaries sees a geometry identical to the exterior of a BTZ black hole. All three of these black holes share a common interior, and the central region $\mathcal{W}$ on the $t = 0$ slice is exactly this shared interior.

Returning to Euclidean signature, note that removing the region $\mathcal{W}$ from the $(z, \mathbf{z})$-plane for all ρ leaves behind six disconnected pieces of the geometry. These are the six "leg" regions, $\mathcal{L}_i$. It is inside these leg regions where the $\rho = \rho_*$ cutoff given in eq. (3.5) fails, since each leg contains one of the concentric series of singularities. So we will need a new prescription to regulate the action in the leg regions.

The naïve cutoff which we will use in each of the leg regions is given by a surface which is isometric to a cone in the $\{Y, Z, \bar{Z}\}$ coordinates. That is, by performing an isometry, we can choose the naïve cutoffs for each of the legs to be cones in coordinates in which the metric takes the form (3.1) – see figure 3.12. So, they are most easily described by introducing another system of coordinates on Euclidean AdS_3,

$$\begin{aligned} Y &= e^{\tau} \operatorname{sech} \tilde{\rho} \,, \\ Z &= e^{\tau + i\theta} \tanh \tilde{\rho} \,, \\ \bar{Z} &= e^{\tau - i\theta} \tanh \tilde{\rho} \,. \end{aligned}$$

In these coordinates, the metric takes the form

$$ds^2 = d\tilde{\rho}^2 + \cosh^2 \tilde{\rho} \, d\tau^2 + \sinh^2 \tilde{\rho} \, d\theta^2 \,. \tag{3.5.0}$$

In these coordinates, the naïve cutoff for each of the leg regions is then a surface of constant $\tilde{\rho}$, which is a cone in the Poincaré coordinates (3.1). The coordinates τ and θ will be related to the physical coordinates in the CFT with

$$\tau = \frac{1}{2}\left(\tilde{f}_i(z) + \bar{\tilde{f}}_i(\bar{z})\right) \,, \qquad \theta = \frac{1}{2i}\left(\tilde{f}_i(z) - \bar{\tilde{f}}_i(\bar{z})\right) \,, \tag{3.5.0}$$

where i labels the six leg regions.

Similarly to what we saw in the central region, the naïve cutoff has the wrong metric. So we will use a cutoff related to this naïve one by a similar shift

$$\tilde{\rho}_* = \ln\left(\frac{2}{\epsilon}\right) - \frac{\tilde{\varphi}_i(z, \bar{z})}{2} \tag{3.5.0}$$

where $\tilde{\varphi}_i(z, \bar{z})$ are each solutions to the *Laplace* equation, given by

$$\tilde{\varphi}_i(z, \bar{z}) = \ln\left(\partial \tilde{f}_i \, \bar{\partial} \bar{\tilde{f}}_i\right) \,. \tag{3.5.0}$$

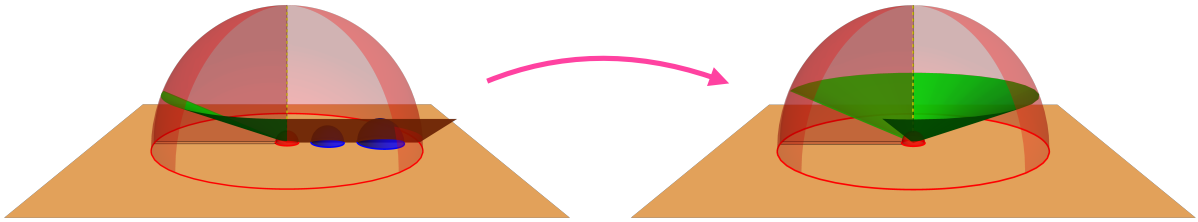

In the central chamber we use a "book page" cutoff, which transitions as we cross each of the horizons to a cone cutoff.

The cone cutoff continues through each of the doors all the way down the infinite sequence of "leg" chambers.

Figure 3.12: We use different "naïve" cutoffs in the central region and the leg regions. Each of these are then shifted to obtain a cutoff with the correct metric. These shifts are controlled by solutions to the Liouville and Laplace equations in the central and leg regions, respectively.

With these choices, the metric on the cutoff surface is the desired flat metric

$$ds^2_{\text{cutoff}} = \frac{dzd\bar{z}}{\epsilon^2} + O(\epsilon^0)\,. \tag{3.5.0}$$

Finally, in order for the full cutoff to be smooth, we need to impose gluing conditions at each of the boundaries Γ_i between the central and leg regions:

$$\begin{aligned}
\varphi(z,\bar{z})|_{\Gamma_i} &= \tilde{\varphi}_i(z,\bar{z})|_{\Gamma_i}\,,\\
\partial\varphi(z,\bar{z})|_{\Gamma_i} &= \partial\tilde{\varphi}_i(z,\bar{z})|_{\Gamma_i}\,,\\
\bar{\partial}\varphi(z,\bar{z})|_{\Gamma_i} &= \bar{\partial}\tilde{\varphi}_i(z,\bar{z})|_{\Gamma_i}\,.
\end{aligned}$$

To summarize, we have split the geometry into several regions – see figure 3.11. In each region, we have a natural way to describe the physical cutoff as the shift of a "naïve" cutoff – see figure 3.12. In the central region, corresponding to the $\mathcal{W}$ in the $(z,\bar{z})$-plane, we will use the cutoff $\rho = \rho_*$ in eq. (3.5). This cutoff has a shift by the Liouville field of a constant ρ "bookpage". In the leg regions $\mathcal{L}_i$, we use the cutoff $\tilde{\rho} = \tilde{\rho}_*$ given in eq. (3.5). There, the shift is made by a solution to the Laplace equation of the constant $\tilde{\rho}$ cone. Although we are describing these cutoffs in different coordinates, the gluing conditions on the Liouville and Laplace solutions guarantee that we are actually describing a single continuous cutoff surface.

Central Region Action

We start by considering the "central" region corresponding to $\mathcal{W}$ defined above. Using the expression for the book page metric (3.4)-(3.4) and integrating over ρ, we find that the volume of the central region is

$$V = \int d^2z \left(\frac{1}{\epsilon^2} + \ln(2/\epsilon)\, e^{\varphi} - \bar{\partial}(\varphi\partial\varphi) + \partial\varphi\bar{\partial}\varphi\right)$$

where we used the equations of motion, $\partial\bar{\partial}\varphi = \frac{1}{2}e^{\varphi}$. Plugging in the induced metric on the asymptotic cutoff surfaces, $\rho = \pm\rho_*$ gives

$$A = \int d^2z \left(\frac{2}{\epsilon^2} + e^{\varphi} + \partial\varphi\bar{\partial}\varphi\right). \tag{3.5.0}$$

Combining these expressions as in eq. (3.5), the action for the central region is given by

$$I_{\mathcal{W}} = \frac{1}{8\pi G_{\text{N}}}\int_{\mathcal{W}} d^2z \left(\partial\varphi\bar{\partial}\varphi + e^{\varphi}\right) - \frac{i}{8\pi G_{\text{N}}}\oint_{\partial\mathcal{W}} dz\ \varphi\partial\varphi - \frac{1}{2G}\left(1 - \ln(2/\epsilon)\right).$$

In the last term, we used the fact that the area of the wormhole region is[10]

$$\int_{\mathcal{W}} d^2z\ e^{\varphi(z,\bar{z})} = 2\pi\,. \tag{3.5.0}$$

We see that, up to the final term, which will be cancelled by counterterms, the action of the central region is the Liouville action for $\varphi(z,\bar{z})$ in the corresponding subregion of the $(z,\bar{z})$-plane, $\mathcal{W}$. This is very similar to what happens in the conical defect case, as discussed in [11].

Leg Region Action

Now consider the contribution to the action of one of the "leg" regions, where the metric takes the form (3.5). Integrating over $\tilde{\rho}$, we find that the total volume is

$$V = \int d^2z \left(\frac{1}{2\epsilon^2} - \frac{1}{4}e^{\tilde{\varphi}_i}\right)$$

For the boundary contribution, we need the area of the surface $\tilde{\rho} = \tilde{\rho}_*$ as defined in eq. (3.5). Then A is given by

$$A = \int d^2z \left(\frac{1}{\epsilon^2} + \frac{1}{2}\partial\tilde{\varphi}_i\bar{\partial}\tilde{\varphi}_i\right). \tag{3.5.0}$$

Combining the bulk and boundary terms together as in eq. (3.5), we find

$$I_{\mathcal{L}_i} = \frac{1}{16\pi G_{\text{N}}}\int_{\mathcal{L}_i} d^2z \left(\partial\tilde{\varphi}_i\bar{\partial}\tilde{\varphi}_i - e^{\tilde{\varphi}_i}\right) - \frac{i}{8\pi G_{\text{N}}}\oint_{\partial\mathcal{L}_i} dz\ \tilde{\varphi}_i\partial\tilde{\varphi}_i\,. \tag{3.5.0}$$

where we used the equations of motion $\partial\bar{\partial}\tilde{\varphi} = 0$, and integrated by parts to extract a boundary term that will combine nicely with the one which we found in the central region.

We see that the action in the each leg region is given by the Liouville action evaluated on a solution to the *Laplace* equation $\tilde{\varphi}_i(z,\bar{z})$ and with the opposite sign for the Liouville

[10] This can be seen by remembering the realization of $\mathcal{W}$ as a quotient of the hyperbolic upper half-plane. Then we see that $\mathcal{W}$ is a hyperbolic octagon with all right angles (with some edges identified). Then the result (3.5) can be derived using the general formula for the area of a hyperbolic polygon: $A = (n-2)\pi - \sum_i \alpha_i$ where n is the number of sides and α_i are the interior angles of the polygon.

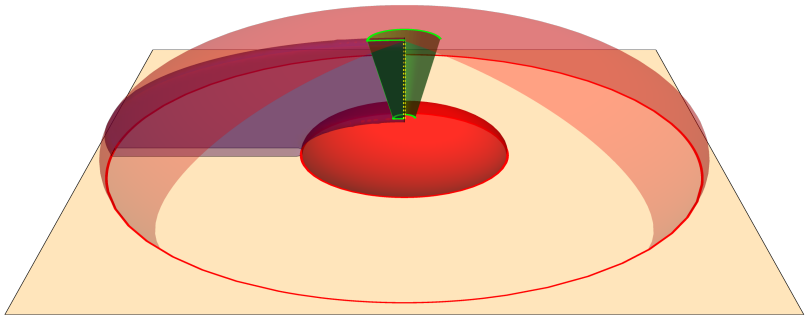

Figure 3.13: The stretched horizon (green cone) crashes into the true horizon (yellow, dashed line) before it goes through the door and enters the central chamber.

cosmological constant (the minus sign in front of $e^{\tilde{\varphi}_i}$ in the first integral above). It may seem strange at first that we are evaluating the Liouville action of a solution to the Laplace equation, but in fact it matches perfectly with the proposal in [76, 87], except for the wrong-sign cosmological constant. Having the correct sign for the Liouville cosmological constant is crucial for reproducing the expected dependence of the three point function (squared) on the location of the operator insertions. Thankfully, eqs. (3.5) and (3.5) are not the only contributions, since as we argued in chapter 2, we must also include a GHY term on the stretched horizons, as we have already indicated in eq. (3.5). The inclusion of this boundary term makes the geometries we are considering analogous to the fixed area states of [18, 19] (see also [88]), since it allows us to fix the metric on the horizon. We will see soon that the inclusion of the Gibbons-Hawking-York term on the stretched horizons exactly flips the sign of the Liouville cosmological constant!

Gibbons-Hawking-York Term on the Horizons

We need to include a GHY terms on each of the stretched horizons. The stretched horizons are simply the surfaces with $\tilde{\rho} = \epsilon$. Computing the induced metric on these surfaces, we find that the volume form is

$$\sqrt{h}\; d\tau d\theta = \epsilon\; e^{\tilde{\varphi}_i} dz d\bar{z} + O(\epsilon^3), \tag{3.5.0}$$

while the extrinsic curvature is given by simply $K = \frac{1}{\epsilon} + O(\epsilon)$.

The stretched horizons extend along each of the six legs. We also need to decide what to do with the stretched horizon in the central region $\mathcal{W}$. We will make what we consider a "minimal" choice. That is, we will have the stretched horizon crash into the true horizon just before it enters the central chamber – see figure 3.13.[11]

With this choice, the GHY terms at the horizons give a contribution only in the leg regions, and we find

$$I_{\text{GHY,hor}} = \frac{1}{8\pi G_{\text{N}}} \sum_i \int \sqrt{h} K = \frac{1}{8\pi G_{\text{N}}} \sum_i \int_{\mathcal{L}_i} d^2 z\; e^{\tilde{\varphi}_i}\,. \tag{3.5.0}$$

[11] This choice may seem unusual and our primary justification will be the agreement of our results with the semiclassical Liouville three-point function. However, see further discussion in section 3.6.

Combining this to the previous leg contributions in eq. (3.5), we see that the sign of the Liouville potential in the leg region is flipped.

Combining eqs. (3.5), (3.5) and (3.5), we have

$$\begin{aligned} I &= I_{\mathcal{W}} + \sum_i \left(I_{\mathcal{L}_i} + I_{\text{GHY,hor}}\right) \\ &= \frac{1}{8\pi G_{\text{N}}} \int_{\mathcal{W}} d^2z \left(\partial\varphi\bar{\partial}\varphi + e^{\varphi}\right) + \frac{1}{16\pi G_{\text{N}}} \sum_i \int_{\mathcal{L}_i} d^2z \left(\partial\tilde{\varphi}_i\bar{\partial}\tilde{\varphi}_i + e^{\tilde{\varphi}_i}\right) \\ &\quad - \frac{i}{8\pi G_{\text{N}}} \sum_i \oint_{|z-z_i|=\epsilon} dz\ \varphi_i\partial\varphi_i - \frac{i}{8\pi G_{\text{N}}} \oint_{|z|=1/\epsilon} dz\ \varphi\partial\varphi - \frac{1}{2G_{\text{N}}}\left(1 - \ln(2/\epsilon)\right). \end{aligned}$$

Notice that the boundary terms from (3.5) have nicely cancelled with the ones in (3.5), since they lie along the common boundary of $\mathcal{W}$ and the $\mathcal{L}_i$'s. This is the importance of the gluing conditions (3.5).

As mentioned before, a procedure for calculating the action of the Liouville solution with three hyperbolic singularities was introduced in [76, 87]. Their result has the correct dependence on the locations of the operator insertions, and the position independent term in their result matches with the semiclassical limit of the DOZZ formula. Their calculation involves the introduction of solutions to the Laplace equation, which can be identified with our $\tilde{\varphi}_i(z,\bar{z})$. They define the regularized Liouville action as

$$\begin{aligned} I_L &= \frac{1}{2\pi} \int_{\mathcal{W}} d^2z \left(\partial\varphi\bar{\partial}\varphi + e^{\varphi}\right) + \frac{1}{2\pi} \sum_{i=1}^{3} \left(\int_{\mathcal{L}_i} d^2z \left(\partial\tilde{\varphi}_i\bar{\partial}\tilde{\varphi}_i + e^{\tilde{\varphi}_i}\right)\right) \\ &\quad - \frac{i}{\pi} \oint_{|z|=1/\epsilon} dz\ \varphi\partial\varphi - \frac{i}{\pi} \sum_{i=1}^{3} \oint_{|z-z_i|=\epsilon} dz\ \tilde{\varphi}_i\partial\tilde{\varphi}_i - \left(4 + \sum_{i=1}^{3}(1 - R_i^2)\right)\ln(\epsilon). \end{aligned}$$

Comparing with our result (3.5), we see

$$I = \frac{c}{6} I_L - \frac{c}{3}(1 - \ln(2)) + \frac{c}{6} \sum_{i=1}^{3} (1 - R_i^2)\ln(\epsilon) \tag{3.5.0}$$

where we used the relation $c = \frac{3}{2G_{\text{N}}}$.

The remaining dependence on the cutoff is canceled when we add the required counterterms, which can be found by examining the two point function – see Appendix B.2. Hence in the end, we have

$$I = \frac{c}{6} I_L - \frac{c}{3}(1 - \ln(2)) \tag{3.5.0}$$

As discussed in [11], the second term arises from the dependence of the DOZZ formula on the Liouville cosmological constant μ when one scales it as $\mu = \frac{1}{4\pi b^2}$ in the semiclassical limit, $b \to 0$. Hence we find

$$e^{-I} \approx |G_L(z_1, z_2, z_3)|^2 \tag{3.5.0}$$

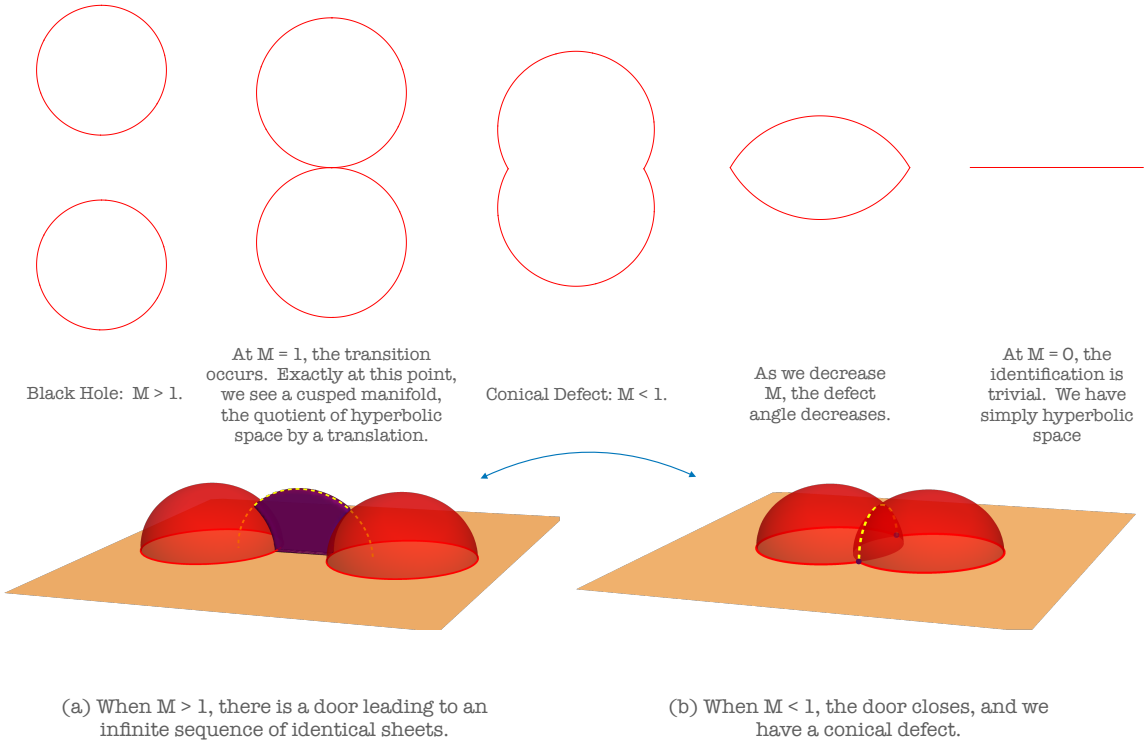

Figure 3.14: **Top:** Boundary picture. As we decrease the mass of the operator insertions, a transition occurs in which the black hole becomes a conical defect. The defect angle for a given mass, M, is $2\pi\left(1-\sqrt{1-M}\right)$. Eventually, as we continue to decrease M, the defect disappears. **Bottom:** Full picture. When the transition between black hole and conical defect is made, the door closes. In the left figure, the yellow dashed line is the black hole horizon, around which the geometry branches infinitely many times, as represented by the purple door. In the right figure, the yellow dashed line represents the conical defect, which appears at the intersection of the domes defining the identification.

where $G_L(z_1, z_2, z_3)$ is the semiclassical Liouville three-point function with a specific normalization related by analytic continuation to the one used in [11], and we have checked the agreement at the classical level. Of course, this result (3.5) with the square of the three-point function is aligned with our discussion in section 3.3.1, where the appearance of the wormhole suggested that the geometric calculation yields a contribution to the variance of the three-point function.

Now we turn to discussion of the relationship between the black hole three-point function geometry and geometries involving defect operators. We will then return to the discussion of the Lorentzian cap, and consider its contribution to the action in more detail.

3.6 Geometric Transitions. Doors and Defects.

Since we are discussing gravity in three dimensions, there is a gap in energy between the vacuum and the first black hole state. For an operator to be dual to a black hole, we need

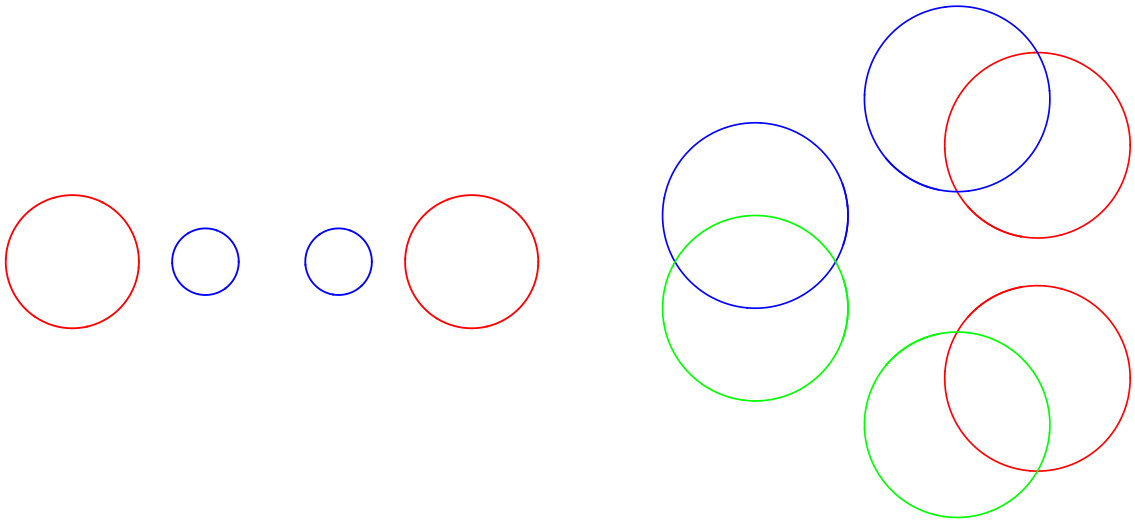

(a) The boundary of the three point function geometry for one choice of identifications

(b) A different choice of identifications that gives the same boundary manifold

Figure 3.15: Two different choices of branch cuts for the boundary of the three-point function geometry with three black hole operator insertions. Circles with the same color are identified, creating the same genus-two surface in both cases.

that its mass to be $M > 1$. So far we have been considering only such black hole operators. However, it is straightforward and illuminating to extend the constructions above to the case where some of the operators have mass $0 < M < 1$, which are dual to conical defects in the bulk.

Consider the two-point function geometry. As we decrease the mass of the operators, the domes used to represent the corresponding identification of hyperbolic space approach each other. As we pass below $M = 1$, the identification used to construct the geometry goes from being a hyperbolic isometry to an elliptic one. In terms of the dome pictures, the transition occurs as the domes collide – see figure 3.14. The resulting intersection of the two domes is the trajectory of a conical defect.

In terms of the Schwarzian solutions, the transition is also apparent. Recall for the black hole case (with $M > 1$), we had

$$f_{\texttt{BH}}(z) = z^{i\sqrt{M-1}}\,. \tag{3.6.0}$$

The fact that the image of the z plane under this function covers the $(Z, \bar{Z})$-plane many times is what necessitated the introduction of the door. On the other hand, with $M < 1$, the exponent is *real*, *i.e.*

$$f_{\texttt{defect}}(z) = z^{\sqrt{1-M}}\,. \tag{3.6.0}$$

The image covers only a portion of the Z plane once, and the door has disappeared.

This story continues naturally to the three-point function case. Here, it is easier to understand the transitions by considering a different choice of fundamental domain – see figure 3.15. The two panels correspond to different choices for the branch cuts of the Schwarzian

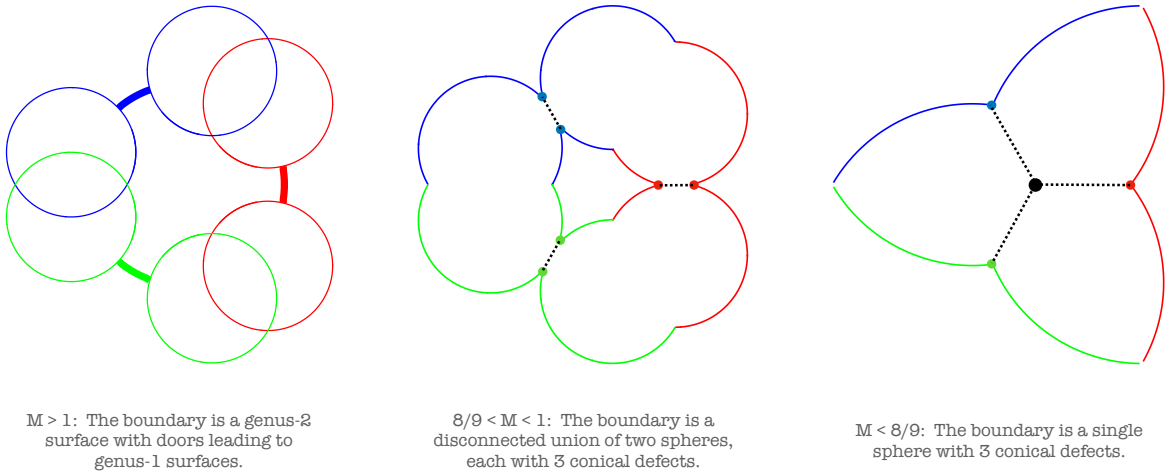

Figure 3.16: The three-point function geometry for three equal-mass operators, seen from above. When M $>$ 1, the identifications create a genus-two surface, which has three doors (thick lines). These divide the asymptotic boundary into two regions (*i.e.* we have a wormhole). As we decrease the mass so that $M < 1$, the black holes are replaced by defects (dashed lines). The doors collapse and close, but the boundary is still divided into two pieces. If we decrease the mass even more, so that $M < 8/9$, the wormhole itself disappears, and the defects join at a vertex (the black dot in the center of the right figure) in the bulk instead. Although they appear flat here, the dashed lines are actually semicircular arcs shooting through the bulk.

solution $f_{\mathtt{3pt}}$. With the choice of identifications shown in figure 3.15(b), we can follow what happens as we decrease the masses of all three operators – see figure 3.16. We see that first, the circles corresponding to a given identification collide, the doors disappear and they are replaced by conical defects at the intersections of the corresponding domes – see figure 3.15(b). These conical defects shoot into the bulk, and travel to another point on "the" asymptotic boundary. However, just as in the black hole case, the boundary is actually divided into two disconnected components, in this case without the need for doors. Thus, we see that we have conical defects flying from one side of a two-sided Euclidean wormhole to the other. This geometry was studied in [11], and its gravitational action was found to reproduce the square of the expected universal HHH three-point function.

As we decrease the masses even more, a second transition occurs when

$$\sum_i \sqrt{1 - M_i} = 1\,. \tag{3.6.0}$$

At this point, the area of the throat of the wormhole $\mathcal{W}$ goes to zero. The wormhole closes up, and instead of travelling from one asymptotic boundary to another, the defects meet at a point in the bulk – see figure 3.16(c). Here we have the single-sided solution studied in [73], where they also found the universal result for the boundary structure constant.

It is also straightforward to consider mixed cases of defect-BH-BH or defect-defect-BH geometries. In these cases, the calculation of the action proceeds with a mixture of what

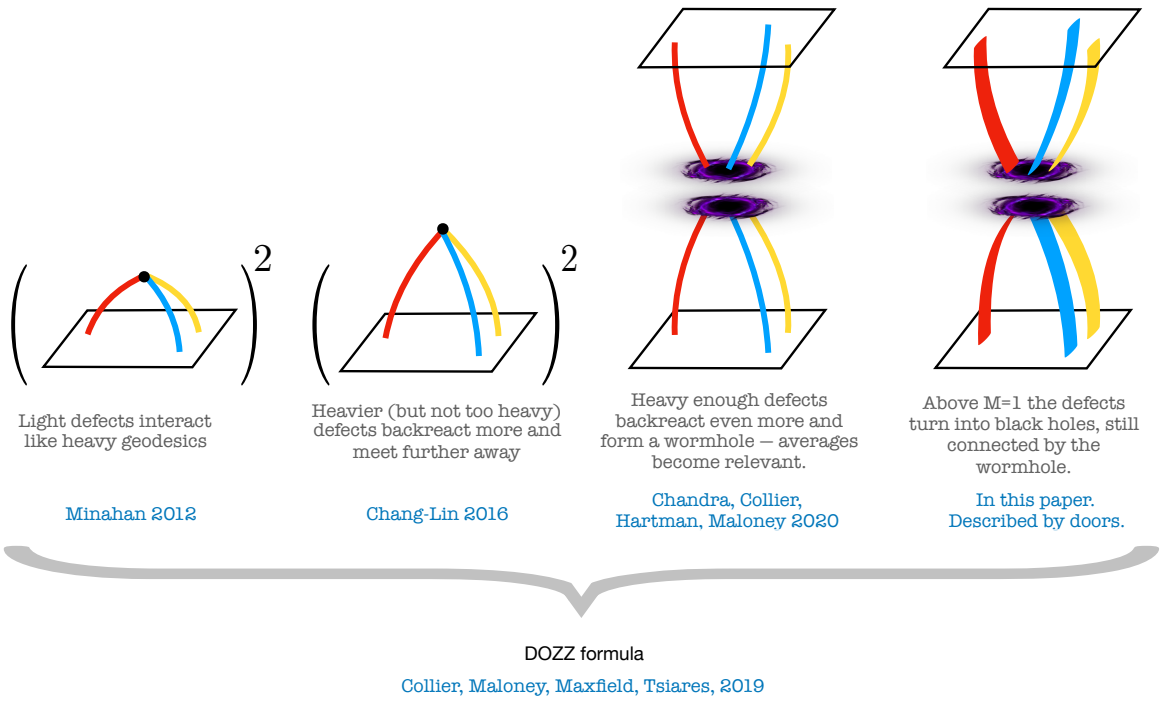

Figure 3.17: Heavy operator correlators in AdS_3/CFT_2 are universally given by the DOZZ formula [65]. Nonetheless, their bulk geometrical description varies quite a bit. Very light defects can be well described by geodesics meeting at an optimal point which minimizes their lengths; as the defects become heavier they interact further from the boundary; these solutions were studied by Chang and Lin in [73]. Eventually they cross a threshold where they would interact at infinity; beyond this point the solution forms a wormhole and becomes double sided, becoming the solution studied by Chandra, Collier, Hartman and Maloney [11]. For even heavier masses, they become black holes and we get a geometry with black holes traversing a wormhole studied in this chapter. The dome picture described herein unifies all these geometries and their interpolations.

we have just done for the three black hole case and what was done in [11] for three defects. We introduce a stretched horizon with GHY term for each black hole operator, and we can choose whether to consider a two-sided geometry or a single-sided one with a Lorentzian cap. The result again has the universal form of the HHH three-point function.

The complete story is summarized in figure 3.17.

Lorentzian Caps and Single-sided Geometries

Now we would like to consider the proposal in section 3.3.2 where continuing the mouth of the wormhole to a Lorentzian cap turns our two-sided Euclidean solution into a single-sided solution. Since the cap is Lorentzian, the corresponding action I_{cap} will contribute to the

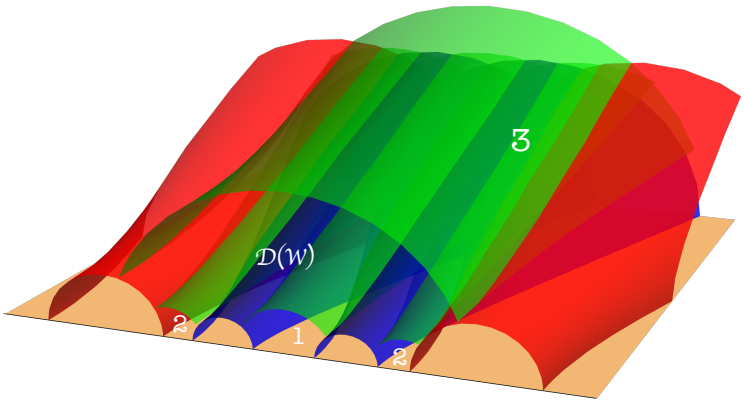

Figure 3.18: Here we show the Lorentzian cap for the 3pt geometry. The domain of dependence of $\mathcal{W}$ is the region between the green surfaces, while the rest of the upper half space lies outside of it. We see that removing the domain of dependence splits the spacetime into three disconnected regions. We associate the three disconnected regions each to one of the operators, and absorb the corresponding phase factor into the definition of the operator.

three-point function as a phase

$$G_3(z_1, z_2, z_3) = e^{-I_{\text{Euclidean}} + iI_{\text{cap}}} \tag{3.6.0}$$

The key result is that the contribution of the Lorentzian geometry to the action, I_{cap} is a sum of separate contributions from each of the three operators.

The Lorentzian cap has a metric obtained by performing a Wick rotation as in eq. 3.3.2 on the wormhole metric (3.4),

$$-dt^2 + \cos^2 t \; e^{\varphi(z,\bar{z})} \; dz d\bar{z} \, . \tag{3.6.0}$$

We glue this Lorentzian geometry with $t > 0$ onto the $\mathcal{W}$ region (*i.e.* the region between to three horizons) at $\rho = 0$.

The area of the throat of the wormhole (*i.e.* the region $\mathcal{W}$) at time $t = 0$ is

$$\int_{\mathcal{W}} d^2 z \; e^{\varphi(z,\bar{z})} = 4\pi \sum_{i=1}^{3} \text{Re}(\eta_i) - 4\pi \, . \tag{3.6.0}$$

where $\eta_i = \frac{1}{2} - \frac{1}{2}\sqrt{1 - M_i}$. Note that if η_i corresponds to a conical defect (with $M_i < 1$), then $\text{Re}(\eta_i) = \eta_i$, while if η_i corresponds to a black hole (with $M_i > 1$), then $\text{Re}(\eta_i) = \frac{1}{2}$. One contribution to the volume of the Lorentzian cap is given by the volume of the region $\mathcal{W}$ for $0 < t < \pi/2$. This contribution is given by

$$V_{\mathcal{W}} = \int_0^{\frac{\pi}{2}} dt \;\; \cos^2(t) \int_{\mathcal{W}} d^2 z \; e^{\varphi(z,\bar{z})} = \pi^2 \sum_{i=1}^{3} \left(\text{Re}(\eta_i) - \frac{1}{3} \right) \, . \tag{3.6.0}$$

The crucial property of this result is that it is a sum of three separate contributions that each depend only on the properties of a single operator.

In the conical defect case, this is the full cap. However, if the geometry contains a black hole, the region $\mathcal{W}$ for $0 < t < \pi/2$ does not cover the full cap. It contains only the domain of dependence of $\{z \in \mathcal{W}, t = 0\}$. However, the geometry at the surface at $t = \pi/2$ is smooth, *i.e.* it is only a coordinate singularity, and so we may choose to include further portions of the Lorentzian geometry beyond this surface. For example, we choose to include the entire interior region of the black hole(s). Again it is crucial to note that the additional geometry will be comprised of a disconnected component for each black hole operator – see figure 3.18. Since these regions lie outside of the domain of dependence of $\mathcal{W}$, their geometry (*e.g.* whether they contain shockwaves or any other disturbances) are not determined by the boundary condition we have supplied. If we simply analytically continue the given solution, the geometry of these regions is identical to the Einstein-Rosen bridge in a two-sided BTZ geometry with the same mass as the corresponding operator. We will take the interpretation that the details of what appears outside the domain of dependence of $\mathcal{W}$ is part of the definition of the operator associated to that region. So in sum, the action of the Lorentzian cap is

$$I_{\text{cap}} = \frac{1}{4\pi G_{\text{N}}} V_{\mathcal{W}} + \sum_{i=\text{BH}} I_i = \frac{\pi}{4G_{\text{N}}} \sum_i \left(\text{Re}(\eta_i) - \frac{1}{3} \right) + \sum_{i=\text{BH}} I_i \,. \tag{3.6.0}$$

Hence we see that it is the sum of three contributions that each depend only on one of the three operators. Thus, we can absorb the corresponding phase generated by the action of the Lorentzian geometry into the definition of the operators, and we will arrive at a real result for the three-point function.

Hence we arrive at the total action for the single-sided geometry,

$$I_{\text{single-sided}} = \frac{1}{2} I_{\text{wormhole}} + i \sum_i f(i) \,. \tag{3.6.0}$$

Again, it is a nontrivial result that the imaginary term is given by the sum shown above since this allows us to absorb the corresponding phases into the definition of the operators. After eliminating these phases, we recover the three-point function from the single-sided bulk geometry, *i.e.*

$$e^{-I} \approx G_L(z_1, z_2, z_3) \,, \tag{3.6.0}$$

where $G_L(z_1, z_2, z_3)$ is the semiclassical Liouville three-point correlator in [11].

3.7 Discussion

In this chapter we discussed three-dimensional asymptotically AdS_3 geometries that are sourced by the insertion of boundary operators whose scaling dimensions is heavy as the central charge of the holographic CFT_2. The presence of any such operators deforms the AdS geometry by inducing a non vanishing expectation value for the holographic stress tensor, close to the boundary. This is true perturbatively in general dimensions, but in three-dimensions there is an exact solution, due to Bañados [35], that describes such deformation. However, this metric does not describe the full bulk spacetime. When only two black hole operators are inserted, we showed that the full geometry is simply an infinite covering of

the Euclidean BTZ black hole, but when three or more operators are inserted, we found that the completion of the Bañados metric into the bulk is a wormhole geometry involving multiple asymptotic boundaries. To understand this rather non trivial fact we rephrased the construction of the bulk geometry as a quotient of AdS_3 realized by domes and doors. The dome construction is a well know characterization of hyperbolic geometries with an asymptotically AdS_3 metric, and more familiar from the study of black hole thermodynamics, see *e.g.* [89], but the addition of the doors is new as far as we can tell.

As in the description of a Euclidean two-point function geometry in section 3.2, *i.e.* as empty AdS_3 with identifications, the doors are needed to describe the insertion of boundary operators. In particular, approaching a black hole operator insertions means circling around a dome and thus going through the door infinitely many times. When a third operator is inserted, as we discussed in section 3.3, the presence of the doors splits the AdS_3 boundary into multiple asymptotic boundaries and a wormhole appears. An interesting alternative to the Euclidean wormhole[12] is to cut the geometry at the wormhole mouth and glue there a Lorentian cap. In this way the bulk on-shell action can be understood to compute a holographic three-point function, up to phases. We expect that geometries with n-black holes operator insertions are again Euclidean wormholes, since it is straightforward to extend our dome-and-door construction to examine the case with more than three insertions. It would be interesting to understand how these geometries, constructed here using domes and doors, would be described in the language of the recently proposed "Virasoro TQFT" of [90].

For discussion, it is instructive to consider some simplifying regimes. For example, things simplify when the operators are either very light or very heavy. In the first case, three black holes should behave as pointlike probes moving along geodesics meeting at an optimal point in the bulk. Then the correlator should be approximated by *minus* the mass times length of these geodesics so that [91]

$$\begin{aligned} \log C_{123} &\simeq \sum_{i\neq j\neq k} \frac{\Delta_i}{2} \log\left(\frac{(\Delta_i-\Delta_j+\Delta_k)(\Delta_i+\Delta_j-\Delta_k)(\Delta_i+\Delta_j+\Delta_k)}{4\Delta_i^2(\Delta_j+\Delta_k-\Delta_i)}\right) \\ &= -\frac{3}{2}\Delta\log(4/3)<0 \qquad \text{for equal masses} \end{aligned} \tag{3.7.0}$$

For very heavy operators, we also expect things to simplify and indeed we observe that the DOZZ formula as function of insertions points, and at very large conformal dimensions Δ_i, can be nicely captured by the simple integral

$$\log|G_L(z_1,z_2,z_3)|^2 \simeq \frac{c}{3\pi}\int d^2z\sqrt{L\bar{L}} \tag{3.7.0}$$

This integral can be evaluated straightforwardly and matched with the well known asymptotics of DOZZ; it would be great to understand how to derive it directly from a simple gravitational argument (something we partially achieve below where we mention the analytic continutation to negative masses). For $\Delta_i=\Delta$, the above (3.7) gives [66]

$$\log C_{\texttt{BH BH BH}} \simeq \frac{3\Delta}{2}\log(27/16)>0 \tag{3.7.0}$$

[12] We thank Juan Maldacena for bringing this possibility to our attention.

Note that $C_{\texttt{BH BH BH}}$ is exponentially large, while C_{123} for geodesics is exponentially small. The interpolation is drawn schematically in figure 3.19. Perhaps there is a simple CFT explanation for such a drastic change in the scaling of the three-point coupling.[13]

Collecting the results from sections 3.2, 3.3 and 3.6 we provided a uniform geometric picture for interpolating between these extreme regimes. In particular we discussed the geometry as we vary from the regime in which the geometry sourced by the operator insertions matches the result for the geodesic computation, and it grows into finite defect operators, until the regime where the geometry describes black hole operators, for which we have found a wormhole.

A more general consideration that our three-dimensional explorations are strongly demanding is the following: What will happen in higher dimensions when we try to extend a three-point geometry beyond the Fefferman-Graham patch, all the way into the bulk? and what geometric picture underlies the interpolation between geodesics and huge operator insertions? Will we find a wormhole, or will we rather find a single horizon with the topology obtained by fattening three geodesics meeting at a point into a three-legged sphere? Perhaps neither is true and something even more exotic will arise. In [1], we also advocated the possibility of a conifold-like solution with three spacetime bananas. It would be fascinating to develop new analytical or numerical techniques for finding the three-point function geometry in higher dimensions.

Relatedly, in [59], the authors predict that the typical structure constant of three very heavy global primary operators, with equal dimensions $\Delta_i = \Delta$, is at leading order independent from the spacetime dimensions, and reads

$$\log C_{\texttt{Heavy Heavy Heavy}} \simeq \frac{3\Delta}{2} \log(36/16) \tag{3.7.0}$$

What is the holographic counterpart of this very unusual universality? We do not know of any other example where a physical quantity computed by a gravitational action is independent from the spacetime dimensions.

Another observation highlighted in [59] is that by reconsidering (3.7) in two dimensions, it follows that the leading order result for the structure constants of huge primaries is much larger than (3.7), which is valid for huge Virasoro primaries, and that we obtain holographically as explained in this chapter. Indeed, the fact that we are reproducing (3.7) and not (3.7) makes sense since the stress-tensor expectation (3.1) we start with is the expectation of T in the presence of three Virasoro primaries. It would be very interesting to construct the *typical* stress tensor expectation value (3.1) when O_Δ are global primaries corresponding to descendants of Virasoro primaries with a level comparable to the dimension and redo the analysis of this chapter with that effective $L(z)$ as starting point.[14] Will that reproduce (3.7)? Can that be translated to a boundary graviton computation as discussed in [59]?

[13] Note that if we consider a correlation function of very large operators in a gauge theory, we often get exponentially large results precisely indicating that the number of contractions (*i.e.* the entropy) is huge. For example, see the discussion of C_{123} for three operators dual to LLM geometries in chapter 2 There the result is exponentially large for any R-charges $J_i \sim N^2$.

[14] If the level is $O(1)$ the expectation value will lead to the very same (3.1) as can be checked by a straightforward 2d CFT computation in the semiclassical limit where c, Δ scale together to infinity.

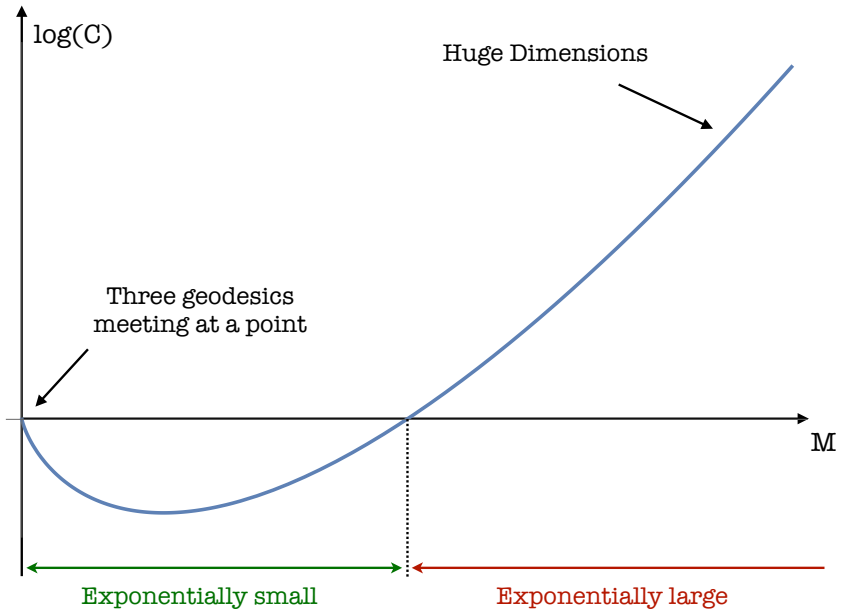

Figure 3.19: As we go from small to large masses (*i.e.* conformal dimensions), $\log C$ changes sign. The structure constant is thus exponentially small for "small" masses and exponentially large for "large" masses.

Will that computation better hint at the higher d generalization for which we only have the preliminary ideas alluded to in chapter 2?

Perhaps some intuition can be obtained from the following observation. The large dimension prediction of [59] can be cast as the statement that the structure constant of three huge operators of dimension Δ_i should be approximately given by a very simple ratio of factorials

$$C_{\texttt{Heavy}_1\ \texttt{Heavy}_2\ \texttt{Heavy}_3} \simeq \frac{(\Delta_1+\Delta_2+\Delta_3)!}{2^{\Delta_1}(\Delta_1)!\times 2^{\Delta_2}(\Delta_2)!\times 2^{\Delta_3}(\Delta_3)!} \tag{3.7.0}$$

as can be checked by comparing the Stirling approximation of the square of this expression to the leading expectation value for three heavy operators contained in the second line of eq. (7.51) in [59]. Clearly, (3.7) is begging for a combinatorial interpretation! If we interpret the denominator as coming from the normalization of the operators and the numerator as coming from the genuine interaction the task is to figure out how to generate $(\Delta_1+\Delta_2+\Delta_3)!$. Is there any (set of) Feynman diagrams that could produce such simple dependence in a large N gauge theory for instance?[15] Can the topology of such diagrams hint at a dual gravity picture? Since the main interaction factor only depends on the sum of all dimensions, this naively would suggest that the three operators merge into some big object in the bulk, akin to

[15] One naive suggestion would be to have one big bulk vertex with $\Delta_1+\Delta_2+\Delta_3$ fields connected to the three boundary operators, each with Δ_i fields. The number of ways to pick constituents from this bulk vertex to connect to the boundary would then easily produce such factorials. This is naive because vertices with n indistinguishable legs would naturally come with a $1/n!$ prefactor thus cancelling this factorial.

the interaction meeting point of three light geodesics, in contradistinction with the wormhole picture we encountered for Virasoro primaries.[16]

Another regime where things could simplify and help our intuition is the Heavy-Heavy-Light correlators when the light operator is not neutral, implying that the two heavy operators can not be the same by charge conservation [92, 93]. Then the light operator is most probably not just a probe geodesics. It would interesting to understand the implications of this statement on the gravity side.

Finally, let us add an intriguing observation concerning negative masses as a way to explore the physics of huge mass operators, at least holographically. The idea is to explore this unphysical regime as a trick to study the analytic continuation of the on-shell action for potisive and large masses. We shall see now that this idea allows for a shortcut derivation of the asymptotics (3.7). The key observation is that when black holes have negative mass, most, if not all of the geometry can be reached by staying below the wall (the surface where the Bañados metric has zero determinant). We explain this in detail in appendix B.3. The simplest scenario to discuss is the two-point function with insertions at zero and infinity. There the $\det(g) = 0$ wall is a cone which when mapped back to global coordinates is located at some finite $r > r_h$ when M is positive, *e.g.* see discussion around eq. (3.9) in chapter 2 and appendix B.3. But when $M < 0$ the wall actually corresponds to $r = 0$, which is the location of the naked singularity. Thus, the Bañados patch covers the full geometry in this case! A naïve estimate of the bulk geometry in this case then reads

$$-I = \frac{c}{6\pi}\int_{\epsilon/x<|z|<x/\epsilon} d^2z\,\sqrt{L(z)\bar{L}(\bar{z})} = \frac{c|M|}{12}\int_{\epsilon/x}^{x/\epsilon}\frac{dR}{R}\frac{1}{R} = -2\Delta\log(x/\epsilon) \tag{3.7.0}$$

This contribution alone gives $e^{-S} = |x/\epsilon|^{c|M|/6} = |x/\epsilon|^{-2\Delta}$ which is the expected growth when $M < 0$. Importantly, it gives precisely the analytic continuation of the full $M > 0$ result derived in chapter 2.

For the Bañados banana with two fixed insertions at z_1 and z_2 – instead of zero and infinity – the picture is a bit more subtle, but the geometry there is still almost all outside the wall. In particular, when $M \to -\infty$ the volume of the region inside the wall is subleading, as explained in Appendix B.3. Thus we reproduce again the expected result.

The negative mass two-point function discussion immediately leads to the plausible picture that perhaps the same will happen for the three-legged geometry: As $M_i \to -\infty$, the geometry outside the wall is almost the full geometry. Then it is straightforward to compute the bulk action from the Bañados patch and one obtains that the action on-shell is related to the integral of $\sqrt{L\bar{L}}$. For three points we immediately reproduce (3.7) and thus (3.7) for large negative mass. If we assume no essential singularity at infinity, the large positive mass result follows by analytic continuation. This is a much simpler derivation than the one from the Liouville field in section 3.5! Does a similar shortcut yield the asymptotic large mass behaviour

[16] This is also quite different from the combinatoric result arising from the interaction of three fully symmetric LLM large operators as computed in chapter 2. There the combinatorics final result took the form of a product of terms depending on effective dimensions $\Delta_{ij} = (\Delta_i + \Delta_j - \Delta_k)/2$ hinting as a sort of splitting of each external LLM geometry into two effective geometries of dimension Δ_{ij} with pairwise interactions between these effective geometries taking place.

of higher point functions as well in terms of the integral of the corresponding $\sqrt{L\bar{L}}$'s?[17]

Also, is there a counterpart of this picture for large negative mass in higher dimensions? Should it lead to (3.7)?

Maybe not; perhaps for global primaries things are more subtle (not only for large masses but for any masses). Maybe the typical three point function of huge CFT operators corresponds to a gravitational picture of three black holes dressed by a complicated cloud of matter and gravitons as speculated in [59]. Conversely, according to that scenario – which we are not necessarily endorsing or finding any sort of evidence for in our explorations – the holographic dual of the three huge black holes geometry is *not* just a typical three point function of very heavy operators in the dual CFT. What would it be?

[17] Of course, the result for higher point functions would not be as universal. For a four-point function, for instance, we have

$$L(z) = -\frac{1}{(z-z_1)(z-z_2)(z-z_3)(z-z_4)}\left(\sum_i \frac{M_i \prod_{j\neq i} z_{ij}}{4(z-z_i)} + U\right)$$

where the constant U is a theory dependent constant which is not a simple function of the dimensions and central charge.

Bibliography

[1] J. Abajian, F. Aprile, R. C. Myers, and P. Vieira, *Holography and Correlation Functions of Huge Operators: Spacetime Bananas*, arXiv:2306.15105.

[2] J. Abajian, F. Aprile, R. C. Myers, and P. Vieira, *Correlation Functions of Huge Operators in AdS_3/CFT_2: Domes, Doors and Book Pages*, arXiv:2307.13188.

[3] J. M. Maldacena, *The Large N limit of superconformal field theories and supergravity*, *Adv. Theor. Math. Phys.* **2** (1998) 231–252, [hep-th/9711200].

[4] D. Harlow and D. Stanford, *Operator Dictionaries and Wave Functions in AdS/CFT and dS/CFT*, arXiv:1104.2621.

[5] E. Witten and S.-T. Yau, *Connectedness of the boundary in the AdS / CFT correspondence*, *Adv. Theor. Math. Phys.* **3** (1999) 1635–1655, [hep-th/9910245].

[6] B. Mukhametzhanov, *Half-wormholes in SYK with one time point*, *SciPost Phys.* **12** (2022), no. 1 029, [arXiv:2105.08207].

[7] P. Saad, S. H. Shenker, and D. Stanford, *JT gravity as a matrix integral*, arXiv:1903.11115.

[8] N. Afkhami-Jeddi, H. Cohn, T. Hartman, and A. Tajdini, *Free partition functions and an averaged holographic duality*, *JHEP* **01** (2021) 130, [arXiv:2006.04839].

[9] A. Maloney and E. Witten, *Averaging over Narain moduli space*, *JHEP* **10** (2020) 187, [arXiv:2006.04855].

[10] A. Maloney and E. Witten, *Quantum Gravity Partition Functions in Three Dimensions*, *JHEP* **02** (2010) 029, [arXiv:0712.0155].

[11] J. Chandra, S. Collier, T. Hartman, and A. Maloney, *Semiclassical 3D gravity as an average of large-c CFTs*, *JHEP* **12** (2022) 069, [arXiv:2203.06511].

[12] J. Abajian, F. Aprile, R. C. Myers, and P. Vieira, *Correlation Functions of Huge Operators in AdS_3/CFT_2: Domes, Doors and Book Pages*, arXiv:2307.13188.

[13] R. A. Janik, P. Surowka, and A. Wereszczynski, *On correlation functions of operators dual to classical spinning string states*, *JHEP* **05** (2010) 030, [arXiv:1002.4613].

[14] G. T. Horowitz and A. Strominger, *Black strings and P-branes*, *Nucl. Phys. B* **360** (1991) 197–209.

[15] R. C. Myers and O. Tafjord, *Superstars and giant gravitons*, *JHEP* **11** (2001) 009, [hep-th/0109127].

[16] K. S. Thorne, R. H. Price, and D. A. Macdonald, eds., *BLACK HOLES: THE MEMBRANE PARADIGM*. Yale University Press, 1986.

[17] G. W. Gibbons and S. W. Hawking, *Action Integrals and Partition Functions in Quantum Gravity*, *Phys. Rev. D* **15** (1977) 2752–2756.

[18] C. Akers and P. Rath, *Holographic Renyi Entropy from Quantum Error Correction*, *JHEP* **05** (2019) 052, [arXiv:1811.05171].

[19] X. Dong, D. Harlow, and D. Marolf, *Flat entanglement spectra in fixed-area states of quantum gravity*, *JHEP* **10** (2019) 240, [arXiv:1811.05382].

[20] J. W. York, Jr., *Role of conformal three geometry in the dynamics of gravitation*, *Phys. Rev. Lett.* **28** (1972) 1082–1085.

[21] S. W. Hawking, *THE PATH INTEGRAL APPROACH TO QUANTUM GRAVITY*, pp. 746–789. Cambridge University Press, 1980.

[22] M. Parikh and F. Wilczek, *An Action for black hole membranes*, *Phys. Rev. D* **58** (1998) 064011, [gr-qc/9712077].

[23] V. Balasubramanian, J. de Boer, V. Jejjala, and J. Simon, *The Library of Babel: On the origin of gravitational thermodynamics*, *JHEP* **12** (2005) 006, [hep-th/0508023].

[24] A. Belin and J. de Boer, *Random statistics of OPE coefficients and Euclidean wormholes*, *Class. Quant. Grav.* **38** (2021), no. 16 164001, [arXiv:2006.05499].

[25] D. Cassani, "Black Holes and Semiclassical Quantum Gravity." https://laces.web.cern.ch/LACES19/BlackHoleLectures_LACES2019_online.pdf. see sect. 5.2.

[26] R. Emparan, C. V. Johnson, and R. C. Myers, *Surface terms as counterterms in the AdS / CFT correspondence*, *Phys. Rev. D* **60** (1999) 104001, [hep-th/9903238].

[27] K. Skenderis and S. N. Solodukhin, *Quantum effective action from the AdS / CFT correspondence*, *Phys. Lett. B* **472** (2000) 316–322, [hep-th/9910023].

[28] K. Skenderis, *Lecture notes on holographic renormalization*, *Class. Quant. Grav.* **19** (2002) 5849–5876, [hep-th/0209067].

[29] G. W. Gibbons, M. J. Perry, and C. N. Pope, *The First law of thermodynamics for Kerr-anti-de Sitter black holes*, *Class. Quant. Grav.* **22** (2005) 1503–1526, [hep-th/0408217].

[30] J. T. Liu and W. A. Sabra, *Mass in anti-de Sitter spaces*, *Phys. Rev. D* **72** (2005) 064021, [hep-th/0405171].

[31] A. Batrachenko, J. T. Liu, R. McNees, W. A. Sabra, and W. Y. Wen, *Black hole mass and Hamilton-Jacobi counterterms*, *JHEP* **05** (2005) 034, [hep-th/0408205].

[32] A. Christodoulou and K. Skenderis, *Holographic Construction of Excited CFT States*, *JHEP* **04** (2016) 096, [arXiv:1602.02039].

[33] C. Fefferman and C. R. Graham, *Conformal invariants*, *Astérisque* **S131** (1985) 95–116.

[34] C. Fefferman and C. R. Graham, *The ambient metric*, *Ann. Math. Stud.* **178** (2011) 1–128, [arXiv:0710.0919].

[35] M. Bañados, *Three-dimensional quantum geometry and black holes*, *AIP Conf. Proc.* **484** (1999), no. 1 147–169, [hep-th/9901148].

[36] R. A. Janik and R. B. Peschanski, *Asymptotic perfect fluid dynamics as a consequence of Ads/CFT*, *Phys. Rev. D* **73** (2006) 045013, [hep-th/0512162].

[37] R. A. Janik and R. B. Peschanski, *Gauge/gravity duality and thermalization of a boost-invariant perfect fluid*, *Phys. Rev. D* **74** (2006) 046007, [hep-th/0606149].

[38] A. Serantes and B. Withers, *Convergence of the Fefferman-Graham expansion and complex black hole anatomy*, *Class. Quant. Grav.* **39** (2022), no. 24 245010, [arXiv:2207.07132].

[39] J. L. Cardy, *Anisotropic Corrections to Correlation Functions in Finite Size Systems*, *Nucl. Phys. B* **290** (1987) 355–362.

[40] A. Petkou, *Conserved currents, consistency relations and operator product expansions in the conformally invariant O(N) vector model*, *Annals Phys.* **249** (1996) 180–221, [hep-th/9410093].

[41] H. Liu and A. A. Tseytlin, *$D = 4$ superYang-Mills, $D = 5$ gauged supergravity, and $D = 4$ conformal supergravity*, *Nucl. Phys. B* **533** (1998) 88–108, [hep-th/9804083].

[42] J. Penedones, *TASI lectures on AdS/CFT*, in *Theoretical Advanced Study Institute in Elementary Particle Physics: New Frontiers in Fields and Strings*, pp. 75–136, 2017. arXiv:1608.04948.

[43] V. Iyer and R. M. Wald, *Some properties of Noether charge and a proposal for dynamical black hole entropy*, *Phys. Rev. D* **50** (1994) 846–864, [gr-qc/9403028].

[44] S. S. Gubser and A. Nellore, *Ground states of holographic superconductors*, *Phys. Rev. D* **80** (2009) 105007, [arXiv:0908.1972].

[45] A. L. Fitzpatrick and K.-W. Huang, *Universal Lowest-Twist in CFTs from Holography*, *JHEP* **08** (2019) 138, [arXiv:1903.05306].

[46] Y.-Z. Li, Z.-F. Mai, and H. Lü, *Holographic OPE Coefficients from AdS Black Holes with Matters*, *JHEP* **09** (2019) 001, [arXiv:1905.09302].

[47] A. L. Fitzpatrick, J. Kaplan, and M. T. Walters, *Virasoro Conformal Blocks and Thermality from Classical Background Fields*, *JHEP* **11** (2015) 200, [arXiv:1501.05315].

[48] A. L. Fitzpatrick, K.-W. Huang, D. Meltzer, E. Perlmutter, and D. Simmons-Duffin, *Model-dependence of minimal-twist OPEs in $d > 2$ holographic CFTs*, *JHEP* **11** (2020) 060, [arXiv:2007.07382].

[49] E. Hijano, P. Kraus, E. Perlmutter, and R. Snively, *Witten Diagrams Revisited: The AdS Geometry of Conformal Blocks*, *JHEP* **01** (2016) 146, [arXiv:1508.00501].

[50] Z. W. Chong, H. Lu, and C. N. Pope, *BPS geometries and AdS bubbles*, *Phys. Lett. B* **614** (2005) 96–103, [hep-th/0412221].

[51] J. T. Liu, H. Lu, C. N. Pope, and J. F. Vazquez-Poritz, *Bubbling AdS black holes*, *JHEP* **10** (2007) 030, [hep-th/0703184].

[52] N. Bobev, A. Kundu, K. Pilch, and N. P. Warner, *Supersymmetric Charged Clouds in AdS_5*, *JHEP* **03** (2011) 070, [arXiv:1005.3552].

[53] H. Lin, O. Lunin, and J. M. Maldacena, *Bubbling AdS space and 1/2 BPS geometries*, *JHEP* **10** (2004) 025, [hep-th/0409174].

[54] K. Skenderis and M. Taylor, *Anatomy of bubbling solutions*, *JHEP* **09** (2007) 019, [arXiv:0706.0216].

[55] S. Corley, A. Jevicki, and S. Ramgoolam, *Exact correlators of giant gravitons from dual N=4 SYM theory*, *Adv. Theor. Math. Phys.* **5** (2002) 809–839, [hep-th/0111222].

[56] K. Costello and S. Li, *Twisted supergravity and its quantization*, arXiv:1606.00365.

[57] K. Costello and D. Gaiotto, *Twisted Holography*, arXiv:1812.09257.

[58] K. Budzik and D. Gaiotto, *Giant gravitons in twisted holography*, *JHEP* **10** (2023) 131, [arXiv:2106.14859].

[59] N. Benjamin, J. Lee, H. Ooguri, and D. Simmons-Duffin, *Universal Asymptotics for High Energy CFT Data*, arXiv:2306.08031.

[60] V. Balasubramanian and P. Kraus, *A Stress tensor for Anti-de Sitter gravity*, *Commun. Math. Phys.* **208** (1999) 413–428, [hep-th/9902121].

[61] S. de Haro, S. N. Solodukhin, and K. Skenderis, *Holographic reconstruction of space-time and renormalization in the AdS / CFT correspondence*, *Commun. Math. Phys.* **217** (2001) 595–622, [hep-th/0002230].

[62] M. M. Roberts, *Time evolution of entanglement entropy from a pulse*, *JHEP* **12** (2012) 027, [arXiv:1204.1982].

[63] K. Krasnov, *Holography and Riemann surfaces*, *Adv. Theor. Math. Phys.* **4** (2000) 929–979, [hep-th/0005106].

[64] S. Carlip, *The (2+1)-Dimensional black hole*, *Class. Quant. Grav.* **12** (1995) 2853–2880, [gr-qc/9506079].

[65] S. Collier, A. Maloney, H. Maxfield, and I. Tsiares, *Universal dynamics of heavy operators in CFT_2*, *JHEP* **07** (2020) 074, [arXiv:1912.00222].

[66] J. Cardy, A. Maloney, and H. Maxfield, *A new handle on three-point coefficients: OPE asymptotics from genus two modular invariance*, *JHEP* **10** (2017) 136, [arXiv:1705.05855].

[67] A. Belin, C. A. Keller, and I. G. Zadeh, *Genus two partition functions and Rényi entropies of large c conformal field theories*, *J. Phys. A* **50** (2017), no. 43 435401, [arXiv:1704.08250].

[68] M. Cho, S. Collier, and X. Yin, *Genus Two Modular Bootstrap*, *JHEP* **04** (2019) 022, [arXiv:1705.05865].

[69] H. Dorn and H. J. Otto, *Two and three point functions in Liouville theory*, *Nucl. Phys. B* **429** (1994) 375–388, [hep-th/9403141].

[70] A. B. Zamolodchikov and A. B. Zamolodchikov, *Structure constants and conformal bootstrap in Liouville field theory*, *Nucl. Phys. B* **477** (1996) 577–605, [hep-th/9506136].

[71] J. Teschner, *On the Liouville three point function*, *Phys. Lett. B* **363** (1995) 65–70, [hep-th/9507109].

[72] D. Harlow, J. Maltz, and E. Witten, *Analytic Continuation of Liouville Theory*, *JHEP* **12** (2011) 071, [arXiv:1108.4417].

[73] C.-M. Chang and Y.-H. Lin, *Bootstrap, universality and horizons*, *JHEP* **10** (2016) 068, [arXiv:1604.01774].

[74] C. T. Asplund, A. Bernamonti, F. Galli, and T. Hartman, *Holographic Entanglement Entropy from 2d CFT: Heavy States and Local Quenches*, *JHEP* **02** (2015) 171, [arXiv:1410.1392].

[75] S. Carlip and C. Teitelboim, *Aspects of black hole quantum mechanics and thermodynamics in (2+1)-dimensions*, *Phys. Rev. D* **51** (1995) 622–631, [gr-qc/9405070].

[76] L. Hadasz and Z. Jaskolski, *Classical Liouville action on the sphere with three hyperbolic singularities*, *Nucl. Phys. B* **694** (2004) 493–508, [hep-th/0309267].

[77] T. Faulkner, *The Entanglement Renyi Entropies of Disjoint Intervals in AdS/CFT*, arXiv:1303.7221.

[78] V. Balasubramanian, P. Hayden, A. Maloney, D. Marolf, and S. F. Ross, *Multiboundary Wormholes and Holographic Entanglement*, *Class. Quant. Grav.* **31** (2014) 185015, [arXiv:1406.2663].

[79] J. M. Maldacena and L. Maoz, *Wormholes in AdS*, *JHEP* **02** (2004) 053, [hep-th/0401024].

[80] J. Cotler and K. Jensen, *AdS_3 gravity and random CFT*, *JHEP* **04** (2021) 033, [arXiv:2006.08648].

[81] J.-M. Schlenker and E. Witten, *No ensemble averaging below the black hole threshold*, *JHEP* **07** (2022) 143, [arXiv:2202.01372].

[82] G. Di Ubaldo and E. Perlmutter, *AdS_3/RMT_2 Duality*, arXiv:2307.03707.

[83] S. Aminneborg, I. Bengtsson, D. Brill, S. Holst, and P. Peldan, *Black holes and wormholes in (2+1)-dimensions*, *Class. Quant. Grav.* **15** (1998) 627–644, [gr-qc/9707036].

[84] D. R. Brill, *Multi - black hole geometries in (2+1)-dimensional gravity*, *Phys. Rev. D* **53** (1996) 4133–4176, [gr-qc/9511022].

[85] K. Skenderis and B. C. van Rees, *Holography and wormholes in 2+1 dimensions*, *Commun. Math. Phys.* **301** (2011) 583–626, [arXiv:0912.2090].

[86] L. A. Takhtajan and L.-P. Teo, *Liouville action and Weil-Petersson metric on deformation spaces, global Kleinian reciprocity and holography*, *Commun. Math. Phys.* **239** (2003) 183–240, [math/0204318].

[87] L. Hadasz and Z. Jaskolski, *Polyakov conjecture for hyperbolic singularities*, *Phys. Lett. B* **574** (2003) 129–135, [hep-th/0308131].

[88] X. Dong, D. Marolf, P. Rath, A. Tajdini, and Z. Wang, *The spacetime geometry of fixed-area states in gravitational systems*, *JHEP* **08** (2022) 158, [arXiv:2203.04973].

[89] H. Maxfield, S. Ross, and B. Way, *Holographic partition functions and phases for higher genus Riemann surfaces*, *Class. Quant. Grav.* **33** (2016), no. 12 125018, [arXiv:1601.00980].

[90] S. Collier, L. Eberhardt, and M. Zhang, *Solving 3d Gravity with Virasoro TQFT*, arXiv:2304.13650.

[91] J. A. Minahan, *Holographic three-point functions for short operators*, *JHEP* **07** (2012) 187, [arXiv:1206.3129].

[92] J. Escobedo, N. Gromov, A. Sever, and P. Vieira, *Tailoring Three-Point Functions and Integrability II. Weak/strong coupling match*, *JHEP* **09** (2011) 029, [arXiv:1104.5501].

[93] P. Yang, Y. Jiang, S. Komatsu, and J.-B. Wu, *D-branes and orbit average*, *SciPost Phys.* **12** (2022), no. 2 055, [arXiv:2103.16580].

[94] Y. Jiang, S. Komatsu, and E. Vescovi, *Structure constants in $\mathcal{N} = 4$ SYM at finite coupling as worldsheet g-function*, *JHEP* **07** (2020), no. 07 037, [arXiv:1906.07733].

APPENDICES

Appendix A

Appendix for Chapter 2

A.1 Euclidean Rotation

In this section we describe the GtP map with marked points 0 and ∞ as a certain *rotation* in embedding coordinates. This rotation is precisely the one used in [13] to map spinning strings in global AdS to Euclidean strings in Poincaré AdS with two-point function boundary conditions. Here we will promote it to a local change of coordinates.

In embedding coordinates,[1] AdS admits the following standard parametrisations

`global Lorentzian`		`Euclidean Poincare`	
X_i	$= r\ \Omega_i\,,\quad i \geq 1$	X_{i+1}	$= x^i/\tilde{z}\,,\quad i \geq 1$
	$\vdots$	X_1	$= \frac{1}{2\tilde{z}}(1 - R^2 - \tilde{z}^2)$
X_0	$= \sqrt{1+r^2}\,\sin t$	X_0	$= x^0/\tilde{z}$
X_{-1}	$= \sqrt{1+r^2}\,\cos t$	X_{-1}	$= \frac{1}{2\tilde{z}}(1 + R^2 + \tilde{z}^2)$

(A.1.0)

where Ω_i are spherical coordinates, and $R^2 = \sum_{i=0}^{d-1}(x^i)^2$. Black holes will live in $D = d+1$ dimensions, with d being the spacetime dimension of the AdS boundary.

Recall the Schwarzschild black hole solution in global with Lorentzian signature is,

$$\texttt{global} \quad ; \quad ds_D^2 = \frac{dr^2}{g_{\tau\tau}(r)} - g_{\tau\tau}(r)dt^2 + r^2 d\Omega_{D-2}^2 \tag{A.1.0}$$

We will change signature by considering $\tau = -it$. Our starting point is then the following relations

$$\begin{aligned} dt &= \tfrac{X_{-1}\,dX_0 - X_0\,dX_{-1}}{1+r^2} \\ dr &= \tfrac{X_0\,dX_0 + X_{-1}\,dX_{-1}}{r} \qquad ; \qquad r = \sqrt{X_{-1}^2 + X_0^2 - 1} \\ d\Omega_{D-2}^2 &= -\tfrac{dr^2}{r^2} + \tfrac{1}{r^2}\textstyle\sum_{i\geq 1} dX_i^2 \end{aligned} \tag{A.1.0}$$

[1] We use $-X_{-1}^2 - X_0^2 + \sum_i X_i^2 = -1$ for Lorentzian and $-X_{-1} + X_0^2 + \sum_i X_i^2 = -1$ for Euclidean.

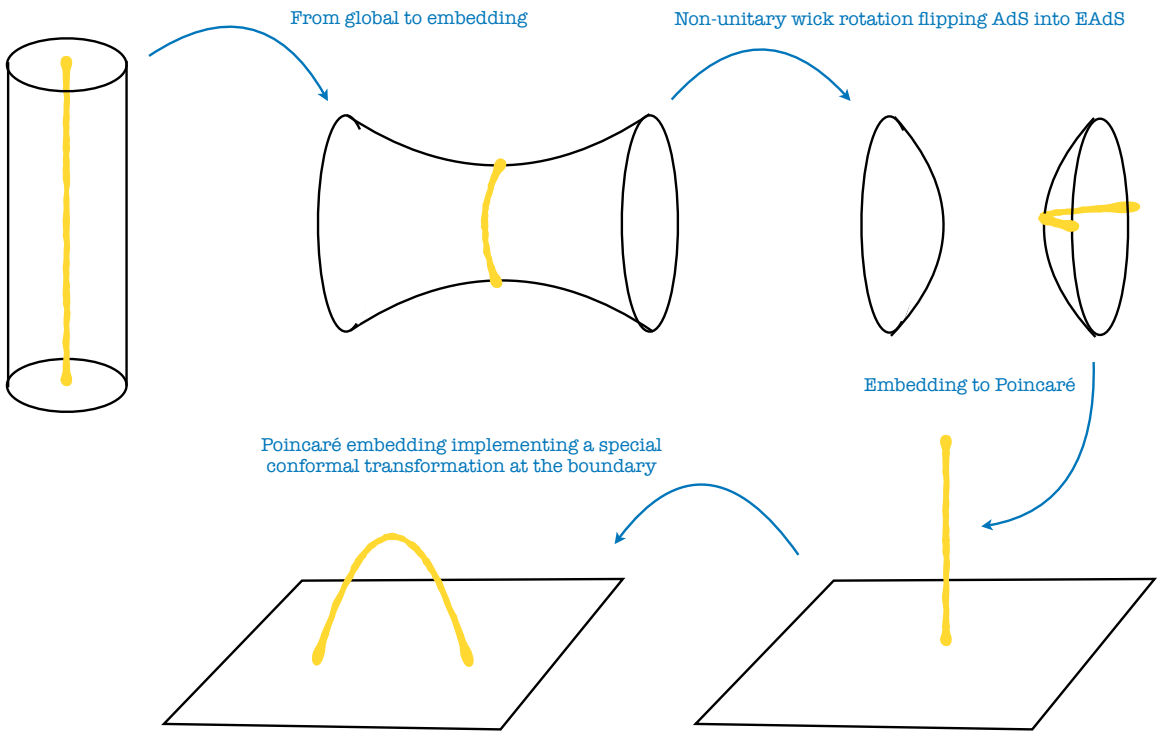

Figure A.1: Schematic for the sequence of transformations from `global` AdS with Lorentzian signature to the euclidean Poincaré patch. Starting with a tubular object in the middle of AdS, we end up with a banana shape with two insertion points at the boundary of AdS. The direct transformation from the top left to the bottom right pictures is eq. (2.2.1).

which we can use to rewrite eq. (A.1). Then, the rotation of [13] into Euclidean AdS is $X_0 \to iX_1$ and $X_1 \to X_0$. Once we perform this rotation on eq. (A.1), we will rewrite the result by the using Euclidean Poincaré patch, *i.e.* the second column of table (A.1). This gives the change of coordinates in the differential form,

$$\begin{bmatrix} d\tau \\ dr \end{bmatrix} = \frac{1}{\tilde{z}} \begin{bmatrix} \frac{R\tilde{z}}{\tilde{z}^2+R^2} & \frac{\tilde{z}^2}{\tilde{z}^2+R^2} \\ 1 & -\frac{R}{\tilde{z}} \end{bmatrix} \begin{bmatrix} dR \\ d\tilde{z} \end{bmatrix} \tag{A.1.0}$$

where R, Ω_i are polar coordinates in Poincaré AdS. As it turns our the $d\Omega$ are invariant, since in fact we are preserving rotational symmetry. Upon integration, we find

$$\tau = \frac{1}{2}\log(\tilde{z}^2 + R^2) \qquad \text{and} \qquad r = \frac{R}{\tilde{z}}\,, \tag{A.1.0}$$

which is precisely the AdS-unitary transformation in eq. (2.2.1).

A.2 Geodesics in the banana background

In this appendix, we show how to solve the problem of a geodesic the background of a two-point function black hole, and for concreteness we will specialize to AdS_5 and AdS_3. Other odd bulk dimensions (*i.e.* even boundary dimensions) can be analyzed with the same tools that we provide, but expressions become more complicated. We are working with the cone metric eq. (2.2.1).

A.2.1 AdS_5 geodesics

We can always put the four external points on a two-dimensional plane, through a conformal transformation, therefore the geodesic can be restricted to explore a three-dimensional space, the plane plus the holographic direction. We have $\tilde{z}(s)$, $R(s)$ and $\phi(s)$ or equivalently $\eta \equiv \tilde{z}/R$, $\rho \equiv \log(R)$ and ϕ. The latter will simplify the problem since they are essentially the same as in global coordinates (2.2.1).

Now, the cone geometry (2.2.1) is invariant under dilations $(R, \tilde{z}) \to \lambda(R, \tilde{z})$ and $SO(d-1)$ rotations. For the three-dimensional problem, we have two conserved charges for geodesics which we denote as $\mathcal{E}$ and $\mathcal{J}$. By using these charges, we obtain first order equations

$$\phi' = \pm \frac{\mathcal{J}\eta\eta'}{\sqrt{\mathcal{J}^2 M\eta^6 - (\mathcal{J}^2+M)\,\eta^4 - \eta^2\,(\mathcal{J}^2+\mathcal{E}^2-1)+1}} \tag{A.2.1}$$

$$\rho' = \pm \frac{\mathcal{E}\eta\eta'}{(1+\eta^2-M\eta^4)\sqrt{\mathcal{J}^2 M\eta^6 - (\mathcal{J}^2+M)\,\eta^4 - \eta^2\,(\mathcal{J}^2+\mathcal{E}^2-1)+1}} - \frac{\eta\eta'}{\eta^2+1} \tag{A.2.2}$$

In total the solution is parametrized by four integration constants, $\mathcal{E}, \mathcal{J}$ and C_ρ, C_ϕ from these first order equations.

It is straightforward to solve eq. (A.2.2) for empty AdS with $\mathcal{J} = 0$. This gives the semicircle in the form,

$$\big[R(\eta) - R_0\big]^2 + \big[\tilde{z} = \eta R(\eta)\big]^2 = L^2 \quad ; \quad \begin{array}{c} R = \frac{C}{\mathcal{E} \pm \sqrt{1-(\mathcal{E}^2-1)\eta^2}} \\ \mathcal{E} = \frac{R_0}{L} \quad ; \quad C = \frac{R_0^2 - L^2}{L} \end{array} \tag{A.2.2}$$

The signs $\pm$ provide a parametrization for the two branches of the semicircle, each one going from one insertion point at $z = 0 \to \eta = 0$ up to the turning point $\eta_\star$, where the derivatives blow up. This is given by the solution of $1 - (\mathcal{E}^2 - 1)\eta_\star^2 = 0$. Note that since $\eta \geq 0$, in our conventions $\mathcal{E} \geq 1$. The limit where the insertion points are close to each other is the limit $\mathcal{E} \to \infty$, since $\eta_\star$ and thus $\tilde{z}_\star$ goes to zero. Note also the connection with global coordinates, since we can rewrite

$$\rho' + \frac{\eta\eta'}{\eta^2+1} = \frac{d}{ds}\frac{\log\left(z(s)^2 + R(s)^2\right)}{2} = \tau'(s) \tag{A.2.2}$$

Of course, ϕ in the cone is the same as in global coordinates.

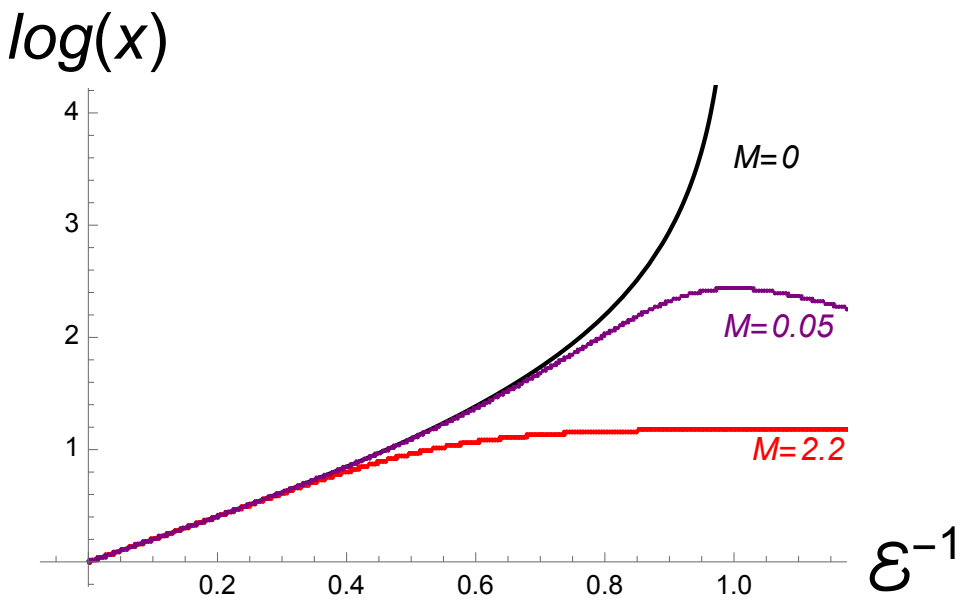

Figure A.2: We plot the right hand side of eq. (A.2.1) on the line $x = \bar{x} \geq 1$. The result can be written through elementary functions, and it reads

$$\log(x) = H_+ + H_- \quad ; \quad H_\pm = \mp \frac{\mathcal{E}}{\sqrt{1+4M}} \frac{1}{\sqrt{1-(\mathcal{E}^2-1)\eta_\mp^2 - M\eta_\mp^4}} \times \left(\coth^{-1}\left[\frac{\sqrt{1-(\mathcal{E}^2-1)\eta_\mp^2 - M\eta_\mp^4}}{2-(\mathcal{E}^2-1)\eta_\mp^2} \right] \pm \frac{i}{2} \right)$$

with $\eta_\pm^2 = (1 \pm \sqrt{1+4M})/(2M)$. For empty AdS, $\log(x)$ blows up at $\mathcal{E} = 1$, which implies that there is a geodesic for any two insertion points, with no limits on their separation. For the black hole, $M > 0$, the range of $\log(x)$ is bounded, thus real geodesics connect insertion points only up to some distance.

In the black hole case, the polynomial in the square root is a cubic in η^2 and has three zeros. One (and only one of them) of them is finite for $M \to 0$ and $\mathcal{J} \to 0$. This one defines the turning point $\eta_* > 0$. By construction this turning point has a good limit to empty AdS.

Eqs. (A.2.1) and (A.2.2) can be integrated to obtain the shifts. For the right-hand side, we sum the integrals from $0 \leq \eta \leq \eta_\star$ for the first branch and the $\eta_\star \leq \eta \leq 0$ for the second branch. For the left-hand side, we then consider the external points as described in figure 2.8. In sum we find

$$\underbrace{-i \log \sqrt{x/\bar{x}}}_{\Delta\phi} = 2 \int_0^{\eta_*} d\eta \frac{\mathcal{J}\eta}{\sqrt{\mathcal{J}^2 M\eta^6 - (\mathcal{J}^2+M)\eta^4 - \eta^2(\mathcal{J}^2+\mathcal{E}^2-1)+1}}$$

$$\underbrace{\log \sqrt{x\bar{x}}}_{\Delta\rho} = 2 \int_0^{\eta_*} d\eta \frac{\mathcal{E}\eta}{(1+\eta^2-M\eta^4)\sqrt{\mathcal{J}^2 M\eta^6 - (\mathcal{J}^2+M)\eta^4 - \eta^2(\mathcal{J}^2+\mathcal{E}^2-1)+1}}$$

These integrals express the physical insertion points $x, \bar{x}$ in terms of $\mathcal{E}$ and $\mathcal{J}$. They can be

computed but the result is written terms of elliptic functions so not very illuminating, and so we omit it.

A somewhat subtle point in the computation is that for some $x, \bar{x}$, a real solution to these equations will not exist, see figure A.2. Implicitly, we invert the relation (A.2.1) in a finite domain where this inverse exists (with a real solution) and analytically continue from there to access the result for any $x, \bar{x}$.

To obtain the action we can directly substitute eqs. (A.2.1) and (A.2.2) into the action to find

$$S(M) = m\left(\int_{\epsilon}^{\eta_*} + \int_{\frac{\epsilon}{\sqrt{x\bar{x}}}}^{\eta_*}\right)\frac{d\eta}{\eta}\frac{1}{\sqrt{\mathcal{J}^2 M\eta^6 - \eta^4\left(\mathcal{J}^2+M\right) - \eta^2\left(\mathcal{J}^2+\mathcal{E}^2-1\right)+1}} \tag{A.2.2}$$

Note that when computing $S(M) - S(0)$ the ϵ divergent terms coming from the lower integration limit drop out nicely and we can simply take $\epsilon \to 0$ there. This combination is what gives us the relevant four point function with stripped off two-point function prefactors.

We will now make progress analytically in the result by taking some limits.

Small black holes $M \to 0$

If we expand the equations above at small M all integrals become trivial to compute in terms of functions like log and arctan. We then easily find

$$\begin{aligned}
S(M) - S(0) = M&\left(-\frac{\left(z^2+4z+1\right)(\bar{z}-1)\log(z)}{4(z-1)(z-\bar{z})} + \frac{(z-1)\left(\bar{z}^2+4\bar{z}+1\right)\log(\bar{z})}{4(z-\bar{z})(\bar{z}-1)} - \frac{3}{2}\right) \\
+M^2&\left(\frac{8z^2\bar{z}^2+z^2\bar{z}+z\bar{z}^2-106z\bar{z}+43\bar{z}^2+\bar{z}+43z^2+z+8}{16(z-\bar{z})^2}\right. \\
&-\frac{(z-1)\left(z^2\bar{z}^4-2z^2\bar{z}^3+6z^2\bar{z}^2+24z^2\bar{z}+5\bar{z}^4-10z\bar{z}^3+24\bar{z}^3-48z\bar{z}^2+6\bar{z}^2-10z\bar{z}-2\bar{z}+5z^2+1\right)\log\bar{z}}{16(z-\bar{z})^3(\bar{z}-1)} \\
&+\frac{(\bar{z}-1)\left(z^4\bar{z}^2-2z^3\bar{z}^2-10z^3\bar{z}+6z^2\bar{z}^2-48z^2\bar{z}+24z\bar{z}^2-10z\bar{z}+5\bar{z}^2+5z^4+24z^3+6z^2-2z+1\right)\log z}{16(z-1)(z-\bar{z})^3} \\
&+\frac{\left(z^4\bar{z}^3-2z^4\bar{z}^2-5z^4\bar{z}+z^3\bar{z}^4+16z^3\bar{z}^3+8z^3\bar{z}^2-32z^3\bar{z}-2z^2\bar{z}^4+8z^2\bar{z}^3+24z^2\bar{z}^2+8z^2\bar{z}-5z\bar{z}^4-32z\bar{z}^3+8z\bar{z}^2+16z\bar{z}-5\bar{z}^3-2\bar{z}^2+\bar{z}-5z^3-2z^2+z\right)\log z\log\bar{z}}{16(z-\bar{z})^4} \\
&-\frac{(\bar{z}-1)^2\left(z^6\bar{z}+z^5\bar{z}^2+16z^5\bar{z}-4z^4\bar{z}^2-13z^4\bar{z}-6z^3\bar{z}^2-80z^3\bar{z}+20z^2\bar{z}^2-13z^2\bar{z}+25z\bar{z}^2+16z\bar{z}+\bar{z}+25z^5+20z^4-6z^3-4z^2+z\right)\log^2 z}{32(z-1)^2(z-\bar{z})^4} \\
&\left.-\frac{(z-1)^2\left(z^2\bar{z}^5-4z^2\bar{z}^4-6z^2\bar{z}^3+20z^2\bar{z}^2+25z^2\bar{z}+z\bar{z}^6+16z\bar{z}^5+25\bar{z}^5-13z\bar{z}^4+20\bar{z}^4-80z\bar{z}^3-6\bar{z}^3-13z\bar{z}^2-4\bar{z}^2+16z\bar{z}+\bar{z}+z\right)\log^2\bar{z}}{32(z-\bar{z})^4(\bar{z}-1)^2}\right) + O(M^3)
\end{aligned} \tag{A.2.3}$$

The first line is just the conformal block for the graviton exchange as we saw in the main text. The second line should correspond to an exchange of two gravitons. Indeed we find an infinite sum precisely compatible with that interpretation (it is infinite since the two massless

gravitons can easily form states of any spin and twist)

$$\texttt{blue} \;=\; c^{(1)}_{4,2}\times \mathcal{F}_{4,2}(w,\bar{w}) \qquad , \qquad (w,\bar{w})=(1-z,1-\bar{z}) \tag{A.2.-2}$$

$$\texttt{magenta} \;=\; \sum_{J=0}^{\infty}\sum_{\Delta=\max(8,4+J)}^{\infty} c^{(2)}_{\Delta,J}\mathcal{F}_{\Delta,J}(w,\bar{w}) \tag{A.2.-1}$$

where $c^{(1)}=-1/120$. We could find several trajectories for $c^{(2)}$ but not a closed expression. For example

$$c^{(2)}_{4+J,J}=-\frac{\sqrt{\pi}2^{-2J-5}(J-2)J\left(J^4+6J^3+35J^2+78J-72\right)\Gamma(J-3)}{(J+2)(J+4)(J+6)\Gamma\left(J+\frac{3}{2}\right)}\,, \qquad J=4,6,8,\ldots$$

$$c^{(2)}_{\Delta,0}=-\frac{\pi 4^{-\Delta-4}\left(32\Delta^6-429\Delta^5+1410\Delta^4+1660\Delta^3-10472\Delta^2+2144\Delta+7680\right)\Gamma\left(\frac{\Delta}{2}-1\right)^2}{5(\Delta-5)\Gamma\left(\frac{\Delta-1}{2}\right)\Gamma\left(\frac{\Delta+3}{2}\right)}\,,$$
$$\Delta=8,10,12,\ldots$$

And so on.

It would be interesting to see what changes in higher curvature gravity. In particular, it would be interesting if some structure constants would become negative for swampland values of these curvature coefficients.

Radial Geodesics and OPE

Another regime where we get remarkable simplifications is when we put the four points on a line. Then $x=\bar{x}$, and therefore $\mathcal{J}=0$. All formulae in section (A.2.1) simplifies and for example the action simply reads

$$S(M)-S(0)=-\frac{m}{2}\log(1+4M-2\mathcal{E}^2+\mathcal{E}^4)-(M\to 0) \tag{A.2.-4}$$

which is thus parametrically a function of x. It is nice to consider the OPE expansion for $x\to 1$ so that the geodesic stays close to the boundary. This limit is the limit of large energy $\mathcal{E}\gg 1$, and we can expand all expressions in that limit trivially to any desired OPE order and for any mass M. Using $w=1-x$ we find

$$\begin{aligned} S(M)-S(0) \;=\;& -\frac{M}{40}w^4-\frac{M}{20}w^5-\frac{M}{14}w^6-\frac{5M}{56}w^7+\left(-\frac{5M}{48}-\frac{11M^2}{14400}\right)w^8 \\ &+\left(-\frac{7M}{60}-\frac{11M^2}{3600}\right)w^9+\left(-\frac{7M}{55}-\frac{37M^2}{4928}\right)w^{10}+\left(-\frac{3M}{22}-\frac{1081M^2}{73920}\right)w^{11} \\ &+\left(-\frac{15M}{104}-\frac{1011M^2}{40768}w-\frac{89M^3}{1872000}\right)w^{12}+\left(-\frac{55M}{364}-\frac{39083M^2}{1019200}-\frac{89M^3}{312000}\right)w^{13} \\ &+\left(-\frac{11M}{70}-\frac{82079M^2}{1478400}-\frac{21991M^3}{22176000}\right)w^{14}+\left(-\frac{13M}{80}-\frac{4525M^2}{59136}-\frac{1657M^3}{633600}\right)w^{15} \\ &+O(w^{16}) \end{aligned} \tag{A.2.-3}$$

Note that although this is not a small M expansion, it is automatically organized as one as expected physically. Namely, the more subleading the OPE is, the more *primary* gravitons are being exchanged and thus more powers of M appear. The linear and quadractic terms in M agree with general limit of the previous section when taken the line.

A.2.2 AdS_3 geodesics

In this case the problem is simpler, since the blackening factor $f(r) = r^2+1-M$ is polynomial. We will introduce the quantity $r_h^2 = M-1$. Note that there are two regimes: the black hole regime where $M > 1$ and $r_h \geq 0$ is real, the defect regime where $0 \leq M \leq 1$ and r_h is imaginary. We will be careful in the following in finding expressions for the geodesic where the transitions is smooth.

The AdS_3 equations of motions are

$$\phi' = \pm \frac{\mathcal{J}\eta\eta'}{\sqrt{r_h^2\mathcal{J}^2\eta^4 - (\mathcal{E}^2+\mathcal{J}^2+r_h^2)\eta^2+1}}$$
$$r' = \pm \frac{\mathcal{E}\eta\eta'}{(1-r_h^2\eta^2)\sqrt{r_h^2\mathcal{J}^2\eta^4 - (\mathcal{E}^2+\mathcal{J}^2+r_h^2)\eta^2+1}} - \frac{\eta\eta'}{\eta^2+1}$$

The square root contains only a quadratic expression in η^2, so there are only two roots.

$$\eta_\pm^2 = \frac{\mathcal{J}^2+r_h^2+\mathcal{E}^2 \pm \sqrt{(\mathcal{J}^2+r_h^2+\mathcal{E}^2)^2 - 4\mathcal{J}^2 r_h^2}}{2\mathcal{J}^2 r_h^2} \tag{A.2.-7}$$

The turning point corresponds to $\eta_\star = \eta_-$, since this is the one that can go to the boundary $\eta = 0 = z$. As in AdS_5 – see eqs. (A.2.1) and (A.2.1) – we can integrate these expressions to find the shifts in ϕ and r. One might notice that the square root in $\eta_\pm$ is simply,

$$(\mathcal{J}^2+r_h^2+\mathcal{E}^2)^2 - 4\mathcal{J}^2 r_h^2 \quad = \prod_{\substack{s_1=\pm \\ s_2=\pm}} (\mathcal{J} + s_1 r_h + i s_2 \mathcal{E}) \tag{A.2.-7}$$

Then, the combinations that appear after doing the integrals are such that the result can be written as

$$\underbrace{-i\log\sqrt{x/\bar{x}}}_{\Delta\phi} = \frac{\log\frac{(\mathcal{J}+r_h+i\mathcal{E})(\mathcal{J}+r_h-i\mathcal{E})}{(\mathcal{J}-r_h-i\mathcal{E})(\mathcal{J}-r_h+i\mathcal{E})}}{2r_h} \quad ; \quad \underbrace{\log\sqrt{x\bar{x}}}_{\Delta\rho} = \frac{\log\frac{(\mathcal{J}-r_h+i\mathcal{E})(\mathcal{J}+r_h-i\mathcal{E})}{(\mathcal{J}-r_h-i\mathcal{E})(\mathcal{J}+r_h+i\mathcal{E})}}{2ir_h}$$

These function have a smooth transition from the defect to the black hole regime. It is also interesting to see how both remain real. In the defect regime, r_h is imaginary. By checking the argument of the log on the r.h.s. of $\Delta\phi$, this is a phase, and so $\Delta\phi$ is real, similarly, by checking the argument of the log on the r.h.s. of $\Delta\rho$, this is a radius, so $\Delta\rho$ is again real. In the black hole regime r_h is real, and the opposite happens.

We can now compute the action for the geodesic, by substituting ϕ' and r',

$$S(M) = m\left(\int_{\frac{\epsilon}{1}}^{\eta_*} + \int_{\frac{\epsilon}{\sqrt{z\bar{z}}}}^{\eta_*}\right)\frac{d\eta}{\eta}\frac{1}{\sqrt{(M-1)\mathcal{J}^2\eta^4 - (\mathcal{E}^2+\mathcal{J}^2+M-1)\eta^2+1}}$$

This integral receives no contribution from $\eta_\star$, and it is log divergent,

$$S(M) = -\frac{m}{2}\log\left[\frac{\epsilon^4}{16x\bar{x}}\prod_{s_1=\pm,s_2=\pm}(\mathcal{J}+s_1 r_h + is_2\mathcal{E})\right]$$

The next step is to invert $\mathcal{E},\mathcal{J}$ in terms of $\Delta\rho,\Delta\phi$, thus $x,\bar{x}$. For real values of $\mathcal{E},\mathcal{J}$ the range of $x,\bar{x}$ is restricted on a certain domain, which is less than the whole boundary of AdS. With this understanding we find,

$$\begin{aligned} S(M) &= -\frac{m}{2}\log\left[\frac{\epsilon^4 r_h^4}{4x\bar{x}}\frac{1}{(\cosh(ir_h\Delta\rho)-\cosh(r_h\Delta\phi))^2}\right] \\ &= -\frac{m}{2}\log\left[\frac{\epsilon^4 r_h^4 x^{-ir_h-1}\bar{x}^{-ir_h-1}}{(1-x^{-ir_h})^2(1-\bar{x}^{-ir_h})^2}\right] \end{aligned}$$

For $r_h = i$, *i.e.* empty AdS, the result becomes $S(0) = -\frac{m}{2}\log[\frac{\epsilon^4}{(1-x)^2(1-\bar{x})^2}]$. The geodesic 4pt correlator in the BTZ background is

$$\begin{aligned} \frac{\langle\phi_H(0)\phi_L(1)\phi_L(x)\phi_H(\infty)\rangle}{\langle\phi_H(\infty)\phi_H(0)\rangle\langle\phi_L(x)\phi_L(1)\rangle} &= e^{-(S(M)-S(0))} = \\ &= \left[(1-M)\frac{(1-x)x^{\frac{\sqrt{1-M}-1}{2}}(1-\bar{x})\bar{x}^{\frac{\sqrt{1-M}-1}{2}}}{(x^{\sqrt{1-M}}-1)(\bar{x}^{\sqrt{1-M}}-1)}\right]^m \end{aligned}$$

Note this is invariant under $x\to 1/x$ and $\bar{x}\to 1/\bar{x}$, as it should. Quite nicely, the result is simply the Virasoro block in the t-channel orientation. In the defect regime, we can expand at small M to get,

$$\frac{\langle\phi_H(0)\phi_L(1)\phi_L(x)\phi_H(\infty)\rangle}{\langle\phi_H(\infty)\phi_H(0)\rangle\langle\phi_L(x)\phi_L(1)\rangle} = 1 + \frac{mM}{24}\left((1-x)^2{}_2F_1(2,2,4;1-x) + c.c.\right) + O(M^2) \quad \text{(A.2.-8)}$$

which at leading order is just the stress tensor global conformal block.

A.3 Schur 3-pt functions: a new exact and non-extremal result

In this appendix we will derive a new exact formula for three-point function of half-BPS operators given by fully symmetric (or anti-symmetric) characters. As will any three-point

function of half-BPS correlators, this correlation function can be computed at tree level, by working out the combinatoric of Wick contractions.

There are plenty of exact three-point correlators of half-BPS operators computed in this way in the the literature but most of them – if not all – were computed for extremal correlators where the length of one operator is equal to the sum of the other two and thus there are no propagators between those two smaller operators. The main novelty of this appendix is that we will consider a maximally non-extremal correlator where all fields are connected to all fields.

The starting point reads

$$\left\langle \prod_{i=1}^{3} \det[1 + t_i\, Y_i \cdot \Phi_i(x_i)]^{\pm 1} \right\rangle = \tag{A.3.1}$$

$$= C \int \prod_{i \neq j} d\rho_{ij} e^{\frac{2N}{g^2} \sum\limits_{i<j} \rho_{ij}\rho_{ji}} (1 - \hat{\rho}_{12}\hat{\rho}_{12} - \hat{\rho}_{13}\hat{\rho}_{31} - \hat{\rho}_{23}\hat{\rho}_{32} + \hat{\rho}_{12}\hat{\rho}_{23}\hat{\rho}_{31} + \hat{\rho}_{13}\hat{\rho}_{32}\hat{\rho}_{21})^{\pm N}$$

This formula is derived following [93, 94]: One (1) introduces a set of auxiliary fields χ to cast the determinants as Gaussian integrals[2]; (2) integrates out the scalars Φ to obtain a quartic action in the auxiliary field; (3) introduce a second set of auxiliary fields ρ to render that quartic interation quadractic using the usual Hubbard-Stratonovich trick; (4) integrate out the now quadractic fields χ to arrive at (A.3.1).

The dependence on the generating function variables t_j and on the positions and polarizations on the right hand side of (A.3.1) is hidden inside the hatted variables

$$\hat{\rho}_{ij} \equiv \rho_{ij} \times \sqrt{4 t_i t_j \frac{Y_i \cdot Y_j}{x_{ij}^2}}\,. \tag{A.3.0}$$

Each determinant is a generating function of characters of fully anti-symmetric (+ sign) or symmetric (− sign) characters so to get the correlation function of the desired characters we simply need to pick up the corresponding powers of t_j on the right hand side by using the usual Binomial expansion to expand out

$$(1 - \hat{\rho}_{12}\hat{\rho}_{12} - \hat{\rho}_{13}\hat{\rho}_{31} - \hat{\rho}_{23}\hat{\rho}_{32} + \hat{\rho}_{12}\hat{\rho}_{23}\hat{\rho}_{31} + \hat{\rho}_{13}\hat{\rho}_{32}\hat{\rho}_{21})^{\pm N} \tag{A.3.0}$$

Because there are six terms in this expression we can cast it as a five-fold binomial sum where each of the six terms is raised to an integer power. The power of the last and next-to the last terms needs to be the same to get a non-trivial result and this kills one of the five sums. Since we are interested in fixed powers of t_1, t_2 and t_3 we set three extra constraints on the powers arising in these four sums killing three of them. So we are left with a single sum for the desired character three-point function (here specializing to the anti-symmetric

[2]Depending on what sign we want on the left hand side we use fermions or bosons.

case for simplicity):

$$\langle \mathcal{O}_{\chi^{anti}_{j_1}} \mathcal{O}_{\chi^{anti}_{j_2}} \mathcal{O}_{\chi^{anti}_{j_3}} \rangle = C \left(\frac{Y_1 \cdot Y_2}{x_{12}^2}\right)^{(j_1+j_2-j_3)/2} \left(\frac{Y_2 \cdot Y_3}{x_{23}^2}\right)^{(j_2+j_3-j_1)/2} \left(\frac{Y_1 \cdot Y_3}{x_{13}^2}\right)^{(j_1+j_3-j_2)/2} \tag{A.3.1}$$

$$\times \sum_{n=0}^{N/2} \binom{N}{2n,\ \frac{j_1+j_2+j_3}{2}-3n} \binom{\frac{j_1+j_2+j_3}{2}-3n}{\frac{j_1+j_2-j_3}{2}-n,\ \frac{j_1+j_3+-j_2}{2}-n} \binom{2n}{n} (-1)^{\frac{j_1+j_2+j_3}{2}}$$

$$\times \langle (\rho_{12}\rho_{21})^{\frac{j_1+j_2-j_3}{2}} \rangle \langle (\rho_{13}\rho_{31})^{\frac{j_1+j_3-j_2}{2}} \rangle \langle (\rho_{23}\rho_{32})^{\frac{j_2+j_3-j_1}{2}} \rangle$$

where the averages in the last line are with respect to to the Gaussian measure in eq. (A.3.1) so they can be trivially evaluated. (For symmetric characters we get a similar expression with $N \to -N$ and the sum running up to infinity.) Once we evaluate the integrals we can simply preform the sum: We get an hypergeometric function. We should also normalize properly the two-point function to get a properly defined three-point function. Keeping track of all those simple normalization factors, we obtain eq. (2.5.2).[3]

[3]Formula (2.5.2) is for symmetric characters. For anti-symmetric simply replace $N \to -N$ there.

Appendix B

Appendix for Chapter 3

B.1 Solutions of AdS_3 Einstein Gravity

A striking consequence of the simplicity of gravity in three dimensions is that the general asymptotically AdS_3 solution can be written in closed Bañados form given in eq. (3.1). That is,

$$ds^2 = \frac{dy^2 + dzd\bar{z}}{y^2} + L(z)dz^2 + \bar{L}(\bar{z})d\bar{z}^2 + y^2 L(z)\bar{L}(\bar{z})dzd\bar{z}\,. \tag{B.1.0}$$

This solution is determined in terms of a holomorphic function $L(z)$ and an anti-holomorphic function $\bar{L}(\bar{z})$, which are proportional to the holomorphic and anti-holomorphic components of the boundary stress tensor. The problem of finding solutions corresponding to configurations in the boundary CFT_2 therefore reduces to finding the boundary stress tensor (3.1). Such an expansion is available in higher-dimensional Einstein gravity as well, but uniquely in three dimensions, the expansion truncates for the general solution.

B.1.1 The det(g) Wall

While it is possible to construct a solution corresponding to any boundary stress tensor as an expansion near the conformal boundary, this expression will typically only describe the solution in a coordinate patch. To see this, consider the determinant of the metric, which yields

$$\det(g) = \frac{\left(1 - y^4 L(z)\bar{L}(\bar{z})\right)^2}{4\ y^6} \tag{B.1.0}$$

So we see that the metric degenerates when the numerator vanishes, which happens at

$$y = \left(L(z)\bar{L}(\bar{z})\right)^{-1/4} \tag{B.1.0}$$

Note that when the boundary stress tensor has poles, as it does when there are local operator insertions in the CFT_2, this surface will extend all the way to the conformal boundary at $y = 0$. In order to calculate the bulk action, we first need to extend the geometry past this surface.

B.1.2 Extending the Solution

Since every solution to Einstein gravity is locally isometric, there exists a change of variables that puts the metric of the general solution (B.1) into the form of the standard Poincaré upper half plane metric on Euclidean AdS_3,

$$ds^2 = \frac{dY^2 + dZd\bar{Z}}{Y^2} \tag{B.1.0}$$

The task of extending the solution can be informed by considering the explicit form of this map from the general solution to Euclidean AdS_3. Remarkably, the explicit expression for this map is known [62]. The map is given explicitly by

$$\begin{aligned}
Y &= y\,\frac{4(\partial f\,\bar{\partial}\bar{f})^{3/2}}{4\,\partial f\,\bar{\partial}\bar{f} + y^2\,\partial^2 f\,\bar{\partial}^2\bar{f}}\,,\\
Z &= f(z) - \frac{2y^2\,(\partial f)^2\,\bar{\partial}^2\bar{f}}{4\,\partial f\,\bar{\partial}\bar{f} + y^2\,\partial^2 f\,\bar{\partial}^2\bar{f}}\,,\\
\bar{Z} &= \bar{f}(\bar{z}) - \frac{2y^2\,(\bar{\partial}\bar{f})^2\,\partial^2 f}{4\,\partial f\,\bar{\partial}\bar{f} + y^2\,\partial^2 f\,\bar{\partial}^2\bar{f}}\,.
\end{aligned}$$

Here the functions $f(z)$ and $\bar{f}(\bar{z})$ are related to the boundary stress tensor through the Schwarzian equations

$$\begin{aligned}
\{f, z\} &\equiv \frac{f'''(z)}{f'(z)} - \frac{3}{2}\left(\frac{f''(z)}{f'(z)}\right)^2 = -2L(z)\\
\{\bar{f}, \bar{z}\} &= -2\bar{L}(\bar{z})\,.
\end{aligned}$$

At the conformal boundary $y = 0$, we have

$$Z = f(z) \quad ; \qquad \bar{Z} = \bar{f}(\bar{z})\,. \tag{B.1.0}$$

The functions f and $\bar{f}$ will generically have branch points, and the image under the map (B.1.2) will be a region in Euclidean AdS_3 bounded by surfaces that are the images of surfaces on either side of the branch cuts. These surfaces are identified with each other to produce the solution (B.1). To find the completion of this solution, we need to extend the identification surfaces into the rest of AdS_3. The map into AdS_3 is not necessarily injective. So the completion of the solution (B.1) can be thought of as a subregion of a covering space of Euclidean AdS_3 with its boundary glued together in a way that can be "read off" from the functions f and $\bar{f}$.

Note that the functions f and $\bar{f}$ are only unique up to isometries of Euclidean AdS_3. Given solutions, f_0 and $\bar{f}_0$, to the Schwarzian equations (B.1.2), we can construct a family of solutions

$$\begin{aligned}
f(z) &= \frac{af_0(z) + b}{cf_0(z) + d}\\
\bar{f}(\bar{z}) &= \frac{\bar{a}\bar{f}_0(\bar{z}) + \bar{b}}{\bar{c}\bar{f}_0(\bar{z}) + \bar{d}}
\end{aligned}$$

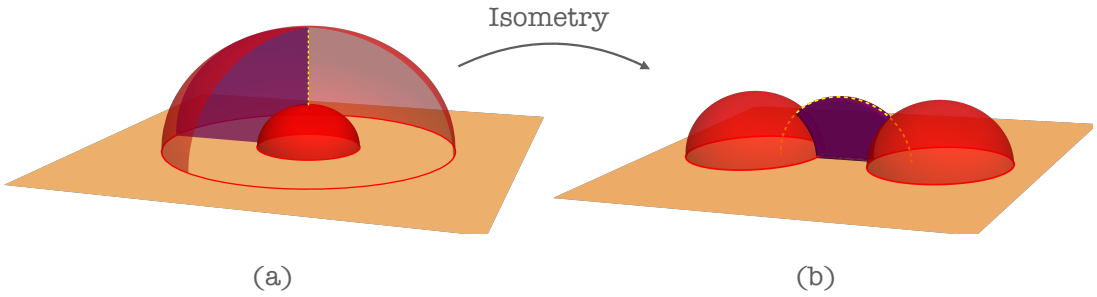

Figure B.1: Replacing $f \to \frac{af+b}{cf+d}$ acts on the domes-and-doors pictures as an isometry of Euclidean AdS_3. For example, here we show the effect of such a change on the representation of the two-point function geometry. Since we have only changed things by an isometry, the resulting geometry is the same.

When we perform such a Möbius transformation on f, the Roberts map (B.1.2) extends this change into the bulk.

The Roberts map with the new f is the same as the old Roberts map, composed with an isometry of Euclidean AdS_3. For example we can perform such an isometry by replacing $f_{\texttt{2pt}}$ with a new f related by a Möbius transformation in order to change the domes-and-doors picture from figure B.1(a) to figure B.1(b). The freedom to perform such Möbius transformations can be useful for putting the domes-and-doors constructions into nice standard configurations, such as the one in figure 3.6.

B.2 Black Hole Two-Point Function in AdS_3

The black hole two-point function was treated in chapter 2. Here, we perform the same calculation, in AdS_3, in a language similar to that which we used to treat the three-point function. This allows us to determine the correct counterterms to add in the case of the three-point function.

B.2.1 Geometric Setup

We consider the black hole two-point function geometry, which can be described using the metric

$$ds^2 = d\tilde{\rho}^2 + \cosh^2\tilde{\rho}\, d\tau^2 + \sinh^2\tilde{\rho}\, d\theta^2 \tag{B.2.0}$$

where the coordinates range over

$$0 < \tilde{\rho} < \infty\,,$$
$$0 < \tau < 2\pi R_h\,,$$
$$-\infty < \theta < \infty\,.$$

We will calculate the Einstein-Hilbert action of this geometry by cutting off the radial coordinate at

$$\tilde{\rho}_{\text{cutoff}} = \ln\left(\frac{2}{\epsilon}\right) - \frac{\tilde{\varphi}(z,\bar{z})}{2}\,, \tag{B.2.0}$$

as described in section 3.5. As in eq. (3.5), the coordinates $z, \bar{z}$ are related to the coordinates τ, θ with

$$\tau = \frac{1}{2}\left(\tilde{f}(z) + \bar{\tilde{f}}(\bar{z})\right) \quad ; \qquad \theta = \frac{1}{2i}\left(\tilde{f}(z) - \bar{\tilde{f}}(\bar{z})\right)\,. \tag{B.2.0}$$

Further, the solution to the Laplace equation is given by

$$\tilde{\varphi}(z,\bar{z}) = \ln\left(\partial\tilde{f}\,\bar{\partial}\bar{\tilde{f}}\right)\,. \tag{B.2.0}$$

With these choices, we have that the metric on the cutoff surface is

$$ds^2_{cutoff} = \frac{dz d\bar{z}}{\epsilon^2} + O(\epsilon^0) \tag{B.2.0}$$

B.2.2 Calculating the Action

The contributions to the action coming from the bulk and the asymptotic boundary for our solution are given by

$$I_0 = \frac{1}{4\pi G_{\text{N}}}\int_{\mathcal{M}} d\tilde{\rho}\; d^2z\sqrt{g} - \frac{1}{8\pi G_{\text{N}}}\int_{\partial\mathcal{M}} d^2z\sqrt{h} = \frac{1}{4\pi G_{\text{N}}}\left(V - \frac{1}{2}A\right) \tag{B.2.0}$$

Now, we have

$$\begin{aligned} \frac{1}{4\pi G_{\text{N}}}\int_0^{\tilde{\rho}_{cutoff}} d\tilde{\rho}\sqrt{g} &= \frac{1}{8\pi G_{\text{N}}\,\epsilon^2} - \frac{e^{\tilde{\varphi}(z,\bar{z})}}{16\pi G_{\text{N}}} + O(\epsilon^2)\,, \\ -\frac{1}{8\pi G_{\text{N}}}\sqrt{h} &= -\frac{1}{8\pi G_{\text{N}}\,\epsilon^2} - \frac{\partial\tilde{\varphi}\bar{\partial}\tilde{\varphi}}{16\pi G_{\text{N}}} + O(\epsilon^2)\,. \end{aligned} \tag{B.2.1}$$

Combining these results, we find

$$I_0 = \frac{1}{16\pi G_{\text{N}}}\int d^2z\left(-\partial\tilde{\varphi}\bar{\partial}\tilde{\varphi} - e^{\tilde{\varphi}(z,\bar{z})}\right)\,. \tag{B.2.0}$$

As discussed in chapter 2, we must also add a Gibbons-Hawking-York boundary term on the stretched horizon $\tilde{\rho} = \epsilon$, which yields

$$I_{\text{GHY,hor}} = \frac{1}{8\pi G_{\text{N}}}\int d^2z\; e^{\tilde{\varphi}(z,\bar{z})}\,. \tag{B.2.0}$$

Finally, we get

$$I = I_0 + I_{\text{GH,hor}} = \frac{1}{16\pi G_{\text{N}}}\int_{\partial\mathcal{M}} d^2z\left(-\partial\tilde{\varphi}\bar{\partial}\tilde{\varphi} + e^{\tilde{\varphi}(z,\bar{z})}\right) \tag{B.2.0}$$

Note that using the equations of motion, we have $\partial\tilde{\varphi}\bar{\partial}\tilde{\varphi} = \bar{\partial}(\tilde{\varphi}\partial\tilde{\varphi})$. So we see that

$$\int d^2z\;\partial\tilde{\varphi}\bar{\partial}\tilde{\varphi} = \int d^2z\;\bar{\partial}(\tilde{\varphi}\partial\tilde{\varphi}) = i\oint dz\;\tilde{\varphi}\partial\tilde{\varphi} \tag{B.2.0}$$

and therefore

$$I = \frac{1}{16\pi G_{\text{N}}}\int d^2z\left(\partial\tilde{\varphi}\bar{\partial}\tilde{\varphi} + e^{\tilde{\varphi}(z,\bar{z})}\right) + \frac{i}{8\pi G}\oint dz\;\tilde{\varphi}\partial\tilde{\varphi}\,. \tag{B.2.0}$$

B.2.3 Counterterms

The Laplace solution corresponding to two hyperbolic singularities located at $z = \pm 1$ is given by

$$\tilde{\varphi}_{2pt}(z, \bar{z}) = \ln\left(\frac{4R_h^2}{|z^2-1|^2}\right) \tag{B.2.0}$$

Inserting this into the action above, we find

$$I = \frac{1}{4\pi G_{\text{N}}}\int d^2z\left(-\frac{|z|^2}{|z^2-1|^2} + \frac{R_h^2}{|z^2-1|^2}\right) \tag{B.2.0}$$

where we cut out a region of size ϵ around each of the insertions. The R_h dependent term gives

$$\frac{1}{4\pi G_{\text{N}}}\int d^2z\frac{R_h^2}{|z^2-1|^2} = -\frac{1}{4G_{\text{N}}}R_h^2\ln(\epsilon)\,. \tag{B.2.0}$$

So we see that

$$I = -\frac{1}{4G_{\text{N}}}R_h^2\ln(\epsilon) + C \tag{B.2.0}$$

where the constant C does not depend on R_h.

To fix C, we note that when $R_h^2 = -1$, we should have the vacuum. The vacuum partition function can be calculated from the conformal anomaly [11], and the result is

$$-\ln(Z(S^2)) = -\frac{1}{2G_{\text{N}}}\ln\left(\frac{R}{\epsilon}\right)\,. \tag{B.2.0}$$

So we have

$$I|_{R_h\to -1} = \frac{1}{4G_{\text{N}}}\ln\epsilon + C = -\frac{1}{2G_{\text{N}}}\ln\left(\frac{R}{\epsilon}\right)\,, \tag{B.2.0}$$

which allows us to read off the value of the constant C,

$$C = -\frac{1}{2G_{\text{N}}}\ln R + \frac{1}{4G_{\text{N}}}\ln\epsilon\,. \tag{B.2.0}$$

Finally, we find the action (B.2.3) becomes

$$I = \frac{1}{4G_{\text{N}}}(1-R_h^2)\ln\epsilon - \frac{1}{2G_{\text{N}}}\ln R\,. \tag{B.2.0}$$

Hence, to leading order, the action is given by

$$I \simeq \frac{1}{4G_{\text{N}}}(1-R_h^2)\ln\epsilon\,, \tag{B.2.0}$$

and so for each operator, we must add a counterterm of the form

$$I_{ct}(R_h) = -\frac{1}{8G_{\text{N}}}(1-R_h^2)\ln\epsilon\,. \tag{B.2.0}$$

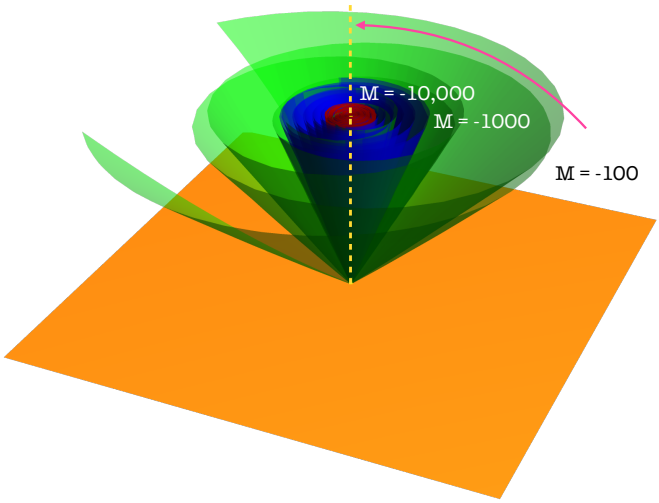

Figure B.2: Here we show the image of the $\det(g) = 0$ surface in empty AdS_3. We show the surface for $M = -100$ (green), -1000 (blue), and $-10,000$ (red). As the figure suggests, the wall shrinks towards the conical excess at $\tilde{\rho} = 0$ (the dashed yellow line in the figure) as we increase $|M|$. This shrinking is enough to compensate for the fact that the range of the angular coordinate θ is growing as $O(\sqrt{|M|})$, resulting in a volume that is only $O(M^0)$.

B.3 Negative Mass

It is interesting to consider analytically continuing the two- and three-point geometries to include insertions with negative masses. Consider first the two-point case, with operators of mass M placed at 0 and ∞ for convenience. Recall that when the mass is positive, we encountered a "wall" at

$$y = \frac{1}{(L\bar{L})^{1/4}} = 2\sqrt{\frac{z\bar{z}}{|M|}} \tag{B.3.0}$$

where $\det(g) = 0$. Some of the geometry was hidden behind this wall, and we needed to extend beyond this point to evaluated the two-point function. In the case where the mass is negative, we still have that the determinant of the metric vanishes at $y = 2\sqrt{z\bar{z}/|M|}$. However, when $M < 0$, the coordinate patch below this value of y actually represents the complete geometry. To see this, one need only use the Roberts map (3.1) to check where the $\det(g) = 0$ wall is mapped to in the "domes-and-doors" picture. We find that the wall is mapped into the line $Z = \bar{Z} = 0$. So in the negative mass case, there is no region hidden behind the wall. In fact, the wall is the location of the conical excess sourced by the operator insertions!

In order to calculate the two-point function with negative mass, we would like to consider the Bañados metric (3.1) with the operators at finite points. In this case, the situation is slightly more complicated. The Bañados patch no longer covers everything. However, if we consider the surface where $\det(g) = 0$, and use the map (3.1) to identify it with a surface in empty AdS_3, we find that the resulting surface closes up towards the singularity as we

increase the mass – see figure B.2. Indeed, we find

$$\tilde{\rho}_{\texttt{wall}}(\theta) = O\left(\frac{1}{(-M)^{1/4}}\right) \tag{B.3.0}$$

where $\tilde{\rho}$ and θ are the coordinates introduced in eq. (3.5). The range of θ in these coordinates is $0 < \theta < 2\pi\sqrt{1-M}$. So for large negative M, it is growing like $\sqrt{-M}$. Hence we find that the volume of the region behind the $\det(g) = 0$ wall is, to leading order at large negative M,

$$V_{\text{hidden}} = \int d\tilde{\rho}\, d\tau\, d\theta \cosh\tilde{\rho} \sinh\tilde{\rho} \sim \int \tilde{\rho}\, d\tilde{\rho}\, d\tau\, d\theta \sim \pi\sqrt{1-M}\tilde{\rho}^2_{\texttt{wall}} \int d\tau = O(M^0) \tag{B.3.0}$$

On the other hand, consider the contribution from outside the $\det(g) = 0$ wall in a solution described by the metric (3.1) for arbitrary L, $\bar{L}$. It is given by

$$I_{\texttt{outside}} = \frac{c}{6\pi}\left(V_{\texttt{outside}} - \frac{1}{2}A\right) \tag{B.3.0}$$

where $V_{\texttt{outside}}$ is the bulk volume outside the $\det(g) = 0$ surface,

$$V_{\texttt{outside}} = \int_{y=\epsilon}^{y=1/(L\bar{L})^{1/4}} dy\, d^2z \frac{1-y^4 L(z)\bar{L}(\bar{z})}{y^3} = \int d^2z \left(\frac{1}{2\epsilon^2} - \sqrt{L\bar{L}}\right) + O(\epsilon^2) \tag{B.3.0}$$

and A is the area of the cutoff surface at $y = \epsilon$,

$$A = \int d^2z \frac{1}{\epsilon^2} + O(\epsilon^2) \tag{B.3.0}$$

So we see that the contribution to the action from the patch covered by the expansion near the asymptotic boundary is given by

$$I_{\texttt{outside}} = -\frac{c}{6\pi}\int d^2z \sqrt{L(z)\bar{L}(\bar{z})}\,. \tag{B.3.0}$$

Now, returning to the specific case of the two-point function, we see that the action outside the $\det(g) = 0$ wall is order $O(M^1)$. So at large negative M, the leading contribution comes from outside the wall, and is given by simply (B.3). We expect that a similar statement is true for the three-point function, since in that case, we find that the contribution outside the wall matches with the expected universal result at leading order in large negative mass.